

See discussions, stats, and author profiles for this publication at: <https://www.researchgate.net/publication/323428558>

Drilling Simulation and Risk Assessment of the IDDP-2 Geothermal Well in Iceland

Thesis · April 2016

CITATION

1

READS

262

1 author:



Alexander Scherff

Technische Universität Clausthal

8 PUBLICATIONS 4 CITATIONS

SEE PROFILE

Some of the authors of this publication are also working on these related projects:



Master Thesis Presentation: Drilling Simulation and Risk Assessment of the IDDP-2 Geothermal Well In Iceland [View project](#)



Master Thesis Presentation: 3-D Modelling of the IDDP-2 Geothermal Reservoir at Reykjanes, Southern Iceland [View project](#)



TU Clausthal
Clausthal University of Technology

Master Thesis

By

Alexander Scherff

Drilling Simulation and Risk Assessment of the IDDP-2 Geothermal Well in Iceland

1. Supervisor: Prof. Dr. G. Falcone*
2. Supervisor: Prof. Dr.-Ing. C. Teodoriu**
3. Assistant Advisor: Prof. Dr. W. Blendinger

* Professor at Cranfield University, UK

** Associate Professor at University of Oklahoma, USA

Institute of Petroleum Engineering ite
Clausthal University of Technology

12th April 2016



A 26 credit units Master's thesis

© Alexander Scherff, 2016

Clausthal University of Technology
Institute of Petroleum Engineering
Petroleum Engineering, Department of Drilling and Production
Agricolastraße 10
38678 Clausthal-Zellerfeld, Germany
Tel.: +49-5323-72-2239
Mail: info@tu-clausthal.de
<https://www.ite.tu-clausthal.de/en/>



Declaration:

I hereby confirm that I have prepared this master thesis independently by myself. All information taken from other sources and being reproduced in this thesis are clearly referenced.

.....

Date and Signature

Erklärung:

Hiermit versichere ich, dass ich die Arbeit selbständig verfasst und keine anderen als die angegebenen Quellen und Hilfsmittel benutzt habe und dass alle Stellen dieser Arbeit, die wörtlich oder sinngemäß aus anderen Quellen übernommen wurden, als solche kenntlich gemacht wurden und dass die Arbeit in gleicher oder ähnlicher Form noch keiner anderen Prüfungsstelle vorgelegt wurde.

Des Weiteren erkläre ich, dass ich mit der öffentlichen Bereitstellung meiner Abschlussarbeit in der Instituts-und/oder Universitätsbibliothek einverstanden/ nicht einverstanden bin.

.....

Datum und Unterschrift

Abstract

The Reykjanes Peninsula in Southern Iceland hosts the landward extension of the Mid-Atlantic-Ridge, where the North American and European plates drift away from each other. The Reykjanes geothermal field is a promising place to exploit within the framework of the Iceland Deep Drilling Project, which has already led to the drilling of the IDDP-1 well. The Reykjanes reservoir is supposed to contain supercritical fluids at approximately 5,000 m of depth. The interest in producing supercritical fluids stems from their energy content being about ten times higher than that of conventional dry steam geothermal systems. The magma-enhanced Reykjanes reservoir lies in a volcanic and tectonic active environment. The planned drilling of the IDDP-2 well is a challenging process and has to cope with very high temperature and pressure, and the intensely fractured subsurface. A thorough well design, including the selection of adequate downhole equipment can help minimize the likelihood of drilling and completion problems that could compromise the success of the entire project.

The goal of this thesis is twofold: to simulate the drilling process and possible load cases for the well completions and, to identify and discuss the associated hazards according to a risk assessment of the project. The relative motion of the North American and European plates continuously increases the local stress field, which poses the risk of a sudden release and subsequent occurrence of volcano-tectonic earthquakes at the drilling site. This could cause subsequent volcanism and/or the re-opening of fractures along which molten magma can flow upwards and, in the worst case, damage the well equipment and surface facilities. A simulation of the most dramatic scenario of circulation loss into the fractured formation has revealed a high potential of two failure modes. The drop of mud in the annulus can cause a burst, whereas a fully evacuated string collapses due to high external load from the cement column. The simulation of an unexpected influx of geofluids defines a critical situation for deeper casing sections. Thermal stress and cycling reduces the yield of the joints and connections making them more prone to fail. Temperature modelling has shown that the mud flow rate and inlet temperature significantly influence the bottomhole fluid temperatures.

A reliable well design defines the success of this project, which directly depends on a thorough modelling of bottomhole conditions, simulation of probable load cases and assessment of potential risks.

Kurzfassung

Die Halbinsel Reykjanes im Südwesten Islands liegt unmittelbar an der verlängerten Spreizungsachse des Mittelozeanischen Rückens, an dem die Nordamerikanische und die Europäische Platten auseinanderdriften. Das angrenzende Geothermiefeld ist ein prädestinierter Ort zur Erschließung einer Lagerstätte, welches in einer Tiefe von etwa 5,000 m überkritische Fluide ermöglicht zu fördern. Das IDDP-2 Bohrprojekt erfolgt im Rahmen des „Iceland Deep Drilling Project“, kurz IDDP, welches mit der IDDP-1 Bohrung bereits einen ersten Versuch unternahm. Das Interesse an überkritischen Fluiden rührt von deren um das Zehnfache erhöhten Energieanteil gegenüber herkömmlichen Trockendampf Geothermiesystemen. Die erwarteten Temperatur- und Druckbedingung im Bohrloch, von etwa 400 °C und 250 bar, erfordern eine sorgfältige Auswahl der Bohrmaterialien und Konstruktion des Bohrstranges, um mögliche Gefahrenpotentiale zu minimieren.

Der Rahmen dieser Masterarbeit verfolgt, Erstens, die Simulation des Bohrprozesses sowie mögliche Belastungszustände während des Bohrens und, Zweitens, die Identifizierung und Beschreibung der Gefahren im Rahmen einer Risikoanalyse. Die Relativbewegung der beiden tektonischen Platten beeinflusst das lokale Stressfeld und führt durch spontane Entladung der Spannungen zu regelmäßig auftretenden Erdbeben, die zur Beeinträchtigung des Bohrprozesses und zur Beschädigung von Bohranlagen und des Bohrstranges führen könnten. Die induzierte Reaktivierung von Störungen kann zum Aufstieg geschmolzenen Magmas führen, welcher fatale Schäden an abgeteufte Bohrungen hervorrufen kann. Der stark zerklüftete Untergrund kann hohe Bohrspülungsverluste zur Folge haben und zur Einbeulung oder einem Bruch der Verrohrung führen. Eine Belastung der Verrohrung im Falle einer vollständigen Evakuierung oder eines Absenkens der Bohrspülung im Ringraum zeigt in der Simulation mögliche technische Versagen. Die Simulation eines plötzlichen Zustromes von Untergrundwässern zeigt, dass die tieferliegenden Verrohrungen brechen könnten. Thermische Beanspruchungen, die durch extreme Temperaturwechsel entstehen, verringern die Plastizitätsbedingungen des Gestänges, welches damit anfälliger für technisches Versagen wird. Die Modellierung der Bohrlochtemperaturen während des Spülvorganges zeigt einen signifikanten Einflussfaktor durch die Fließrate und der Zuflusstemperatur der Bohrspülung.

Die Modellierung der Bohrlochbedingungen, Simulation wahrscheinlicher Belastungszustände und die Risikoanalyse erlauben eine zuverlässige Bohrstrangkonstruktion und sichern folglich den Erfolg des Projektes.

Acknowledgements

I offer my gratitude to my accompanying supervisors Prof. Dr. G. Falcone, Prof. Dr. C. Teodoriu and Prof. Dr. W. Blendinger, whose know-how and experience in geology, geothermal engineering and drilling have had a crucial impact on the success of this project. I appreciate the assistance, guidance and encouragement throughout the realization of this master thesis. The work atmosphere and meetings were always filled with creativity, professionalism and joy.

I have to deeply thank my family, parents and friends which were a very important pillar all along my master studies.

Table of Contents

ABSTRACT	4
KURZFASSUNG	5
ACKNOWLEDGEMENTS	6
LIST OF FIGURES	9
LIST OF TABLES	11
ABBREVIATIONS	12
NOMENCLATURE	12
1. INTRODUCTION	13
1.1 THE REYKJANES GEOTHERMAL FIELD	14
1.2 SUPERCRITICAL RESERVOIR.....	16
1.3. RISK ASSESSMENT	17
1.4. DRILLING SIMULATION AND TEMPERATURE MODELLING.....	18
2. METHODS	21
2.1. LITERATURE REVIEW AND DATA ACQUISITION	21
2.2. FIELD DEFINITION.....	22
2.3. INSTALLATION AND SLOT CONFIGURATION	23
2.4. WELLBORE DETAILS.....	24
2.5. GEOLOGY.....	25
2.6. TEMPERATURE AND PRESSURE PROFILES	26
2.7. DEFINITION OF ASSEMBLIES	29
2.8. DRILLING AND COMPLETION PROGRAM.....	31
2.9. TORQUE AND DRAG CALCULATION	34
2.10. HYDRAULICS CALCULATION.....	36
2.11. CASING ANALYSIS	37
2.12. CEMENTING ANALYSIS	42
2.13. RISK PARAMETER	44
3. RESULTS	45
3.1. TORQUE AND DRAG CALCULATION	45
3.2. HYDRAULICS CALCULATION.....	49
3.3. CASING ANALYSIS	55

3.4. CEMENTING ANALYSIS	60
3.5. RISK ANALYSIS.....	64
4. INTERPRETATION	66
4.1. DRILLING SIMULATION	66
4.2. THERMAL MODELLING	70
4.3. RISK ASSESSMENT	71
5. CONCLUSION AND OUTLOOK	74
6. REFERENCES.....	75
7. APPENDIX.....	78
7.1. APPENDIX A: TEMPERATURE AND PRESSURE PROFILES.....	78
7.2. APPENDIX B: INNOVARIG	81
7.3. APPENDIX C: FANN DIAL READING, PLASTIC VISCOSITY AND YIELD POINT OF OBM	81

List of Figures

FIGURE 1: BATHYMETRIC MAP OF THE ATLANTIC OCEAN WITH THE LOCATION OF ICELAND AND REYKJANES. THE REYKJANES RIDGE INTERSECTS ICELAND FROM SOUTH-WEST AND CAUSES ACTIVE ZONES OF RIFTING AND VOLCANISM ON THE REYKJANES PENINSULA (AFTER FRÍÐLEIFSSON ET AL., 2014A)	14
FIGURE 2: GEOLOGICAL MAP OF THE REYKJANES PENINSULA SHOWING MAINLY BASALT LAVA AND SCATTERED HYALOCLASTITE RIDGES. THE PRODUCTION WELLS AND THE PROSPECTIVE IDDP-2 ARE PRIMARILY LOCATED IN THE CENTER OF THE GEOTHERMAL FIELD. THE SOLID BLUE LINE GIVES THE APPROXIMATE POSITION OF THE LANDWARD EXTENSION OF THE MID-ATLANTIC-RIDGE, HERE REPRESENTED BY ITS SEGMENT THE REYKJANES RIDGE (AFTER FRÍÐLEIFSSON ET AL., 2014A)	15
FIGURE 3: PRESSURE-ENTHALPY DIAGRAM FOR PURE WATER WITH ISOTHERMS. LIQUID AND WATER ARE CO-EXISTENT WITHIN THE SHADED. A SUPERCRITICAL FLUID RIGHT ABOVE THE CRITICAL POINT OF PURE WATER (B) WILL SEPARATE INTO TWO PHASES, WATER AND STEAM, IF IT FLOWS UPWARDS (AFTER FRÍÐLEIFSSON ET AL., 2014B)	16
FIGURE 4: SCHEMATIC OF THE CIRCULATING FLUID SYSTEM IN A WELLBORE. (RAYMOND, 1969)	19
FIGURE 5: THE CORNERS OF THE POLYGON DEFINE THE FIELD BLOCK BOUNDARY. THE DRILLING TARGET AND SIMULATION SUBJECT IDDP-2 LIES IN BETWEEN SEVERAL WELLS, ALREADY DRILLED IN THE REYKJANES GEOTHERMAL FIELD.....	23
FIGURE 6: WELL DESIGN OF THE IDDP-2 (AFTER INAGSON ET AL., 2015).....	24
FIGURE 7: IDDP-2 LITHOLOGY LOG. THE NUMBERING ON THE RIGHT HAND SIDE INDICATES THE SELECTION OF FORMATION TOPS FOR THE SIMULATION (AFTER SCHERFF, 2016).....	25
FIGURE 8: PRESSURE PROFILES OF THE IDDP-2 WELL. THE PORE PRESSURE PROFILE IS ACCORDING TO DATA AFTER INAGSON ET AL. (2015). THE FRACTURE PRESSURE PROFILE WAS CALCULATED ON THE BASIS OF THE PENNEBAKER PREDICTION METHOD. THE OVERBURDEN PRESSURE WAS CALCULATED BY THE LITHOSTATIC PRESSURE EQUATION.....	27
FIGURE 9: LEFT: GRAPH SHOWING DIFFERENT TEMPERATURE PROFILES (AFTER INAGSON ET AL., 2015). THE CURVE IN RED DISPLAYS THE DERIVED IDDP-2 TEMPERATURE LOG OF THE TEMPERATURE MODEL IN SCHERFF (2016). THE PROFILES IN BLUE AND BLACK REFER TO THE LOGGED TEMPERATURE OF THE REYKJANES FIELD AND THE BOILING POINT WITH DEPTH CURVE, RESPECTIVELY (AFTER INAGSON ET AL., 2015). THE YELLOW RECTANGULAR HIGHLIGHTS THE TRIPLE JUNCTION WHERE ALL THREE PROFILES MEET. RIGHT: GRAPH SHOWING THE IMPORTED TEMPERATURE PROFILE IN SYSDRILL.	28
FIGURE 10: EXAMPLE OF THE DRILL STRING ASSEMBLY USED TO DRILL THE 17 ½" HOLE FOR THE ANCHOR CASING SECTION. THE VALUES ON THE RIGHT SIDE DEFINE THE NOMINAL OUTER DIAMETER OF EACH SINGLE STRING ELEMENT. THE BASIC DESIGN ORIGINATES FROM A TEMPLATE IN THE CATALOGUE IN SYSDRILL AND WAS THEN MODIFIED ACCORDING TO HOLMGEIRSSON ET AL., (2010), PALSSON ET AL (2014) AND THORHALLSON ET AL. (2014)	29
FIGURE 11: THE FLUID FORMULATION OF THE WATER-BASED MUD ACCORDING TO DATA AFTER INAGSON ET AL. (2015) AND PREDEFINED VALUES IN THE SYSDRILL FLUID CATALOGUE. THE RHEOLOGICAL PROPERTIES REFER TO DATA FROM RAVI ET AL. (2011)	32
FIGURE 12: THE FLUID FORMULATION IS ACCORDING TO PREDEFINED VALUES FOR AN OIL-BASED MUD IN SYSDRILL. THE RHEOLOGICAL PROPERTIES AND DENSITY OF THE MUD REFER TO DATA FROM IBEH ET AL. (2007) AND INAGSON ET AL. (2015)	32
FIGURE 13: ESTIMATED DRILLING PROGRESS CURVE FOR IDDP-2, INCLUDING TIME INTERVALS FOR CASING SETTING, CEMENTING, PREPARATION AND DOWNHOLE MEASUREMENTS (AFTER SAMORKA, 2014).....	34
FIGURE 14: EXAMPLE OF THE TORQUE AND DRAG EDITOR TAB FOR DRILLING THE 21" HOLE SECTION. UP: INPUT PARAMETERS FOR RUNNING THE SIMULATION UNDER NORMAL DRILLING CONDITIONS. DOWN: INPUT PARAMETERS FOR SIMULATING A DRILLING INCIDENT, E.G. STUCK PIPE UNDER ABNORMAL CONDITIONS. BOTH CASES WERE RUN TO CALCULATE THE SURFACE CONDITIONS USING THE SOFT STRING TYPE TO INCLUDE HYDRAULICS (DATA AFTER PALSSON ET AL, 2014 AND HOLMGEIRSSON ET AL., 2010).....	35
FIGURE 15: EXAMPLE OF THE INPUT TAB WITHIN THE HYDRAULICS CALCULATION EDITOR. THE CALCULATION IS BASED ON THE CONSTRUCTED DRILL STRING ASSEMBLY FOR DRILLING THE 21" INTERMEDIATE CASING SECTION. ADDITIONAL SUBOPTIONS, E.G. THERMAL EFFECTS, ARE AVAILABLE FOR THE PUMP PRESSURE CALCULATION.	37
FIGURE 16: SUMMARY OF DEFINED LOAD CASES AND RELATED DESIGN FACTORS FOR AXIAL TENSION AND COMPRESSION, BURST, COLLAPSE AND TRIAXIAL STRESS CRITERION AS SET DEFAULT IN THE SOFTWARE SYSDRILL.	38
FIGURE 17: BURST/ TENSION LOAD CASE WITH THE INITIAL SELECTION OF AXIAL LOADS AND THE DEFINITION OF THE EXTERNAL PRESSURE PROFILE.	39
FIGURE 18: SETUP OF THE COLLAPSE – FULLY EVACUATED LOAD CASE WITH THE SELECTION OF BENDING STRESS, THERMAL YIELD AND THE DEFINITION OF THE EXTERNAL PRESSURE PROFILE.....	40
FIGURE 19: SETTINGS FOR THE COLLAPSE – CIRCULATION LOSS WITH DROP OF MUD LEVEL LOAD CASE. THE EXTERNAL AND INTERNAL PRESSURE CONDITIONS ARE SHOWN IN COMPARISON.	40
FIGURE 20: SETTINGS OF THE BURST – INFLUX OF GEOFLUIDS LOAD CASE. THE INTERNAL PRESSURE CONDITION DEPENDS ON GAS PROPERTIES AND GEOMETRICAL VALUES.....	41
FIGURE 21: EXAMPLE OF A FLUID SCHEDULE FOR CEMENTING THE ANCHOR CASING SECTION. THE RHEOLOGICAL PROPERTIES OF THE CEMENT SLURRY, DISPLACED FLUID AND DRILLING MUD REFER TO DATA AFTER RAVI ET AL. (2011), IBEH ET AL. (2007) AND KELLINGRAY ET AL. (1991).....	42
FIGURE 22: PUMP SCHEDULE FOR CEMENTING THE ANNULUS OF THE ANCHOR CASING.	43
FIGURE 23: HIERARCHICAL CATEGORIZATION OF THE RISK ASSESSMENT. THE MAJOR RISK TYPES ARE RELATED TO SEVERAL HAZARDS	44
FIGURE 24: SUMMARY OF TORQUE AND DRAG CALCULATIONS, SHOWING A DETAILED LISTING OF DIFFERENT ASPECTS OF TENSION, TORQUE AND STRESS DURING DRILLING.	45

FIGURE 25: GRAPHS SHOWING THE TRUE TENSION (LEFT) AND SURFACE STRESSES (RIGHT) AS A FUNCTION OF DEPTH UNDER NORMAL CONDITIONS AND BASED ON THE STIFF STRING MODEL.....	46
FIGURE 26: GRAPH SHOWING THE SURFACE STRESS CONDITIONS FOR DRILLING THE PRODUCTION CASING SECTION AND CIRCULATION OF DRILLING FLUIDS AT A FLOW RATE OF 3,600 L·MIN ⁻¹	47
FIGURE 27: COLLAPSE AND BURST PRESSURE PROFILE OF DRILLING THE PRODUCTION LINER SECTION TO 5,000 M DEPTH.	48
FIGURE 28: GRAPH SHOWING THE EQUIVALENT MUD WEIGHT DURING DRILLING SUCCEEDS. THE EQUIVALENT STATIC AND CIRCULATING DENSITIES EXCEED THE FRACTURE GRADIENT ALONG THE INTERMEDIATE CASING SECTION.	49
FIGURE 29: TEMPERATURE PROFILES SHOWING THE STRING AND ANNULAR TEMPERATURE AFTER CIRCULATING FOR ONE HOUR. THE CONSTANT DENSITY TEMPERATURE PROFILES REPRESENT THE TEMPERATURE AT WHICH THE THERMAL EXPANSION EFFECT IS EQUAL TO THE COMPRESSIBILITY EFFECT.	50
FIGURE 30: EQUIVALENT MUD WEIGHT VERSUS BIT DEPTH DURING DRILLING OF THE ANCHOR CASING. THE GRADIENT OF THE EQUIVALENT CIRCULATING DENSITY INCREASES LESS THAN THE FRACTURE GRADIENT.	51
FIGURE 31: TEMPERATURE PROFILE FOR THE STRING AND ANNULUS AT A FLOW RATE OF 3,600 L·MIN ⁻¹	52
FIGURE 32: PRESSURE PROFILES FOR A TOTAL BIT FLOW AREA OF 1.66 CM ² (LEFT) AND 4 CM ² (RIGHT).	52
FIGURE 33: GRAPH SHOWING THE TEMPERATURE PROFILES FOR THE STRING AND ANNULUS IF CIRCULATING AT A MODERATE FLOW RATE OF 1,800 L·MIN ⁻¹	53
FIGURE 34: UP: DATABASE AND ADDITIONALLY CHECKED OPTIONS FOR THE SIMULATION. DOWN: SUMMARY OF THE SIMULATION RESULTS.	53
FIGURE 35: GRAPHS SHOWING THE EFFECT OF DIFFERENT FLOW RATE TO THE TEMPERATURE DISTRIBUTION ALONG THE HOLE SECTION. A FLOW RATE OF 1,800 L·MIN ⁻¹ (LEFT) GIVES A HIGHER TEMPERATURE THAN CIRCULATING THE FLUIDS AT A STATIC RATE OF 3,600 L·MIN ⁻¹ (RIGHT).	54
FIGURE 36: GRAPHS SHOWING THE STRING PRESSURES AT A HIGH (LEFT) AND LOW (RIGHT) FLOW RATE. A MINIMUM OF 8 CM ² IS REQUIRED TO KEEP THE STRING PRESSURE BELOW THE FRACTURE PRESSURE AT A HIGH FLOW RATE. AT A LOW FLOW RATE, A TOTAL FLOW AREA OF 1.8 CM ² IS ADEQUATE.	54
FIGURE 37: WORST CASE SUMMARY OF ALL SIMULATED COLLAPSE LOAD CURVES. THE COUPLING YIELD REFERS TO THE COLLAPSE RESISTANCE.	55
FIGURE 38: CURVES SUMMARIZING THE SIMULATED SAFETY FACTOR FOR ALL POSSIBLE FAILURE MODES, EXCEPT FOR AXIAL COMPRESSION OR TENSION.	56
FIGURE 39: INTERNAL PRESSURE PROFILES OF THE BURST – 5 M ³ KICK LOAD CASE (LEFT) AND THE SIMULATION OF A KICK WITH A VOLUME OF 50 M ³ (RIGHT).....	56
FIGURE 40: ELLIPSE OF PLASTICITY SHOWING THE COMBINED LOAD AND THE FAILURE MODE LIMITS OF THE 5 M ³ KICK LOAD CASE.	57
FIGURE 41: PASS AND FAIL SUMMARY OF LOAD CASE CALCULATIONS.	57
FIGURE 42: RELATIONSHIP BETWEEN THE DESIGN FACTORS AND THE CALCULATED SAFETY FACTORS FOR AXIAL, BURST, COLLAPSE AND TRIAXIAL ANALYSIS CATEGORIES. THE FACTORS INCLUDE THE SIMULATION RESULTS OF ALL LOAD CASES. THE COLLAPSE DESIGN FACTOR CURVE IS OVERLAPPED BY THE TRIAXIAL DESIGN FACTOR	58
FIGURE 43: GRAPH SHOWING THE EXTERNAL PRESSURE PROFILE IN CASE OF A FULLY EVACUATED CASING STRING. AN ADDITIONAL 70 BAR OF EXTERNAL PRESSURE WOULD EXCEED THE DE-RATED PIPE YIELD LIMIT.....	58
FIGURE 44: ELLIPSE OF PLASTICITY SHOWS THE COLLAPSE AND TRIAXIAL FAILURE MODES FOR A FULLY EVACUATED PRODUCTION LINER.....	59
FIGURE 45: INTERNAL PRESSURE PROFILE ILLUSTRATING THE BURST FAILURE MODE AFTER A CIRCULATION LOSS AND DROP OF THE MUD LEVEL IN THE ANNULUS.	59
FIGURE 46: UP: PUMP SCHEDULE FOR CEMENTING THE INTERMEDIATE CASING SECTION FROM CASING SHOE TO SURFACE. DOWN: FLUID SCHEDULE INCLUDING THE DISPLACED FLUID, CEMENT SLURRY AND THE DRILLING FLUID TO BE PUMPED AT LEAST.	60
FIGURE 47: CHART DISPLAYING THE PLANNED AND ACTUAL FLOW RATE OF THE FREE FALL CALCULATION.....	60
FIGURE 48: CHART SHOWING THE SURFACE PRESSURE AND ANNULAR PRESSURE LOSS DURING CEMENTING OF THE INTERMEDIATE CASING AND BY THE USE OF THE FREE FALL CALCULATION. THE BLACK VERTICAL LINE INDICATES THE ENTRY OF CEMENT INTO THE ANNULUS.	61
FIGURE 49: CHART SHOWING THE SURFACE PRESSURE AND THE ANNULAR PRESSURE LOSS DURING CEMENTING OF THE INTERMEDIATE CASING AND BY THE USE OF THE FREE FALL CALCULATION. THE BLACK VERTICAL LINE INDICATES THE ENTRY OF CEMENT INTO THE ANNULUS.	61
FIGURE 50: FLUID SCHEMATIC OF THE BOREHOLE AND TOP OF THE CEMENT SLURRY IN THE ANNULUS.....	62
FIGURE 51: GRADIENT CURVES OF THE PORE PRESSURE, FRACTURE PRESSURE AND THE PRESSURE EXERTED BY THE EQUIVALENT CIRCULATING DENSITY. THE GRAPH SHOWS THE SIMULATED DEVELOPMENT OF THE EQUIVALENT MUD WEIGHT ALONG THE ENTIRE BOREHOLE.....	62
FIGURE 52: GRAPH SHOWING THE DEVELOPMENT OF THE ECD GRADIENT AT THE BOTTOM OF THE ANCHOR CASING SECTION. THE BLACK VERTICAL LINE INDICATES THE BEGINNING OF FLUID DISPLACEMENT IN THE ANNULUS BY THE CEMENT SLURRY.	63
FIGURE 53: GRAPH DISPLAYING THE GRADIENT PROFILES FOR THE PORE PRESSURE, FRACTURE PRESSURE AND THE EQUIVALENT CIRCULATING DENSITY PRESSURE	63
FIGURE 54: PENNEBAKER CORRELATION CURVE FOR THE EFFECTIVE STRESS RATIO (BOURGOYNE ET AL., 1986).	78
FIGURE 55: TECHNICAL DATA SHEET OF THE INNOVARIG FROM THE GERMAN RESEARCH CENTRE FOR GEOSCIENCES GFZ (WOHLGEMUTH ET AL., 2007).	81

List of Tables

TABLE 1: CLASSIFICATION OF A HAZARD, ACCORDING TO ITS PROBABILITY, SEVERITY AND IMPACT ON THE DRILLING PROCESS.....	17
TABLE 2: LISTING OF DATA SOURCES AND THE DATABASE BEING EXTRACTED FOR THE SIMULATION AND RISK ASSESSMENT.	21
TABLE 3: LISTING OF THE POSITION OF THE FIELD REFERENCE POINT AND THE DRILL SITES WITH THEIR COORDINATE AND TARGET DEPTH (DATA AFTER THE ICELAND ENERGY PORTAL BY THE NATIONAL ENERGY AUTHORITY ORKUSTOFNUN NEA-OS (NEA-OS, 2012).	22
TABLE 4: OVERVIEW OF THE BOREHOLE DIAMETER AND THE INSTALLED CASING SECTIONS, THEIR RESPECTIVE NOMINAL OUTER DIAMETER AND CASING SHOE DEPTH (DATA AFTER INAGSON ET AL., 2015).....	24
TABLE 5: LIST OF FORMATION TOPS, DYKE AND THEIR DEPTH AS DEFINED IN SYSDRILL.....	25
TABLE 6: ITEMIZED LIST OF EACH DRILL STRING ASSEMBLY AS DERIVED BY A COMBINATION OF DATA AND INFORMATION ACCORDING TO THE SYSDRILL CATALOGUE AND DATA AFTER HOLMGREISSON ET AL., (2010), PALSSON ET AL (2014) AND THORHALLSON ET AL. (2014).	30
TABLE 7: DETAILED LISTING OF EACH CASING STRING ASSEMBLY, INCLUDING THE CASING COUPLINGS AND JOINTS IN API OILFIELD UNITS (DATA AFTER INAGSON ET AL., 2015 AND ACCORDING TO THE SYSDRILL CATALOGUE).	30
TABLE 8: TECHNICAL DATA OF THE INNOVARIG AS USED FOR AN INPUT IN SYSDRILL (DATA AFTER WOHLGEMUTH ET AL. (2007), WWW.ICDP-ONLINE.ORG AND THE SYSDRILL MUD PUMP CATALOGUE).....	33
TABLE 9: SUMMARY OF THE INPUT COEFFICIENTS AND VALUES REQUIRED TO MODEL THE THERMAL EFFECT ON CIRCULATING DRILLING FLUIDS (DATA AFTER KÅRSTAD & AADNØY (1998) AND DEFAULT PARAMETERS IN SYSDRILL).....	36
TABLE 10: DEFINITION OF THE KEY FLUID DENSITIES WITHIN THE CASING ANALYSIS EDITOR (DATA AFTER INAGSON ET AL., 2015 AND DEFAULT SETTINGS IN THE CASING AND TUBING ANALYSIS TAB IN SYSDRILL) ...	38
TABLE 11: TABLE SHOWING THE CALCULATED VOLUMES OF THE DISPLACED FLUID, DRILLING FLUID AND CEMENT SLURRY TO CEMENT THE CASING STRING SECTIONS.	43
TABLE 12: COMPARISON OF THE HYDRAULIC EFFECT OF TWO DIFFERENT FLUIDS ON THE HOOK LOAD, SURFACE TORQUE AND THE VON MISES STRESS.....	46
TABLE 13: CALCULATION RESULTS OF THE 17 ½" AND 8 ½" HOLE SECTIONS UNDER NORMAL CONDITIONS.	48
TABLE 14: LOAD CASE SUMMARY FOR THE INTERMEDIATE CASING SECTION. THE VALUES AND WORDS HIGHLIGHTED IN RED SIGNAL CONSIDERABLE RISKS OF FAILURE.	55
TABLE 15: SUMMARY OF THE SIMULATED FAILURE MODES FOR DIFFERENT LOAD CASES AND CASING LEVELS. THE WEAK POINTS INDICATE THE AREA OF IMPROVEMENTS WITH REGARD TO THE PROPOSED WELL DESIGN IN INAGSON ET AL. (2015). THE SUGGESTION OF IMPROVEMENTS ARE GIVEN AS MINIMUM UPGRADE MEASURES	69
TABLE 16: RISK ASSESSMENT SHEET FOR THE IDDP-2 WELL AT REYKJANES, SOUTHERN ICELAND.....	73
TABLE 17: TEMPERATURE DATABASE ACCORDING TO DATA AFTER SCHERFF (2016) AND INAGSON ET AL. (2015). THE GEOTHERMAL GRADIENTS HAVE BEEN AUTOMATICALLY CALCULATED BY THE SOFTWARE SYSDRILL.	79
TABLE 18: PRESSURE DATABASE FOR THE IDDP-2 WELL. THE PORE PRESSURES ARE ACCORDING TO DATA AFTER INAGSON ET AL. (2015). THE FRACTURE PRESSURE IS BASED ON THE PREDICTION METHOD ACCORDING TO PENNEBAKER. THE OVERBURDEN PRESSURE WAS CALCULATED.	80
TABLE 19: LISTING OF RHEOLOGICAL PROPERTIES OF THE OIL-BASED DRILLING FLUID AFTER DATA FROM IBEH ET AL. (2008). THE VALUES REFER TO THE TEST SCHEDULE UNDER A CONSTANT PRESSURE AND VARIABLE TEMPERATURES.	81
TABLE 20: LISTING OF THE RHEOLOGICAL PROPERTIES OF THE OIL-BASED FLUID AFTER DATA FROM IBEH ET AL. (2008). THE VALUES REFER TO THE TEST SCHEDULE UNDER A CONSTANT TEMPERATURE AND VARIABLE PRESSURES.	81

Abbreviations

API	American Petroleum Institute
BHA	Bottomhole Assembly
DF	Design Factor
ECD	Equivalent Circulating Density
HT	High Temperature
ÍS-REY/IDDP-2	Ísland-Reykjanes/Iceland Deep Drilling Project - 2
OBM	Oil-Based Mud
PV	Plastic Viscosity
RPM	Revolutions per Minute
SF	Safety Factor
TVD	True Vertical Depth
UTM	Universal Transverse Mercator
WBM	Water-Based Mud
YP	Yield Point

Nomenclature

"	Inch	Length
°C	Degree Celsius (Centigrade)	Temperature
°C·100m ⁻¹	Degree Celsius per Hundred Meter	Geothermal gradient
°F	Fahrenheit	Temperature
kg·m ⁻³	Kilogram per cubic meter	Density
l·min ⁻¹	Liter per Minute	Flow Rate
lb·ft ⁻¹	Pound per foot	Weight
lbm	Pound-mass	Mass
m·s ⁻²	Meter per second squared	Acceleration
m ³	Cubic Meter	Volume
m ³ ·s ⁻¹	Cubic meter per second	Volumetric flow rate
mm·a ⁻¹	Millimeter per year	Velocity
mPa·s ⁻¹	Mill pascal per second	Viscosity
MW _e	Megawatt (electrical)	Power
N·m	Newton meter	Torque
Pa	Pascal	Pressure
Psi _g	Pounds per inch squared	Pressure
W·m ⁻² ·°C ⁻¹	Watt per meter squared per degree Celsius	Heat transfer coefficient
J·kg ⁻¹ ·°C ⁻¹	Joule per kilogram per degree Celsius	Specific heat capacity
W·cm ⁻¹ ·°C ⁻¹	Watt per centimeter per degree Celsius	Thermal conductivity

1. Introduction

By the turn of the 20th century, a delegation from Iceland introduced, at the World Geothermal Congress in Japan, a concept for the exploitation of a geothermal resource at supercritical conditions (FRÍÐLEIFSSON et al., 2014b). A reservoir whose fluids have exceeded its critical point defines the supercritical condition and hosts so called supercritical fluids. The idea of the concept pursues an ambitious but simple goal of enlarging the accessible part of a geothermal resource base to the inaccessible part in order to significantly increase useful and economic exploitation of geothermal energy by an order of magnitude of energy output. A federation referred to as “Deep Vision” of three Icelandic’s leading energy companies, namely Hitaveita Suðurnesja Orka, Landsvirkjun, Orkuveita Reykjavíkur and the National Energy Authority Orkustofnun initially established the Iceland Deep Drilling Project (IDDP). Experts from the International Scientific Continental Drilling Program, the U.S. National Science Foundation and a Science Applications Group of Advisors affiliated the consortium as add-on science partners. Further funding and engineering assistance are backed by the global leader in lightweight metals technology Alcoa and the Norwegian enterprise Statoil since 2007 (FRÍÐLEIFSSON et al., 2014b).

The first attempt to achieve the goal and produce supercritical fluids was realized with the IDDP-1 at Krafla in Northern Iceland. The drill site is characterized by a volcanic caldera and seemed to be feasible to host a supercritical reservoir. Drilling of this well succeeded to a depth of 2,104 m when unexpected rhyolite magma of 900 °C was penetrated and led to well integrity problems and the final abandonment (PALSSON et al., 2014). A second attempt is going to be realized within the Reykjanes geothermal field on the Reykjanes Peninsula in Southern Iceland (FRÍÐLEIFSSON et al., 2014a). The IDDP-2 well is supposed to approach supercritical fluids in a depth of 5,000 m and at bottomhole conditions of 400 °C and 250 bar (INAGSON et al., 2014). The drilling environment is similar to the first drill site and therefore prognosticates several potential troubles for the drilling process as well as for the downhole equipment. The scope of this master thesis is to evaluate potential failure modes during drilling and to identify the limitations of the downhole equipment under expected high pressure and temperature conditions. The simulation in Sysdrill will help to study the numerous problems and casing load cases during drilling of a geothermal well under extreme conditions. The thesis will also touch the effect of temperature on the downhole equipment and the influence of circulating fluids on the temperature profile along the borehole. A comprehensive simulation can help to prevent similar incidents as have been encountered during drilling of IDDP-1. The assessment of risks is an essential method to identify hazards and to prioritize prevention measures.

1.1 The Reykjanes Geothermal Field

The Reykjanes geothermal field is situated on the Reykjanes Peninsula, south-west of Iceland. The volcanic island is located close to the Arctic Circle between Greenland to the west and Scandinavia to the east (Fig. 1). The landmass of Iceland is divided into the central mountainous Highland and the marginal Lowlands with a flat terrain of the tundra, a typical characteristic for the Reykjanes Peninsula. The geothermal field is about 55 km south-west of Reykjavik and almost entirely surrounded by the Atlantic Ocean (Fig. 2). To date, 12 production wells were

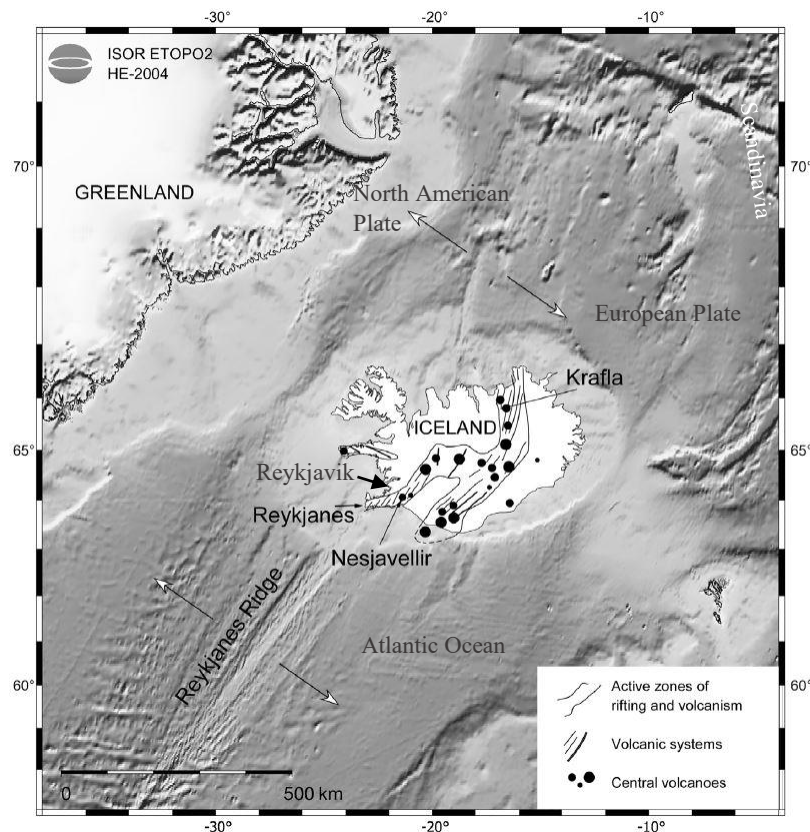


Figure 1: Bathymetric map of the Atlantic Ocean with the location of Iceland and Reykjanes. The Reykjanes Ridge intersects Iceland from south-west and causes active zones of rifting and volcanism on the Reykjanes Peninsula (After FRÍÐLEIFSSON et al., 2014a).

crosses the Atlantic Ocean from south to north. Hot magma erupts along the ocean ridge, forms new ocean crust and from time to time a subaerial volcanic island, such as Iceland (ELDERS & FRÍÐLEIFSSON, 2015).

Yet, active spreading causes extensive volcanism and periodic earthquakes on the Reykjanes Peninsula and central Iceland, in general. These volcanic and tectonic events have created a fissure swarm and a veined reservoir below the hot temperature area. The so called sheeted-dyke complex is a system of fractures, intrusions and faults, which serves as a heat supplier for the geothermal reservoir. The Reykjanes field is covered with postglacial basalt lava flows and hyaloclastite ridges, formed during the last glaciation of Iceland, the Weichselian Ice Age from 120,000 to 10,000 years ago (BISCHOF, 2000; Fig. 2). The upper 1,000 m of the subsurface is

drilled and operate the 100 MWe Reykjanes power plant with geothermal steam and brine (Fig. 2). A spreading axis, just beneath the geothermal field, separates the North American and European lithospheric plate at a spreading rate of $20 \text{ mm} \cdot \text{a}^{-1}$ (EIRIKSSON et al., 1994). The rifting axis constitutes the landward extension of the submarine Reykjanes Ridge, which enters the Reykjanes Peninsula at the southwestern tip. The Reykjanes Ridge represents a segment of the Mid-Atlantic-Ridge that

characterized by the deposition of marine sediments, hyaloclastites and pillow basalt/-breccia from stadial and interstadial cycles during the Ice Age. In greater depth, the sheeted-dyke complex becomes dominant and feeder dykes have delivered magma from a deep source which then has created a vast amount of thick basalt lava sheets, interbedded with widespread pillow basalt/-breccia (SCHERFF, 2016). The Reykjanes geothermal field has similar characteristics to submarine hydrothermal fields, known as Black Smoker. The tectonic and geological setting, plus the fluid chemistry and reservoir conditions make this geothermal system an onshore analogy of a Black Smoker and is therefore of high interest for the scientific community (ELDERS & FRÍÐLEIFSSON, 2015).

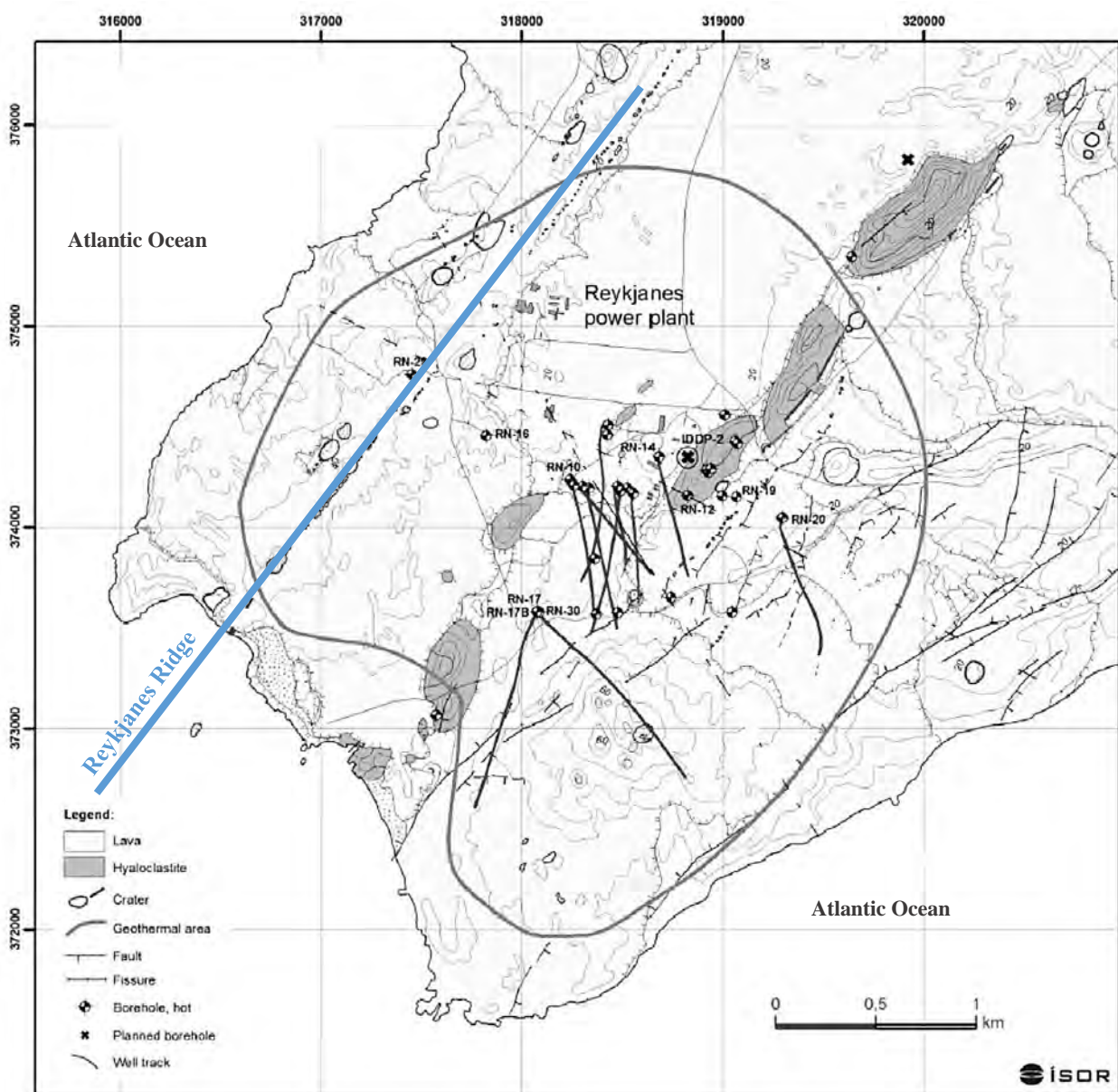


Figure 2: Geological map of the Reykjanes Peninsula showing mainly basalt lava and scattered hyaloclastite ridges. The production wells and the prospective IDDP-2 are primarily located in the center of the geothermal field. The solid blue line gives the approximate position of the landward extension of the Mid-Atlantic-Ridge, here represented by its segment the Reykjanes Ridge (After FRÍÐLEIFSSON et al., 2014a).

1.2 Supercritical Reservoir

The Iceland Deep Drilling consortium plans to drill a 5,000 m deep well into a reservoir of extreme temperature and pressure conditions. At a depth of 5,000 m, the expected temperature and pressure can be as high as 400 °C and 250 bar (INAGSON et al., 2015). These reservoir conditions are beyond the critical point of pure water at ~374 °C and ~221 bar (FRÍÐLEIFSSON et al., 2014b). The Reykjanes reservoir fluids are known to be saline and of similar composition like seawater. Hence, the critical point is shifted towards higher values of ~407 °C and ~298 bar for seawater. Although, the salinity of the reservoir fluid below 3,000 m was not sampled yet, the temperature and pressure conditions down to 5,000 m were extrapolated on the basis of the boiling point with depth curve of seawater with 3.5 % sodium chloride. The region above the critical point is defined as the supercritical state of the fluid, where the liquid and steam phase is indistinctive and only a single phase exists, the so called supercritical fluid. The high temperatures favor the solubility of aggressive gases, like hydrogen, hydrogen sulfide and carbon dioxide, but also the enrichment of metals like iron, zinc and copper (FRÍÐLEIFSSON et al., 2014b). The idea of the Iceland Deep Drilling Project is to produce supercritical fluids in such a way that superheated steam of the same enthalpy will flow to the surface of the well. Hereby, the enthalpy is defined as the sum of the internal energy plus the product of the pressure of the gas in the

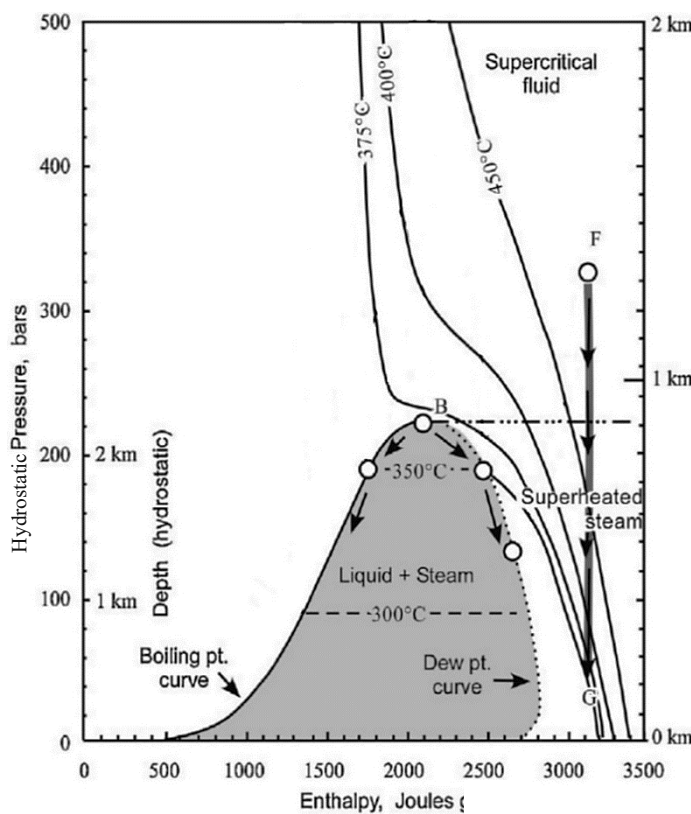


Figure 3: Pressure-enthalpy diagram for pure water with isotherms. Liquid and water are co-existent within the shaded. A supercritical fluid right above the critical point of pure water (B) will separate into two phases, water and steam, if it flows upwards (After FRÍÐLEIFSSON et al., 2014b).

system and its volume. The pathway F-G in Fig. 3 visualizes the aimed scenario. Modelling of the power output of a supercritical fluid has shown that, at a flow rate of $0.67 \text{ m}^3 \cdot \text{s}^{-1}$, the production well can yield about 50 MW_e of electrical energy. This is almost ten times higher than a conventional geothermal well in Iceland, producing from 2,000 m depth at about 235 °C and 30 bar (ELDERS & FRÍÐLEIFSSON, 2015). The analysis of the fluid composition below 3,000 m is of high interest to attain an accurate prediction for the depth of supercritical conditions. A more saline fluid than expected increases the critical point and therefore the depth in order to produce supercritical fluids (HEFU, 2000).

1.3. Risk Assessment

This work will cover the assessment of risks with regard to the project of drilling the well IDDP-2 into a fractured geothermal reservoir. From an engineering point of view, risk is defined as the probability of an accident times the losses per accident. An accidental event defines a significant change from a normal situation that may cause one or more unwanted consequences. The happening of an accident is driven by the exposure towards one or more hazards.

In order to assess the individual risks of the project, a detailed analysis of potential hazards must be done. The identification of hazards is necessary to evaluate the likelihood of technical, environmental and operational risks. Chapter 2.13 describes each single hazard of a defined risk category. Each hazard, which may contribute to a potential risk, will be assigned with a factor that describes the probability, severity and impact on the success of the project (Table 1). The probability of a hazard is expressed between A (frequent) and D (improbable). The classification of the severity goes from 1 to 4, out of which 1 implies a catastrophic and 4 a negligible hazard. Each hazard will have an impact on the achievement of the project, which is assigned a factor between I and III, respectively defined as a low and high impact.

A sophisticated risk assessment of a project refers to the analysis of a sufficient database. The risk assessment of the IDDP-2 project is based on, firstly, the outcome of simulations in Sysdrill and secondly the data and information released in publications dealing with this project. The fact that the simulations mainly refer to data extracted from these publications, show the limitation of the risk assessment. The main influence on the simulation results originate from unknown downhole conditions, which have a significant effect on the mud property or the choice of the cement slurry. Nevertheless, the here presented risk assessment and evaluation is an approach to point out some dangerous parameter, concerning high temperature and high pressure geothermal reservoirs, but also to indicate areas of improvement for similar projects in future.

Table 1: Classification of a hazard, according to its probability, severity and impact on the drilling process.

Probability	Severity	Impact
A – Frequent	1 – Catastrophic	I – High
B – Probable	2 – Critical	II – Moderate
C – Occasional	3 – Marginal	III – Low
D – Improbable	4 – Negligible	

1.4. Drilling Simulation and Temperature Modelling

The concept of drilling a 5,000 m or even deeper well into a reservoir that probably hosts fluids at a supercritical state is a dangerous operation. The drilling equipment is exposed to extreme downhole conditions, including high temperature, high pressure, aggressive gases/fluids and increased in-situ stresses around the borehole. It is of high interest to investigate possible areas of operational, constructional and technical constraints. The drilling simulation aims to survey problems that may arise from drilling at existing downhole conditions.

The software Sysdrill® 10 by Paradigm® is an advanced well planning and drilling engineering application, which was used for the drilling simulation of the IDDP-2 well. The software enables to apply the following calculations and functions, as stated in the Sysdrill manual and the integrated help desk:

- * Well Planning
 - Well path definition and profiling
 - Assembly builder
- * Data Import
 - Temperature and pressure profiles
 - Geology
- * Torque & Drag Analysis
 - Setup of drilling conditions and operation modes
 - Hydraulic effects
- * Hydraulics Calculation
 - Calculation of pump pressure and flow rate
 - Determination of equivalent circulating density
 - Modelling of cuttings transport and bottomhole cleaning
 - Temperature modelling
- * Cementing Analysis
 - Free fall calculation
 - Setup of pumping schedules
- * Casing Analysis
 - Definition of complex load cases
 - Specification of design criteria for the pipe body and connections and every load type

These software features enable to verify whether the proposed IDDP-2 well design in INAGSON et al. (2015) is reliable or requires modifications.

A thorough investigation will be done on the drill string and bit performance, the casing load modes and the temperature distribution during the circulation of the drilling fluid.

The circulation of drilling mud down the drill pipe, through the bit and up the annulus back to the surface affects the temperature profile and distribution around the borehole. A schematic of the circulating fluid system is shown in Fig. 4. The system is comprised of the drill string with a defined radius, r_D , and the borehole with the drilled radius, r_B . In phase 1, the fluid enters the drill pipe with its initial temperature, T_0 ($Z = 0$, $t = 0$), and starts to flow downwards. The string temperature, T_D (Z , t), is then a result of heat convection down the pipe and heat exchange between the pipe and the annulus. At the bottom of the pipe begins phase 2 with the outflow of the fluid through the bit and the inflow into the annulus. At this point, the outflow and inflow temperature assume the same, thus, $T_{out}(Z, t) = T_{in}(Z, t)$. Thus, the reference temperature for the annulus is defined by the string temperature at the bottom of the string or drill bit. The third phase starts with the flow up the annulus and to the surface. The heat convection inside the annulus, the heat exchange between the formation, the flowing fluid in the annulus and the pipe defines the annulus temperature T_A (Z , t). Furthermore, thermal modelling includes appropriate values for the heat transfer coefficient of the borehole, h_f and the annulus, U (Fig. 4; Table 9).

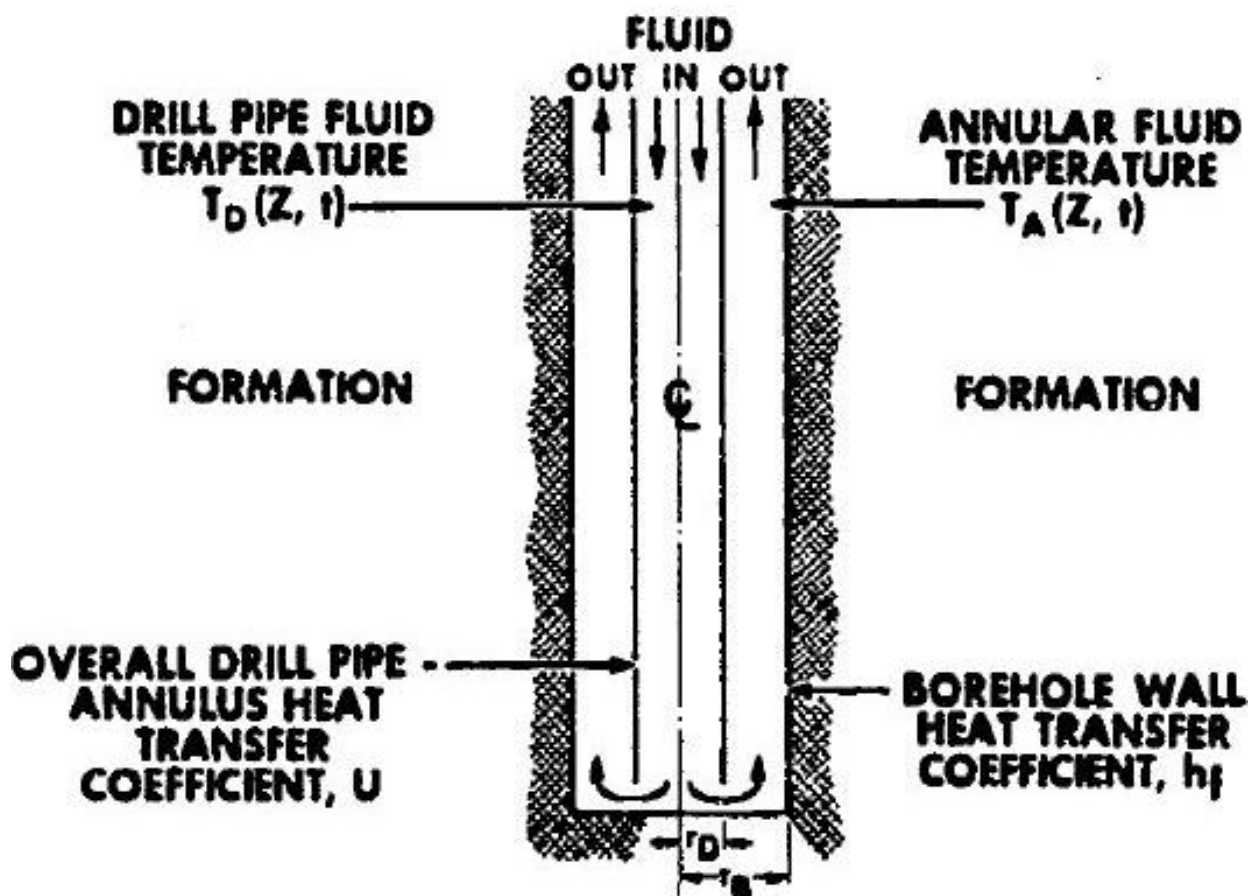


Figure 4: Schematic of the circulating fluid system in a wellbore. (RAYMOND, 1969).

The modelling of thermal effects in Sysdrill, additionally, requires the thermal conductivity, λ_f , and specific heat capacity, c_f , of the formation. The thermal conductivity of volcanic formation in Iceland is almost negligible and therefore assigned a little value (Table 9).

The heat transfer between the formation and the fluids, flowing up the annulus, is exposed to the changing geothermal gradients of the Reykjanes system. The temperature profiles from FRÍÐLEIFSSON (2011) as well as the temperature modelling in SCHERFF (2016) have shown that the upper 1,000 m of the field is characterized by a conductive gradient. The convective geothermal gradient becomes dominating down to a depth of 2,500 m, but shows again a trend back to the conductive gradient profile (FRÍÐLEIFSSON et al., 2014a).

The temperature modelling is based on the following assumptions (After RAYMOND, 1969 & YAN et al., 2014):

1. The heat transfer coefficients, the thermal conductivity and heat capacity of the formation are independent of depth and time.
2. Heat transfer by axial conduction is negligible
3. A radial geothermal gradient is non-existent (steady-state condition)
4. The properties of the fluids, such as heat capacity, thermal conductivity and density, do not show a significant change with temperature
5. Heating of the fluid by viscous dissipation is negligible. The generation of heat due to motion of the fluid is not considered.

The circulation of drilling fluids modifies the temperature profile inside the borehole and the drill string. This influences the local stress field and can cause severe borehole instability (YAN et al., 2013). The thermal effect of mud circulation during drilling was analyzed with the help of changing initial parameters, such as flow rate, circulating time and mud-in temperature. The most affecting parameters on the temperature in the borehole will be analyzed in Chapter 3.2 and further discussed in Chapter 4.2.

According to Paradigm, the temperature modelling relies on a steady-state calculation under consideration of transient effect using a finite difference model. A steady state condition assumes that the heat flux in a radial direction is constant. The implementation of transient effects relate to temperature changes as a function of the circulation time. In finite difference model the wellbore is subdivided into a mesh of nodes and small regions or grid cells.

2. Methods

2.1. Literature Review and Data Acquisition

The integrated well design analysis requires a sufficient database in order to conduct the different calculations regarding torque & drag, hydraulics, cementing, casing and drill string assemblies. Most of the well specific data and information were extracted from online accessible academic papers, reports or presentations which deal with the Iceland Deep Drilling Project in general or the well IDDP-2 in particular. The publication of proceedings from the World Geothermal Congress of 2015 provides a comprehensive coverage of different research subjects regarding IDDP-2, such as fluid chemistry scenarios, structural casing analysis or expected downhole conditions. However, these proceedings lack detailed information about the drilling rig, mud pump system and drilling fluid properties. The additional technical specifications were directly taken from released product information sheets or online databases. The lithological information, for instance formation tops, was retrieved from the generated 3-D facies model of the Reykjanes field (SCHERFF, 2016).

In case of no acquirable data, technical values were assumed and approximated according to engineering judgement. The sources of acquisition and retrieved data and information are summarized in Table 2.

Table 2: Listing of data sources and the database being extracted for the simulation and risk assessment.

Source of Data	Database
IDDP webpage www.iddp.is	Reports and publications Project chronicle and archives Feasibility studies Miscellaneous
ResearchGate, ScienceDirect, OnePetro and Google Scholar	Research articles about IDDP and related subjects
Google Earth/ Maps	Coordinates
Google Search	Miscellaneous information Further reading

2.2. Field Definition

First of all, the new field ÍS-REY/IDDP-2 was created and assigned a field reference point within the World Geodetic System WGS 84 coordinate reference system and the 27N UTM zone. The Reykjanes lighthouse, situated about 1,000 m south-west to the IDDP-2 drill site, was chosen as the field reference point. Next was to define the boundary of the field to be investigated as well as the numerous well sites within the field. The coordinates of the field boundary and wells are listed in Table 3 and additionally shown in Fig. 5. The well specific coordinates and depth were extracted from the Iceland Energy Portal, which is operated by the National Energy Authority Orkustofnun NEA-OS (NEA-OS, 2012). The coordinates of the portal are referenced to the local ISN93 coordinate system and were converted to the UTM system online (HOFER, T., 2015).

Table 3: Listing of the position of the field reference point and the drill sites with their coordinate and target depth (Data after the Iceland Energy Portal by the National Energy Authority Orkustofnun NEA-OS (NEA-OS, 2012).

Element	UTM Northing (m)	UTM Easting (m)	
Field Reference	7077588.64	416101.05	
Field Boundary #1	7078895.00	416650.00	
#2	7078355.00	416650.00	
#3	7078355.00	417758.00	
#4	7078895.00	417758.00	
Well Site	UTM Northing (m)	UTM Easting (m)	True Vertical Depth (m)
IDDP-2	7078643.54	417238.59	5,000
REY-08	7078741.24	417497.76	1,754
REY-09	7078588.49	417357.02	1,445
REY-10	7078532.23	416675.03	2,054
REY-11	7078502.59	416960.04	2,238
REY-12	7078470.08	417254.94	2,506
REY-13	7078811.55	416856.79	831
REY-14	7078662.74	417107.91	2,331
REY-15	7078884.15	417426.07	2,507
REY-18	7078747.00	417495.00	1,815
REY-19	7078477.37	417504.09	2,234
REY-20	7078380.07	417734.22	2,120
REY-22	7078474.00	416992.03	1,680

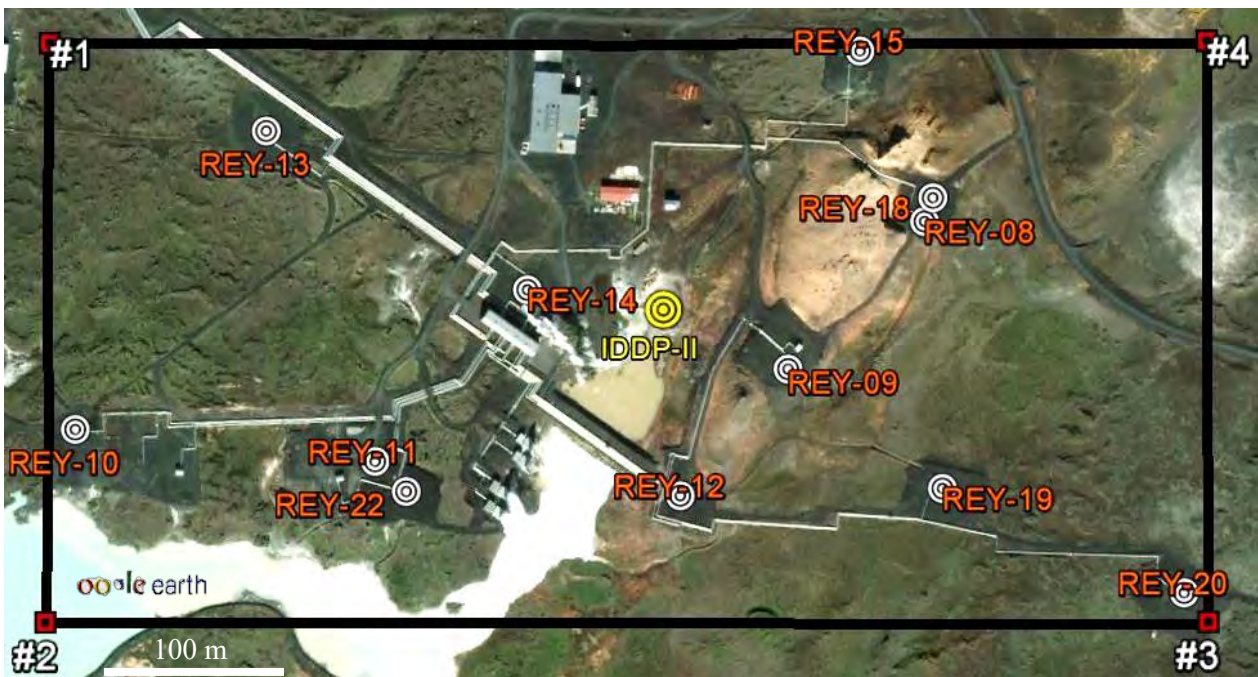


Figure 5: The corners of the polygon define the field block boundary. The drilling target and simulation subject IDDP-2 lies in between several wells, already drilled in the Reykjanes geothermal field.

2.3. Installation and Slot Configuration

A basic requirement for further slot configuration and wellbore description is the definition of the local installation. The information entered is basically the position of IDDP-2 within the defined ÍS-REY/IDDP-2 local grid as already stated in the above Table 3. Furthermore, the vertical datum of the installation of 20 m above the mean sea level was defined. As the coordinate system references grid north, a convergence of 1.51° west to true north is indicated at the installation location by the software. Based on the International Geomagnetic Reference Field model, magnetic north is 14.65° west of true north according to March, 2nd.

Due to a lack of information about the vertical datum it was assumed that both, the slot and rig, correlate with the installation elevation of 20 m above mean sea level. According to this, the temperature and pressure data are referenced to the ground level, respectively the elevation above mean sea level.

2.4. Wellbore Details

As a next step, the wellpath of IDDP-2 was specified with further details. The type of wellbore was set to re-entry since the IDDP consortium was offered to deepen a 2,500 m deep production well and identify the hole as IDDP-2. However, this simulation covers the entire drilling process of a new well in accordance to the proposed well design (INAGSON et al., 2015). The wellpath was generated from top to bottom as a straight borehole with a true vertical depth of 5,000 m. Alongside this wellpath, the proposed hole and casing sections, as published in INAGSON et al. (2015), were defined (Table 4; Fig. 6). At least, the intersected formations from top to bottom were derived from the facies model in SCHERFF (2016) and attached to the wellpath as formation tops (Table 5; Fig. 7).

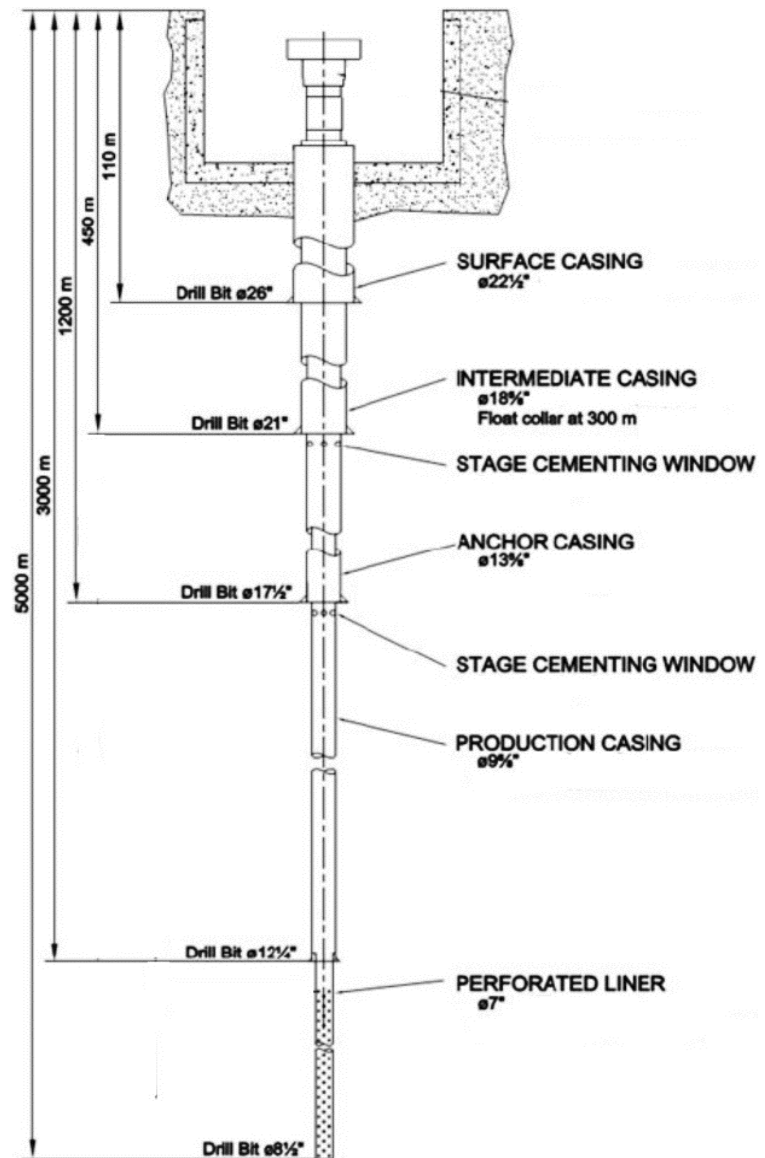


Figure 6: Well design of the IDDP-2 (After INAGSON et al., 2015).

Table 4: Overview of the borehole diameter and the installed casing sections, their respective nominal outer diameter and casing shoe depth (Data after INAGSON et al., 2015).

Hole/ Drill bit diameter (inch)	Casing section	Casing nominal outer diameter (inch)	Casing shoe depth TVD (m)
26	Surface casing	22 ½	110
21	Intermediate casing	18 ⅝	450
17 ½	Anchor casing	13 ⅝	1,200
12 ¼	Production casing	9 ⅝	3,000
8 ½	Perforated liner	7	5,000

2.5. Geology

Geological information, such as formation tops or dykes, were loaded into Sysdrill. The input of data can be visualized in a 3-D view and helps to accurately define or modify the wellpath in order to achieve the drilling goal. A 3-D facies model of the field has been developed in SCHERFF (2016), who provides a derived IDDP-2 lithology log to a depth of around 2,500 m (Fig. 7). The log was simplified in a way that only the most important formation intervals were selected and implemented into the software. A total of 25 formation tops and one subvertical dyke were inserted (Table 5).

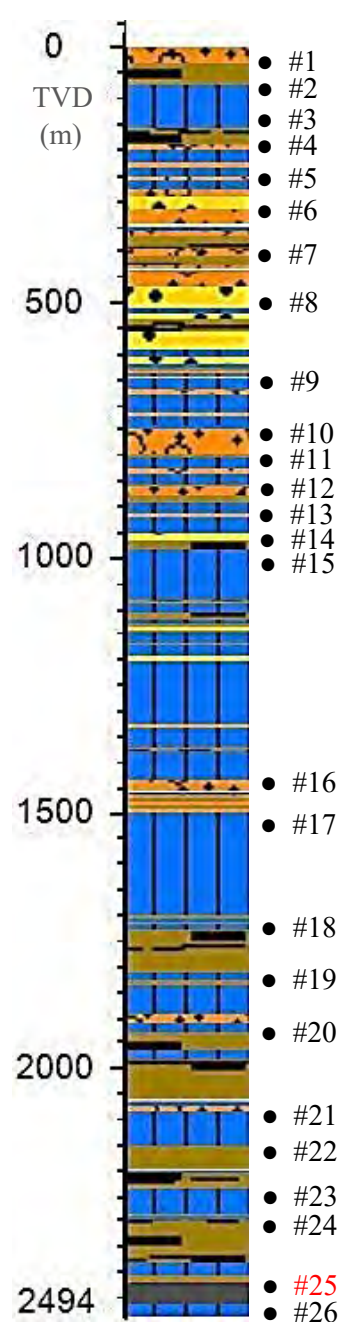


Table 5: List of formation tops, dyke and their depth as defined in Sysdrill.

#	Formation Tops/ Dyke	True Vertical Depth (m)
1	Hyaloclastite	31
2	Pillow basalt/-breccia	71
3	Basalt Lava	155
4	Pillow basalt/-breccia	188
5	Basalt Lava	275
6	Marine Sediments	367
7	Pillow basalt/-breccia	467
8	Marine Sediments	620
9	Basalt Lava	744
10	Hyaloclastite	794
11	Basalt Lava	852
12	Hyaloclastite	890
13	Basalt Lava	961
14	Pillow basalt/-breccia	982
15	Basalt Lava	990
16	Hyaloclastite	1,428
17	Basalt Lava	1,497
18	Pillow basalt/-breccia	1,723
19	Basalt Lava	1,820
20	Pillow basalt/-breccia	1,930
21	Basalt Lava	2,079
22	Pillow basalt/-breccia	2,145
23	Basalt Lava	2,226
24	Pillow basalt/-breccia	2,290
25	Dyke	2,420
26	Basalt Lava	2,437

Figure 7: IDDP-2 lithology log. The numbering on the right hand side indicates the selection of formation tops for the simulation (After SCHERFF, 2016).

2.6. Temperature and Pressure Profiles

The temperature and pressure data are required to perform several engineering calculations, including:

- Mechanical analysis of the drilling assembly (torque and drag tab)
- Thermal effects on the equivalent circulating density, swab and surge effects, pump pressure and flow rate analysis (hydraulics calculation)
- Definition of a pump schedule to optimize circulation modes (cementing analysis)
- Modelling of complex load cases of the casing string (casing analysis tab)

The software allows pressure data to be entered as values or gradients. A solid database includes formation pore, fracture and overburden pressure or gradients. A borehole collapse pressure is optional, but not used for this simulation. The pore pressure was extracted by digitizing the logged pressure profile and boiling point with depth curve after INAGSON et al. (2015). The overburden pressure or stress σ_{ob} was calculated with the following equation:

$$\sigma_{ob} = 0.0001 \times \rho \times g \times h \quad (Eq.1)$$

The overburden load in bar σ_{ob} was calculated using an assumed average bulk density ρ of 2,500 $\text{kg}\cdot\text{m}^{-3}$ and an average gravitational constant g of 9.81 $\text{m}\cdot\text{s}^{-2}$ on Earth at different depth, h . The factor of 0.0001 is needed to convert kilopascal to the more convenient unit bar. The fracture pressures and gradients at each depth was predicted by using the Pennebaker correlation method. The Pennebaker method uses the effective stress ratio F_{σ} and correlates this ratio with the actual depth, regardless of pore pressure gradient. The effective stress or matrix stress ratio is the ratio of the effective horizontal stress and the vertical stress and was empirically estimated from hydraulic fracture data (PENNEBAKER, 1968). The Pennebaker correlation curve for the effective stress ratio is given in Appendix A. The multiplication of the effective stress with the matrix stress σ_z gives the minimum matrix stress, σ_{min} (Eq.2). The matrix stress is the product of the vertical overburden gradient σ_{ob} and the depth minus the formation pore pressure ρ_f . The above mentioned constant bulk density of 2,500 $\text{kg}\cdot\text{m}^{-3}$ yields to an overburden gradient of 0.25 $\text{bar}\cdot\text{m}^{-1}$.

$$\sigma_{min} = F_{\sigma} \times \sigma_z = F_{\sigma} \times [(\sigma_{ob}) \times (depth) - \rho_f] \quad (Eq. 2)$$

The fracture pressure ρ_{ff} was then calculated by using Eq. 3:

$$\rho_{ff} = \sigma_{min} + \rho_f \quad (Eq. 3)$$

The fracture gradient is then the ratio between the fracture pressure and the depth. The pore, fracture and overburden pressure values and gradients are graphically visualized in Fig. 8.

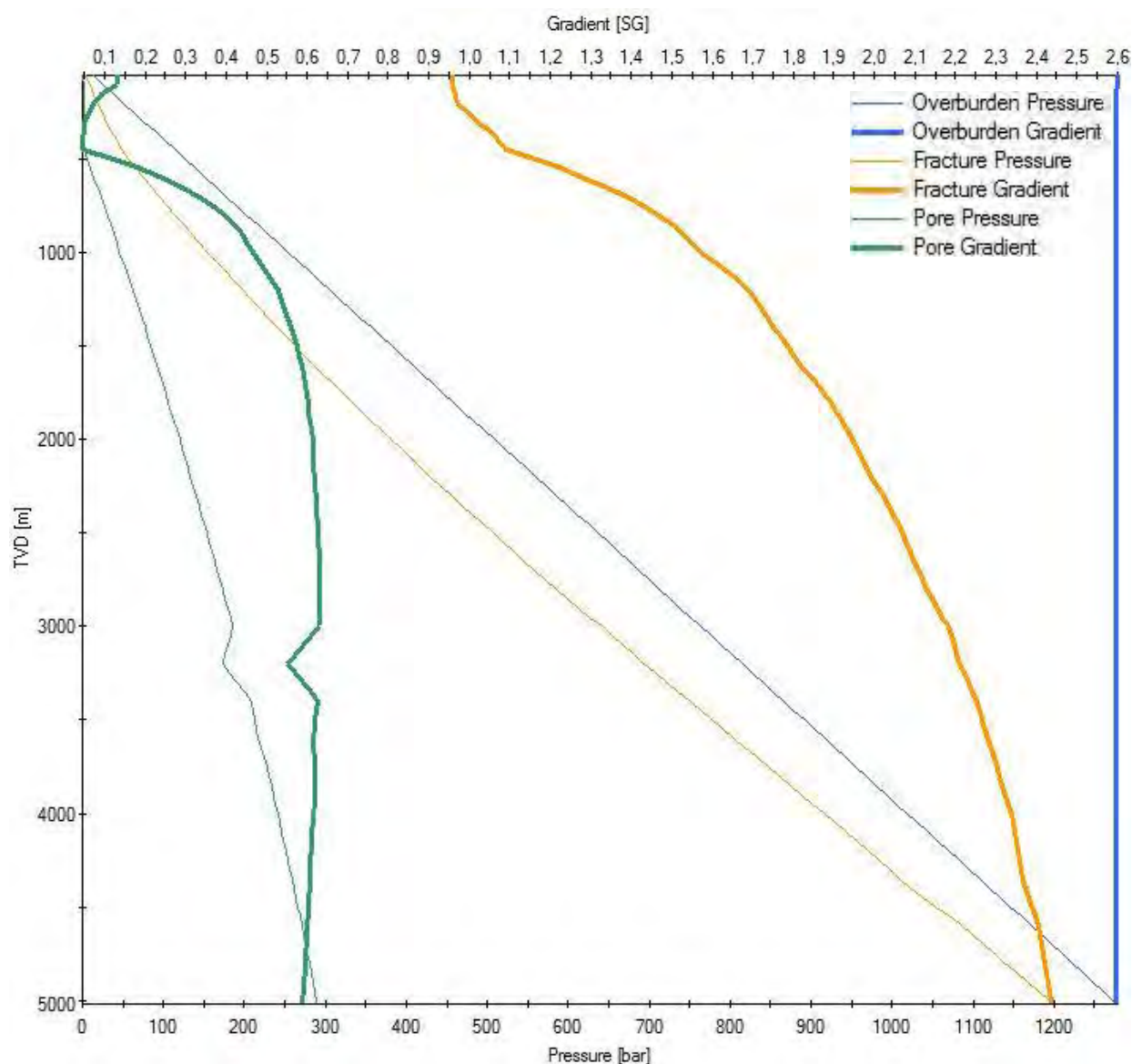


Figure 8: Pressure profiles of the IDDP-2 well. The pore pressure profile is according to data after INAGSON et al. (2015). The fracture pressure profile was calculated on the basis of the Pennebaker prediction method. The overburden pressure was calculated by the lithostatic pressure equation.

The temperature data are based on the derived IDDP-2 temperature log from the temperature model in SCHERFF (2016) and the boiling point with depth curve in INAGSON et al. (2015). The imported temperature data in Sysdrill is therefore a merge between these two profiles. Fig. 9 illustrates the different profiles of the modelled IDDP-2 temperature log, logged temperature of the Reykjanes system and the boiling point with depth curve. As can be seen, these profiles meet at a depth of approximately 1,300 m and temperature of $\sim 285^{\circ}\text{C}$ (yellow rectangular). The imported temperature profile for the simulation in Sysdrill consists of three parts. The upper part above 1,300 m considers the modelled temperature log from SCHERFF (2016). The logged temperature profile of the Reykjanes field define the middle part to a depth of approximately

2,500 m and the lower part of the temperature profile is supposed to follow the boiling point with depth curve according to INAGSON et al. (2015). The temperature profile on the right hand side of Fig. 9 represents the actual temperature data used for the simulation in Sysdrill.

Appendix A provides the imported pressure and temperature values down to a depth of 5,000 m. Furthermore, the lists provide the geothermal gradient and pore pressure gradient, which have automatically been calculated by the software. The fact that the temperature and pressure values were taken by digitizing the temperature curves from INAGSON et al. (2015) and visual extraction of values from the synthetic temperature log in SCHERFF (2016) implies a certain random error of the database.

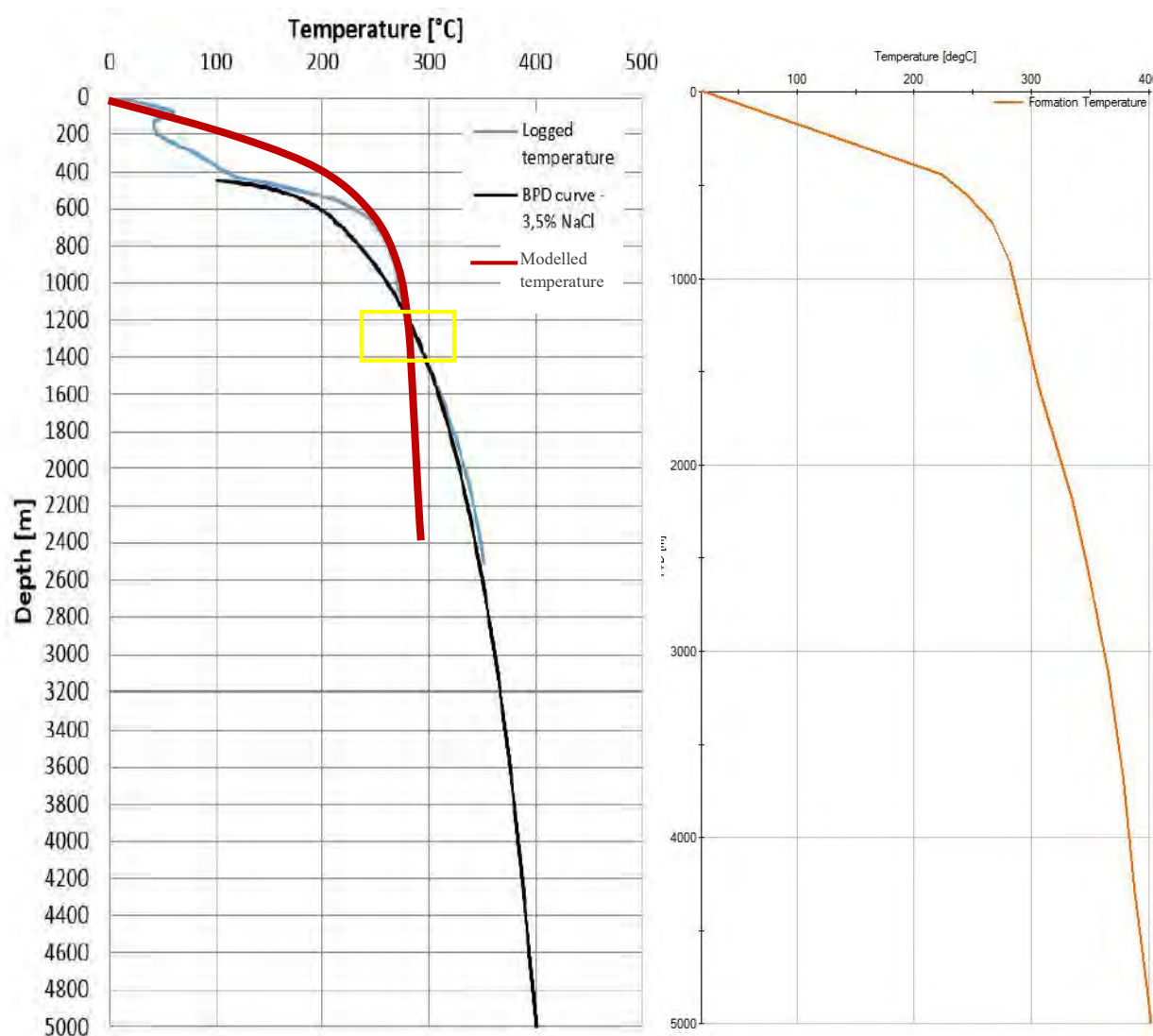


Figure 9: Left: Graph showing different temperature profiles (AFTER INAGSON et al., 2015). The curve in red displays the derived IDDP-2 temperature log of the temperature model in SCHERFF (2016). The profiles in blue and black refer to the logged temperature of the Reykjanes field and the boiling point with depth curve, respectively (After INAGSON et al., 2015). The yellow rectangular highlights the triple junction where all three profiles meet. Right: Graph showing the imported temperature profile in Sysdrill.

2.7. Definition of Assemblies

The drill string and casing assemblies were created prior the beginning of engineering calculations. The defined bottomhole assemblies of selected hole sections are itemized in Table 6. The drill string assemblies were taken from templates provided by the catalogue in Sysdrill. These templates were then individually modified according to the information given about the drill string constructions for drilling the IDDP-1 well at Krafla in Northern Iceland (HOLMGEIRSSON et al., 2010; PALSSON et al., 2014; THORHALLSON et al., 2014).

The constructions do not reflect the final design of the assemblies to be used for drilling the IDDP-2, but represent the implementation of available information and database. The limited information about the IDDP-2 bottomhole assemblies have caused a more or less uniform arrangement of the drill string elements. Heavyweight drill pipes, stabilizers, a shock sub and positive displacement mud motor, drilling jar, drill collars, an inclination tool (Anderdrift) and a roller cone bit are basic elements for almost every drill string.

The example in Fig. 10 shows the 17 1/2" drill string assembly for drilling the anchor casing section. Other drill string assemblies differ in detail, as can be reviewed in Table 6.



5 1/2" 24.7#	5,500 in
Cross Over 5-1/2 to 6-5/8	8,000 in
Heavy Weight Drill Pipes	6,625 in
Drilling Jar	6,625 in
Cross Over 6-5/8 to 7-5/8	9,500 in
8" x 3" Drill Collar	8,000 in
Anderdrift	7,625 in
9 1/2" Drill Collar	9,500 in
Stabiliser	9,500 in
9-1/2" Positive Displacement Motor	9,500 in
Shock Sub	9,500 in
Near Bit Stabilizer	9,500 in
17 1/2" Bit	17,500 in

Figure 10: Example of the drill string assembly used to drill the 17 1/2" hole for the anchor casing section. The values on the right side define the nominal outer diameter of each single string element. The basic design originates from a template in the catalogue in Sysdrill and was then modified according to HOLMGEIRSSON et al., (2010), PALSSON et al (2014) and THORHALLSON et al. (2014).

Table 6: Itemized list of each drill string assembly as derived by a combination of data and information according to the Sysdrill catalogue and data after HOLMGEIRSSON et al., (2010), PALSSON et al (2014) and THORHALLSSON et al. (2014).

21" Hole	17 1/2" Hole	12 1/4" Hole	8 1/2" Hole
5 1/2" 24.7 lbm Drill pipe	5 1/2" 24.7 lbm Drill pipe	5" 19.5 lbm Drill pipe	5" 19.5 lbm Drill pipe
8" Cross over	8" Cross over	5 " HWDP	5 " HWDP
6 5/8" HWDP	6 5/8" HWDP	6 1/2 " Jar	6 1/2 " Jar
9 1/2 " Cross over	6 5/8" Jar	8 " Cross over	6 3/4" Drill collar
9 1/2 " Drill collar	9 1/2 " Cross over	6 5/8" HWDP	6 3/4" Anderdrift
9 1/2 " Stabilizer	8" Drill collar	8 " Cross over	6 3/4" Drill collar
9 1/2 " Drill collar	7 5/8 " Anderdrift	8 " Drill collar	6 1/2 "Stabilizer
9 1/2 " Stabilizer	9 1/2 " Drill collar	8 " Anderdrift	6 1/2 " Shock sub
9 1/2 " Drill collar	9 1/2 " Stabilizer	8 " Drill collar	6 1/2" Near bit stabilizer
9 1/2 " Drill collar	9 1/2 " Positive dis- placement mud motor	8 " Stabilizer	8 1/2" Roller cone bit
21" Roller cone bit	9 1/2 " Shock sub	8 " Positive dis- placement mud motor	
	9 1/2 " Near bit stabilizer	8 " Shock sub	
	17 1/2 " Roller cone bit	8"Near Bit stabilizer	
		12 1/4" Roller cone bit	

The casing strings were designed according to the proposal in INAGSON et al. (2015). The Sysdrill catalogue was used to load the individual casing string assemblies and, additionally, define the couplings. The buttress thread connection type (BTC) was, different than proposed in INAGSON et al. (2015), defined for all casing strings.

Table 7 is a detailed overview about the casing string assemblies, including the nominal weight, outer diameter and steel grades.

Table 7: Detailed listing of each casing string assembly, including the casing couplings and joints in API Oilfield units (data after INAGSON et al., 2015 and according to the Sysdrill catalogue).

18 5/8" , 87.50 lb·ft ⁻¹ Intermediate casing	13 5/8" , 86 lb·ft ⁻¹ Anchor casing	9 5/8" , 53.50 lb·ft ⁻¹ Production casing	7" , 26 lb·ft ⁻¹ Production liner
20" Coupling 87.5 lb·ft ⁻¹ , K-55, BTC	14.299" Coupling 80.7 lb·ft ⁻¹ , T-95, BTC	10.567" Coupling 58.4 lb·ft ⁻¹ , K-55, BTC	7.672" Coupling 28 lb·ft ⁻¹ , K-55, BTC
18 5/8" Joint 87.5 lb·ft ⁻¹ , K-55	13 3/8" Joint 86 lb·ft ⁻¹ , T-95	9 5/8" Joint 53.5 lb·ft ⁻¹ , K-55	7 5/8" Joint 26 lb·ft ⁻¹ , K-55

2.8. Drilling and Completion Program

A planned drilling program for IDDP-2 at Reykjanes is not published in detail, but drafted as shown in Fig. 13. INAGSON et al. (2015) provide a brief description of the proposed casing design program for the prospective IDDP-2 well.

This well design and the determination of the casing shoe depths were determined on the basis of a $1,400 \text{ kg}\cdot\text{m}^{-3}$ ($11.68 \text{ lb}\cdot\text{gal}^{-1}$) drilling fluid (INAGSON et al., 2015). On the basis of the given fluid density, two mud types were defined and integrated in the simulation process. A detailed description of the drilling fluid formulation for drilling the IDDP-2 well is not provided, yet. One of the defined drilling fluids refers to the water-based bentonite mud, used for drilling the IDDP-1 well and most of the wells at Reykjanes (PALSSON et al., 2014; THORHALLSSON et al., 2014). The primary additive was bentonite, which is preferred for geothermal wells with large borehole diameters (CHEMWOTEI, 2011). Lost circulation materials such as fibers, flakes or polymers were also added in case of circulation loss into encountered feeder zones (THORHALLSSON et al., 2003; HOLMGEIRSSON et al., 2010). However, the publications neither provide quantitative information about the density of these additives nor the volume added to the drilling mud. Hence, the values were then assumed. The densities and specific heat capacity of the water and weighting material barite are predefined by the Sysdrill catalogue. A second type of mud refers to an oil-based drilling fluid. The fluid formulation of this mud is simpler since it does not contain any additives. The values for the density and specific heat capacity of the primary base fluid and weighting material are in the same way set according to the fluid catalogue in Sysdrill. The required rheological properties of the water- and oil-based mud were taken from sources, which provide a detailed summary of laboratory experiments.

RAVI et al. (2011) have experimentally analyzed a $2,133 \text{ kg}\cdot\text{m}^{-3}$ ($17.8 \text{ lb}\cdot\text{gal}^{-1}$) water-based mud under high temperature and pressure conditions. This work was used to define the fluid formulation and, moreover, to extract the rheological properties at standard conditions of $\sim 50 \text{ }^\circ\text{C}$ and ambient pressure. The rheological properties and fluid composition of the water-based mud is shown in Fig. 11. In addition to that, an oil-based fluid was defined to compare the effect on the drilling process and the thermal modelling (Fig. 12). IBEH et al. (2007) have investigated an oil-based drilling fluid under ultra-high pressure and high temperature conditions of up to 2,760 bar and $315 \text{ }^\circ\text{C}$, respectively. The fluid has an increased density of $2,157 \text{ kg}\cdot\text{m}^{-3}$ ($18 \text{ lb}\cdot\text{gal}^{-1}$) and is mixed with water at a ratio of 93/7. The tests were run on two different schedules, one at a constant pressure and variable temperature and the other one at a constant temperature and variable pressure. The 600 RPM and 300 RPM dial readings were inserted into the fluid builder

tab, allowing an advanced fluid definition. A detailed listing of these dial readings is given in Appendix C. Both drilling fluids are almost equally weighted with barite, which allows a comparison between these drilling muds (Fig. 11 & Fig. 12).

Nominal Fluid		Primary Base Fluid		Secondary Base Fluid		Weighting Material	
Name	HPHT - WBM	Name	Water	Name		Name	Baryte
Purpose	Drilling Fluid	Type	Water	Type	None	Type	Baryte
Density	1400,00 kg/m ³	Density	1000,00 kg/m ³	Density		Density	4600,00 kg/m ³
Volume	260994,69 l	% Base Fluid	100,00 %	% Base Fluid		Volume	24995,60 l
Mass	365392,56 kg	Volume	221372,62 l	Mass		Mass	114979,75 kg
S. Heat Cap.	2722,36 J/kg.K	Mass	221372,62 kg	% Volume		% Volume	9,58 %
		% Volume	84,82 %	S. Heat Cap.		S. Heat Cap.	565,00 J/kg.K
		S. Heat Cap.	4200,00 J/kg.K				

	Name	Material Type	Fluid Density [kg/m ³]	Volume [l/m ³]	Mass [kg/m ³]	Volume Consumed [l]	Mass Consumed [kg]	Specific Heat Capacity [J/kg.K]
1	Bentonite	Viscosifier	800,00	35,66	28,53	9307,75	7446,20	
2	Solids	Viscosifier	4060,00	20,38	82,74	5318,72	21593,99	

Name	Colour	Fluid Density [kg/m ³]	Fluid Model	PV [mPa.s]	YP [Pa]	Yield Value [Pa]	10 Sec Gel [Pa]	10 Min Gel [Pa]
HPHT - WBM		1400,00	Bingham Plastic	32,00	5,27		1,92	5,75

Figure 11: The fluid formulation of the water-based mud according to data after INAGSON et al. (2015) and predefined values in the Sysdrill fluid catalogue. The rheological properties refer to data from RAVI et al. (2011).

The rheological properties of these reference muds were applied to the proposed $1,400 \text{ kg}\cdot\text{m}^{-3}$ dense fluid, regardless of the big differences in densities. The rheological behavior of the fluids was modelled according to the Bingham plastic model, which describes a linear relationship between the shear stress and shear rate of the fluid. The linearity is achieved once the yield point or shear stress threshold has been reached. The slope of the linear line is the defined as the plastic viscosity (PV). A low plastic viscosity and high yield point (YP) enable a fast drilling process and sufficient cuttings transport out of the hole. The estimated drilling schedule in Fig. 13 has been designed with the help of drilling information from already drilled wells in the surrounding. The plan is to drill and complete the 5,000 m well within three months and subsequently begin the downhole measurements.

Nominal Fluid		Primary Base Fluid		Secondary Base Fluid		Weighting Material	
Name	HPHT - OBM	Name	Oil	Name	Water	Name	Baryte
Purpose	Drilling Fluid	Type	Oil	Type	Water	Type	Baryte
Density	1400,00 kg/m ³	Density	900,00 kg/m ³	Density	1000,00 kg/m ³	Density	4200,00 kg/m ³
Volume	21283,41 l	% Base Fluid	93,00 %	% Base Fluid	7,00 %	Volume	3186,37 l
Mass	29796,77 kg	Volume	16830,25 l	Mass	1266,79 kg	Mass	13382,76 kg
S. Heat Cap.	1479,10 J/kg.K	Mass	15147,22 kg	% Volume	5,95 %	% Volume	14,97 %
		% Volume	79,08 %	S. Heat Cap.	4190,00 J/kg.K	S. Heat Cap.	565,00 J/kg.K
		S. Heat Cap.	2060,00 J/kg.K				

Name	Colour	Fluid Density [kg/m ³]	Fluid Model	PV [mPa.s]	YP [Pa]	Yield Value [Pa]	10 Sec Gel [Pa]	10 Min Gel [Pa]
HPHT - OBM		1400,00	Bingham Plastic	60,00	22,00		5,75	10,53

Figure 12: The fluid formulation is according to predefined values for an oil-based mud in Sysdrill. The rheological properties and density of the mud refer to data from IBEH et al. (2007) and INAGSON et al. (2015).

Two drilling rigs were selected to be able to drill the well, the InnovaRig and the Benntec Euro Rig (ELDERS et al., 2012). It was decided to select the InnovaRig, designed by the German Research Centre for Geosciences GFZ in Potsdam, for this simulation. The necessary input data for the simulation in Sysdrill are listed in Table 8. A detailed technical data sheet of the rig is available in Appendix B. The block weight was assumed according to the technical data sheet. The maximum torque, maximum hook load and mud pit volume have been taken from the technical specification sheet provided by the International Continental Scientific Drilling Program (www.icdp-online.org). The mud pump specifications in WOHLGEMUTH et al. (2007) were taken to select a predefined triplex pump from the Sysdrill pump catalogue. The T-1,600 triplex pump was selected according to similar power generation, maximum pressure and flow rate.

Table 8: Technical data of the InnovaRig as used for an input in Sysdrill (Data after WOHLGEMUTH et al. (2007), www.icdp-online.org and the Sysdrill mud pump catalogue).

Block weight	44.45 tons
Max torque	70,000 N·m
Max hook load	412 tons
Mud pit	15 × 8 × 2 m
Pit heat transfer coefficient	5.68 W·m ⁻² ·°C ⁻¹
Mud pump	T-1,600 Triplex, 1,300 kW

First of all, the 26" hole is drilled to a depth of 110 m to set the surface casing. This depth is necessary to block a problematic water-bearing fissure at approximately 100 m from an inflow. If the inflow cannot be prevented, the problematic zone should be fully cemented. Another feed zone is going to be expected for the intermediate casing section, thus the casing shoe is set at 450 m. A float collar at 300 m depth prevents the drilling mud from entering the casing during its descent and decreases the risk of a collapse. The first stage cementing window is going to be installed just below the casing shoe (Fig. 6). The remaining cement slurry at the bottom of the intermediate casing string will be drilled out. A second stage cementing window is placed below the anchor casing, however, it works as a back-up and only used if no loss of circulation zones are encountered throughout the drilling interval (Fig. 6). It is intended to drill and complete the anchor casing section in about 13 days (Fig. 13). Subsequent drilling of the production casing section crosses the current production zone between 2,000-3,000 m. The expected loss of circulation within this section is counteracted with the help of cement plugs.

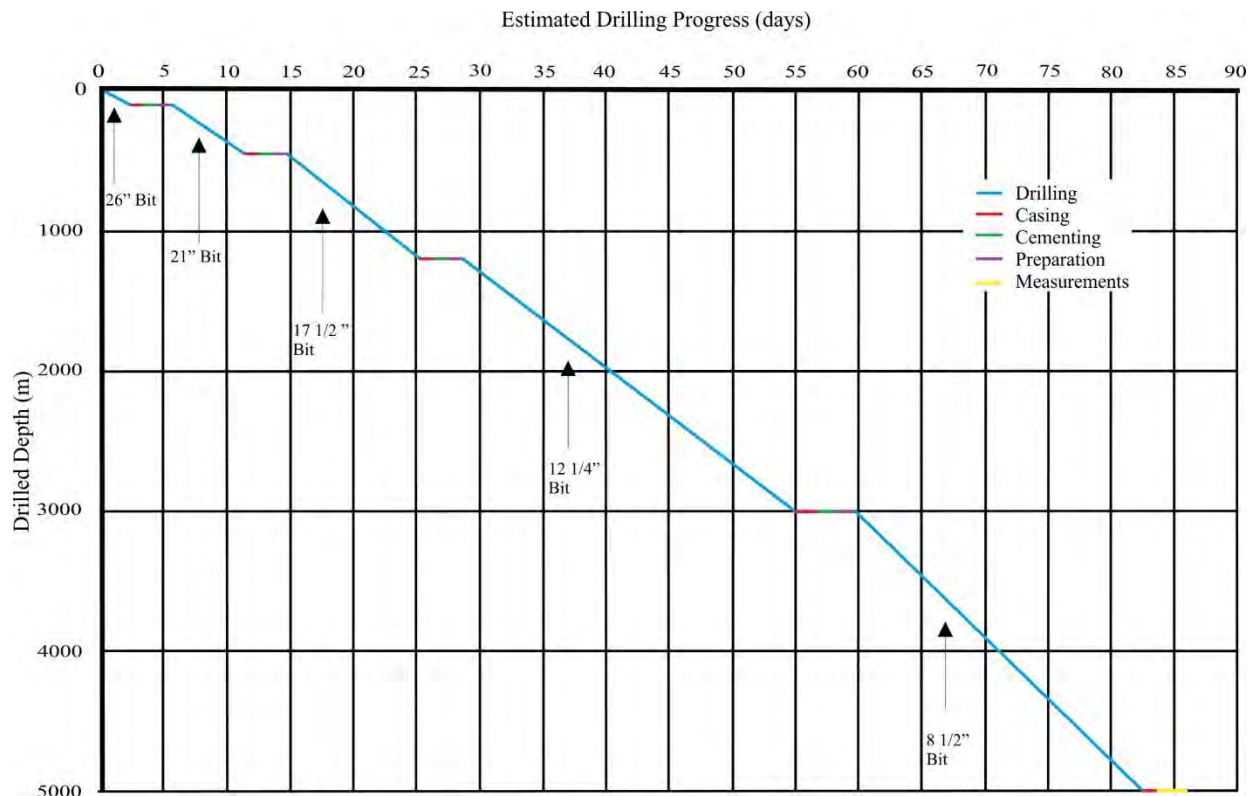


Figure 13: Estimated drilling progress curve for IDDP-2, including time intervals for casing setting, cementing, preparation and downhole measurements (After SAMORKA, 2014).

The cement volume will be kept as low as possible to avoid contamination of the productive zone. On the other hand, the temperature increases at this depth to around 360 °C and a good cement job is of top priority. The extreme conditions require special procedures for drilling and cementing the borehole section. Finally, the 7" production liner section is drilled to a depth of 5,000 m after 80-85 days. The liner overlaps with the bottom of the production casing and shows no perforation for the upper 200 m (INAGSON et al., 2015).

2.9. Torque and Drag Calculation

The integrated torque and drag editor allows the mechanical analysis of a drill string within a particular hole section. A detailed tabular and graphical simulation summary for the relevant aspects of tension, torque and stress is provided in the following Chapter 3.1. The drill string analysis was conducted for drilling the intermediate, anchor and production casing and production liner sections, respectively from 110 m to 5,000 m depth. First of all, the operating conditions and operation modes of each section were defined, as one example is shown for the anchor casing section in Fig. 14. Four operation modes of rotary drilling, rotating off bottom, tripping into and out of the hole were defined. In order to run the torque and drag calculation, the weight on bit, bit torque, rotational speed of the string and drilling penetration rate were inserted.

The input data for the rotary drilling and rotating off bottom modes, as shown in Fig. 14, are adjustments according to measured parameters during drilling of the IDDP-1 well (PALSSON et al., 2014; HOLMGEIRSSON et al., 2010).

The figure displays two screenshots of a software interface for drilling simulation. The top screenshot shows normal drilling conditions, and the bottom screenshot shows abnormal conditions for a stuck pipe simulation. Both screenshots feature a table with columns for Start Depth, End Depth, Depth Interval, Rows, Operating Mode, Name, WOB [Tef], Bit Torque [N.m], RPM [rpm], ROP [m/hr], Include Hydraulics, and Flow Rate [l/min].

Calculate	Surface Conditions	Calculate	Operating Mode	Name	WOB [Tef]	Bit Torque [N.m]	RPM [rpm]	ROP [m/hr]	Include Hydraulics	Flow Rate [l/min]
Start Depth	110,00 m	1	Rotary Drilling	Rotary Drilling	10,00	7500,00	60,00	2,50	<input checked="" type="checkbox"/>	3600,00
End Depth	450,00 m	2	Rotating Off Bottom	Rotating Off Bottom			30,00		<input checked="" type="checkbox"/>	3600,00
Depth Interval	34,00 m	3	Tripping Into Hole	Tripping Into Hole					<input checked="" type="checkbox"/>	3600,00
Rows	10	4	Tripping Out Of Hole	Tripping Out Of Hole					<input checked="" type="checkbox"/>	3600,00

Figure 14: Example of the torque and drag editor tab for drilling the 21" hole section. Up: Input parameters for running the simulation under normal drilling conditions. Down: Input parameters for simulating a drilling incident, e.g. stuck pipe under abnormal conditions. Both cases were run to calculate the surface conditions using the soft string type to include hydraulics (Data after PALSSON et al., 2014 and HOLMGEIRSSON et al., 2010).

The simulation was run under normal and abnormal conditions (Fig. 14). The parameters under normal conditions define an undisturbed and standardized drilling process. Abnormal conditions occur when the pipe is about to get stuck in case of drilling into molten magma, as has happened for the IDDP-1 well (PALSSON et al., 2014). In reality, these drilling parameters behave more dynamic due to changes of the lithology as drilling proceeds (Fig. 7).

The torque and drag calculation was run using the surface calculation option, which determines the surface drilling readings while drilling the specific hole interval. The selected range calculation is a dynamic simulation of the changing hook load, surface stress and surface torque as drilling proceeds (Fig. 14). Furthermore, the editor allows the selection between the stiff and the soft string model. The stiff string model is considered as more realistic as it assumes that only the tool joints or other external upsets are in contact with the borehole wall. In order to accurately calculate the internal and external pressures during drilling, the soft string model must be selected to finally include the hydraulics. The rotating off bottom mode describes any axial movement and bit/formation interaction, reducing the parameter input to the rotational speed of the string. Tripping into or out of hole refers to the removal and replacement of pipe segments or in case of a worn drill bit.

The water- and oil-based muds were separately included in the simulation to evaluate the effect on the torque, tension and stresses. The slips of the associated drilling rig are not specified and, thus, not considered for the simulation.

The torque and drag calculations further takes the friction factor for a specified depth interval into account. The torque and drag editor provides default settings of 0.2 for the cased hole and 0.3 for the open hole section and were kept constant throughout the calculations. The assessment of critical parameters and drill string constraints is the main issue while analyzing the mechanical integrity within the torque and drag calculation tab.

2.10. Hydraulics Calculation

The hydraulic editor tab was used to calculate the required pump pressure, flow rate under a predefined pump pressure and the bit pressure loss. At this stage, the thermal effect of drilling mud circulation was being investigated. In order to do so, the thermal expansion coefficient, γ_t , and the isothermal compressibility coefficient, γ_p , at surface conditions had to be defined for both drilling fluids. These data rely on empirical data from KÅRSTAD & AADNØY (1998) and listed in Table 9. The values for the heat transfer coefficients, thermal conductivity and earth specific heat capacity were kept as default in Sysdrill. The thermal modelling suboption allows the definition of the circulating time, pit volume, mud inlet temperature and air temperature. The pit volume result from the mud pit dimensions of $15 \times 8 \times 2$ m (see Chapter 2.8.). The circulating time, inlet and air temperature were assumed and diversified within a narrow range to study the effects on the annular and string temperature. The loaded annulus includes the average bulk of $2,500 \text{ kg}\cdot\text{m}^{-3}$ and a cuttings diameter of 12 mm, both parameters were assumed. The integration of a loaded annulus allows to model the efficiency of hole cleaning, particularly the cutting transport ratio or cuttings concentration. The predefined pump T-1,600 pump was set to circulate the fluids.

Table 9: Summary of the input coefficients and values required to model the thermal effect on circulating drilling fluids (Data after KÅRSTAD & AADNØY (1998) and default parameters in Sysdrill)

	Water-based mud	Oil-based mud
Thermal expansion coefficient γ_t ($e-10 \text{ Pa}^{-1}$)	3.679	8.847
Isothermal compressibility coefficient γ_p ($e-4 \text{ }^\circ\text{C}^{-1}$)	-4.600	-8.108
Borehole wall heat transfer coefficient ($\text{W}\cdot\text{m}^{-2}\cdot^\circ\text{C}^{-1}$)	170.35	
Annulus heat transfer coefficient ($\text{W}\cdot\text{m}^{-2}\cdot^\circ\text{C}^{-1}$)	5.68	
Formation thermal conductivity ($\text{W}\cdot\text{cm}^{-1}\cdot^\circ\text{C}^{-1}$)	0.039	
Formation specific heat capacity ($\text{J}\cdot\text{kg}^{-1}\cdot^\circ\text{C}^{-1}$)	295.00	
Pit heat transfer coefficient ($\text{W}\cdot\text{m}^{-2}\cdot^\circ\text{C}^{-1}$)	5.68	

Fig. 15 gives an example for the direct inclusion of thermal effects into the hydraulics calculation tab. The modelling of thermal effects takes the predefined geothermal temperature profile into account (Fig. 9).

Figure 15: Example of the input tab within the hydraulics calculation editor. The calculation is based on the constructed drill string assembly for drilling the 21" intermediate casing section. Additional suboptions, e.g. thermal effects, are available for the pump pressure calculation.

Thermal effects due to circulation were investigated for both, the water- and oil-based drilling fluid (Fig. 11 & 12). Swab and surge operations, while running into and pulling out of the hole, were investigated at varying tripping rates. The total flow area of the bit varies with the different assemblies and was automatically calculated by the software on the basis of a drilling bit with five nozzles.

The hydraulics calculation offers a comprehensive analysis of aspects with regard to the pump pressure profile, equivalent circulating density, equivalent static density, tripping operations and hole cleaning. The simulation results of different scenarios will be presented in the following Chapter 3.2.

2.11. Casing Analysis

The casing analysis editor provides the definition and analysis of load cases most likely to occur. A half biaxial casing load method was set default by the program and kept the same for each calculation. This analysis type will affect the burst and collapse load in such a way that the burst load decreases under compression and the collapse load decreases under tension. A full biaxial would affect both loads under compression and tension, whereas a uni-axial analysis type has no effect on the load cases.

Prior casing analysis, the editor requires a comprehensive database. To begin with, initial running speed for casing setting was set to $0.04 \text{ m} \cdot \text{min}^{-1}$ (see Chapter 2.9) and occasionally changed in order to evaluate the effect of higher running speeds on the results of the simulation. The casing couplings and connections were permanently included in each series of calculation. (Table 7; Chapter 2.7.). The calculation requires the insertion of densities of the key fluids and gases to calculate the pressure profiles associated with each load case (Table 10). The mud and cement

slurry densities were kept the same for each section and refer to the predefined values as explained in Chapter 2.8 and 2.12. All other density values for gas, mix water and air were kept as defined by default in Sysdrill.

Table 10: Definition of the key fluid densities within the casing analysis editor (Data after INAGSON et al., 2015 and default settings in the casing and tubing analysis tab in Sysdrill)

Fluid/ Gas	Density (kg·m ⁻³)
Drilling mud	1,400
Cement slurry	1,750
Gas	235
Mix water	1,030
Air	1.29

Four load cases were defined, which might possibly occur during drilling and completion operations. Each load case was assigned a design factor for axial, burst, collapse and triaxial analysis (Fig. 16).

Name	Axial Tension DF	Axial Compression DF	Burst DF	Collapse DF	Triaxial DF	Cxn Axial Tension DF	Cxn Axial Compression DF	Cxn Burst DF	Cxn Collapse DF	Calculate	Type
Initial										<input checked="" type="checkbox"/>	Initial
Burst/Tension	1.70	1.70	1.25	1.25	1.30					<input checked="" type="checkbox"/>	Installation
Collapse - Fully evacuated	1.70	1.70	1.25	1.25	1.30					<input checked="" type="checkbox"/>	Post Cemented
Collapse - Circulation loss, Drop of mud level	1.30	1.30	1.20	1.00	1.25	1.30	1.30	1.20	1.00	<input checked="" type="checkbox"/>	Post Cemented
Burst - Influx of geofluids	1.30	1.30	1.20	1.00	1.25	1.30	1.30	1.20	1.00	<input checked="" type="checkbox"/>	Gas Kick

Figure 16: Summary of defined load cases and related design factors for axial tension and compression, burst, collapse and triaxial stress criterion as set default in the software Sysdrill.

The load cases and specified design factors were taken from predefined templates available in the load case catalogue in Sysdrill. The lower the design factor the more approaches the load stress towards the yield stress of the casing string and related couplings or connections. The sufficiency of a design factor was evaluated by the simulated safety factor, which defines the ratio between the yield stress and load stress. Every load case was assigned to a specific type of simulation condition, for instance, post cemented or gas kick. The relevant types are shown in Fig. 16 and will be explained in the following.

The load case editor allows to check several additional calculation options including casing wear during drilling activities and thermal effects on the yield strength of the casing string equipment (Fig. 15). The thermal yield option is based on a defined temperature profile and was used to simulate the degradation of the casing yield strength. The inclusion of thermal axial loads is available for post cemented calculations.

In the following, the individual load cases and their different standard settings are explained.

Initial

By default an initial load case is defined as a reference for any other load case that include the ‘cement is set’ option. The initial condition includes axial loads due to bending stresses and piston forces. Furthermore, the internal and external pressure profiles are subjected to the properties of the drilling mud. The temperature for this case is adapted from the predefined geothermal temperature profile. The stresses, present prior to the cementation of the string, were analyzed according to this load case setup.

Burst/ Tension

The combination of burst and tension was run under installation conditions, which means that the casing is free hanging in a column of fluid. The default settings with checked bending stresses and piston forces were kept as they are. The external pressure profile includes the fluid gradients of the mud and cement slurry in the annulus (Fig. 17).

The fluid gradient of the drilling mud inside the casing string defines the internal pressure profile. The related top depth reference and density of the fluids are referenced to the input data as defined earlier in the casing analysis editor. Any applied load, either internal or external, would shift the pressure profile from the mud and cement slurry. The determination of critical applied loads was analyzed.

External		Internal							
↓	→	Type	Direction	Top Depth Ref	Top Depth Offset [m]	Top Depth [m]	Density Ref	Density [kg/m3]	
1		Fluid Gradient	From Above	Slot		0,00	Mud	1400,00	
2		Fluid Gradient	From Above	Top Cement Lead		450,00	Cement Lead	1750,00	

Figure 17: Burst/ tension load case with the initial selection of axial loads and the definition of the external pressure profile.

Collapse – fully evacuated

A collapse load case was run under the conditions that the cement was already set and the casing section is fully evacuated (Fig. 18). Hence, the internal pressure profile shows an almost unchanged fluid gradient since the density of air approaches to zero. The external pressure profile was built from the mud and lead cement gradients in the annulus. The set cement slurry behaves as a porous matrix and contains pore fluid, thus, the pore pressure gradient must be included from the previous casing shoe downwards. This load case simulates a poor cement job.

	Type	Direction	Top Depth Ref	Top Depth Offset [m]	Top Depth [m]	Density Ref	Density [kg/m ³]	Pressure Ref
1	Fluid Gradient	From Above	Rig Datum		0,00	Mud	1400,00	
2	Fluid Gradient	From Above	Top Cement Lead		450,00	Cement Lead	1750,00	
3	Gradient Profile	Absolute	Prev Casing Shoe		450,00			Pore Pressure

Figure 18: Setup of the collapse – fully evacuated load case with the selection of bending stress, thermal yield and the definition of the external pressure profile.

Collapse – Circulation loss with drop of mud level

This load case simulates the internal pressure profile after a drop in the annulus mud level due to an encountered lost circulation zone. This case reflects a post cementation case and includes the bending stresses. The external and internal pressure conditions for the anchor casing section are shown in Fig. 19.

	Type	Direction	Top Depth Ref	Top Depth Offset [m]	Top Depth [m]	Density Ref	Density [kg/m ³]	Pressure Ref
1	Fluid Gradient	From Above	Rig Datum		0,00	Mud	1400,00	
2	Fluid Gradient	From Above	Top Cement Lead		450,00	Mix Water	1030,00	
3	Gradient Profile	Absolute	Prev Casing Shoe		450,00			Pore Pressure

	Type	Dir	Top Depth Ref Type	Top Depth Offset [m]	Top Depth [m]	Density Ref	Density [kg/m ³]
1	Fluid Gradient	From Above	Rig Datum		0,00	Air-Empty	1,89
2	Fluid Gradient	From Below	Calculated		0,00	Next Mud	1400,00
3	Fluid Gradient	Absolute	Rig Datum		0,00	Fracture Gradient	1690,00

Figure 19: Settings for the collapse – circulation loss with drop of mud level load case. The external and internal pressure conditions are shown in comparison.

The external pressure profile includes the mud and mixed water fluid pressure gradients. Similar to above load case, a pore pressure gradient was defined from the previous casing shoe. The internal pressure profile basically arise from the drilling mud gradient and the fracture gradient for the open hole section.

Burst – Influx of geofluids

This load case was defined to simulate a hypothetical influx of geofluids at the current production zone between 2,500-3,000 m or at the bottom of IDDP-2. The term geofluids refer to any subsurface fluids, however, only brine, steam and supercritical fluids are expected to flow into the wellbore. The influx volume, to be simulated, is in the range of 5 to 10 m³. The underground blowout was simulated for the anchor, production casing and liner sections. The specific gravity will be different at these depths and depends on the type of geofluids as well as on the temperature. The density of supercritical fluids have a wide range and can be similar to gas but also liquid. The salinity of the Reykjanes system will also affect the specific gravity of the geofluid, causing the underground blowout. The specific gravity of water steadily declines and reaches a value of 0.68 at around 300 °C. The temperature at 3,000 m and 5,000 m will be in the range of 360 to 400 °C. This simulation was by assuming a static specific gravity of 0.60, which takes the depth relationship of the specific gravity into account and seems to be a good approximation for the Reykjanes and supercritical fluids. The external pressure condition is identical to the previous load case. The internal pressure condition is defined by appropriate values of the kick volume and specific gas gravity. In addition to that, the average string diameter and open hole diameter need to be inserted. The design criteria for an underground blowout holds relatively low design factors (Fig. 16). The input values of the external and internal pressure conditions are shown Fig. 20.

The screenshot shows the software interface for defining a burst – influx of geofluids load case. The 'Gas Kick' option is selected under 'Applied Loads'. The 'Internal (Gas Kick)' tab is active, showing a table with the following data:

#	Type	Direction	Top Depth Ref	Top Depth Offset [m]	Top Depth [m]	Density Ref	Density [kg/m ³]	Pressure Ref
1	Fluid Gradient	From Above	Rig Datum		0.00	Mud	1400.00	-
2	Fluid Gradient	From Above	Top Cement Lead		450.00	Mix Water	1030.00	-
3	Gradient Profile	Absolute	Prev Casing Shoe		450.00			Pore Pressure

Below the table, the following parameters are defined:

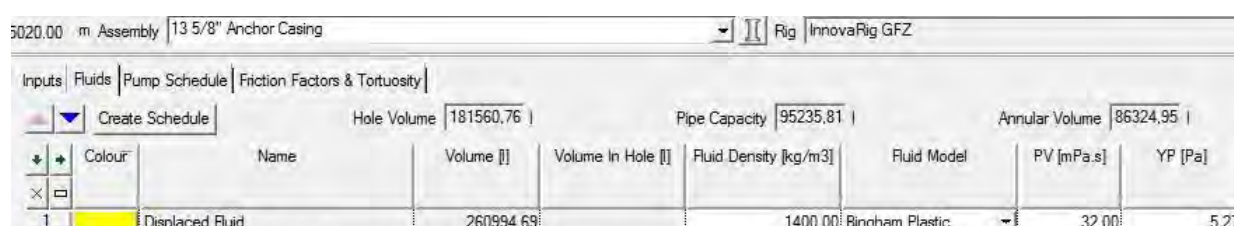
- Kick Volume: 5.00 m³
- Bubble Entry MD: 5020.00 m
- Gas Gravity: 0.60 SG
- Open Hole Diameter: [] mm
- Ave. String Diameter: 127.000 mm
- Mud Density: 1400.00 kg/m³

Figure 20: Settings of the burst – influx of geofluids load case. The internal pressure condition depends on gas properties and geometrical values.

2.12. Cementing Analysis

INAGSON et al. (2015) provide a brief description about the selection of the cement slurry. According to that, it is preferred to pump the API class G cement mixed with silica flour in concentrations of 40 % BWOC¹. Silica flour is an additive which counteracts the decline of the cement strength above 110 °C. Additionally, the cement is mixed with expanded perlite, high temperature retarder, fluid loss additives and bentonite (PALSSON et al., 2014). The density of the cement ranges between 1,700 and 1,800 kg·m⁻³ (INAGSON et al., 2015). A quantitative breakdown of the cement slurry is not required for cementing calculations in Sysdrill. Instead, the rheological properties of plastic viscosity and yield point must be known and defined in the fluids input tab (Fig. 21). Rheological measurements of a 1,920 kg·m⁻³ API class G cement, with silica flour and retarder, yielded to 29 mPa·s⁻¹ and 23 Pa for the plastic viscosity and yield point, respectively (KELLINGRAY et al., 1991). These values apply to a pressure of 405 bar and a temperature of 106 °C and are considered as suitable for the use of this simulation.

A cementing analysis was performed for the intermediate, anchor and production casing sections. The editor provides three calculation types, including the free fall, fixed bottomhole pressure and fixed flow rate option. A fixed flow rate calculation was not performed for this simulation. Some basic input data is required to run the remaining two calculation types. First of all, the fluids and slurries to be pumped down the borehole must be defined regarding their pump volume, density, plastic viscosity and yield point. Fig. 21 demonstrates the general fluid schedule as uniformly used for each borehole section. The displaced fluid equals the water- or oil-based mud and its rheological properties (Fig. 11 & 12). The pumped lead cement refers to the preferred API class G cement and its rheological properties as described above. The volume of the cement slurry is different for each hole section and depends on the individual cement program. A full cementation from bottom to top is intended for the surface and intermediate casing sections, whereas a good cementing job around the casing shoe and in-between the casings is scheduled for the anchor and production casing sections (INAGSON et al., 2015). Table 11 shows the required volumes of the displaced fluid, drilling mud and cement slurry to cement the sections according to the previously described cementing programs.



Inputs	Fluids	Pump Schedule	Friction Factors & Tortuosity				
<div style="display: flex; justify-content: space-between;"> Create Schedule Hole Volume 181560,76 Pipe Capacity 95235,81 Annular Volume 86324,95 </div>							
Colour	Name	Volume [l]	Volume In Hole [l]	Fluid Density [kg/m ³]	Fluid Model	PV [mPa·s]	YP [Pa]
1	Displaced Fluid	260994,69		1400,00	Bingham Plastic	32,00	5,27

Figure 21: Example of a fluid schedule for cementing the anchor casing section. The rheological properties of the cement slurry, displaced fluid and drilling mud refer to data after RAVI et al. (2011), IBEH et al. (2007) and KELLINGRAY et al. (1991).

¹ BWOC means 'by weight of cement' and describes the amount (in percent) of dry form of a material added to cement.

The cementing calculation tab provides a graphic visualization of the well, which was used to set the top of the cement for the individual casing sections. The software then automatically calculated the required volumes for the mud and slurry on the basis of the hole and annulus capacity. The Bingham Plastic model was uniformly used throughout the different cementing analysis.

Table 11: Table showing the calculated volumes of the displaced fluid, drilling fluid and cement slurry to cement the casing string sections.

Sections	Hole Volume (m ³)	Annular Volume (m ³)	Displaced Fluid Volume (m ³)	Drilling Fluid Volume (m ³)	Cement Slurry Volume (m ³)
Intermediate	93	21.3	61	71.5	21.5
Anchor	181.6	86.3	114.6	95.3	48.2
Production	258.9	135.8	133.9	123	12

A two stage-cementing method with two installed cementing windows, below the intermediate and anchor casing strings, should help to perform a sophisticated cement job at this depth (Fig. 6). Another prerequisite to run the cementing calculation is to set the pump schedule. This was done by defining the pump volume and flow rate of the cement slurry as well as displacing drilling fluid. The flow rate to pump the cement was assumed to 500 l·min⁻¹. Fig. 22 shows the pump schedule as designed for the anchor casing section.

Operation	Fluid	Volume Pumped [m ³]	Flow Rate [l/min]	hh:mm	Pump	Liner	Total Vol Pumped [m ³]	Total Time [hr]	Efficiency [%]
1	Pump fluid - Lead Cement - API Class G	48.20	500.00	1h:36m	T-1600	152.400	48.20	1.61	97
2	Pump fluid - HPHT - WBM	95.24	3600.00	0h:26m	T-1600	152.400	143.44	2.05	97

Figure 22: Pump schedule for cementing the annulus of the anchor casing.

The software automatically calculates the required total time and volume of the specific cement operation. The friction factors for the cased and open hole sections were set equal to those defined in the torque and drag calculation (Chapter 2.9.).

The cementing analysis was run by using the free fall option, which is important to understand the effect of density differences between the cement slurry and the drilling mud. The free fall calculation type uses the defined flow rates of the displaced fluid, drilling mud and cement slurry. The specified rate represents the minimum flow rate used to overcome the differential in fluid density between the string and the annulus when the fluids stop to move under their own weight. A graphical and tabular summary of the cementing analysis will show the transient effect on the equivalent mud weight, equivalent circulating density, surface and downhole pressure conditions and hook load while pumping (Chapter 3.4.).

2.13. Risk Parameter

The risk assessment will identify and evaluate several hazards to be encountered during realization of the IDDP-2 project. The evaluation of hazards and assessment of risks rely on information and data released in academic publications, but also the results of the different simulations in Sysdrill. The assessment is split into a technical and non-technical category with defined risk types and related hazards (Fig. 23).

The non-technical aspects of geological and geothermal risks involve hazards related to volcanism, tectonic movement, temperature and pressure conditions, heat flow, permeability and the feasibility of a supercritical reservoir. The technical aspects regarding drilling and well completion risks are basically assessed on the outcome of the simulations. These two major technical risks cover the effect of borehole conditions on the drilling process, mud properties, drilling hydraulics, well design and cement job. The process of drilling involves the probability of circulation loss and an underground blowout. Several defined load cases will help to identify and assess possible failure modes. The assessment and evaluation of risks are summarized in an assessment sheet that gives an overview about the probability, impact, severity and prevention measures of each hazard.

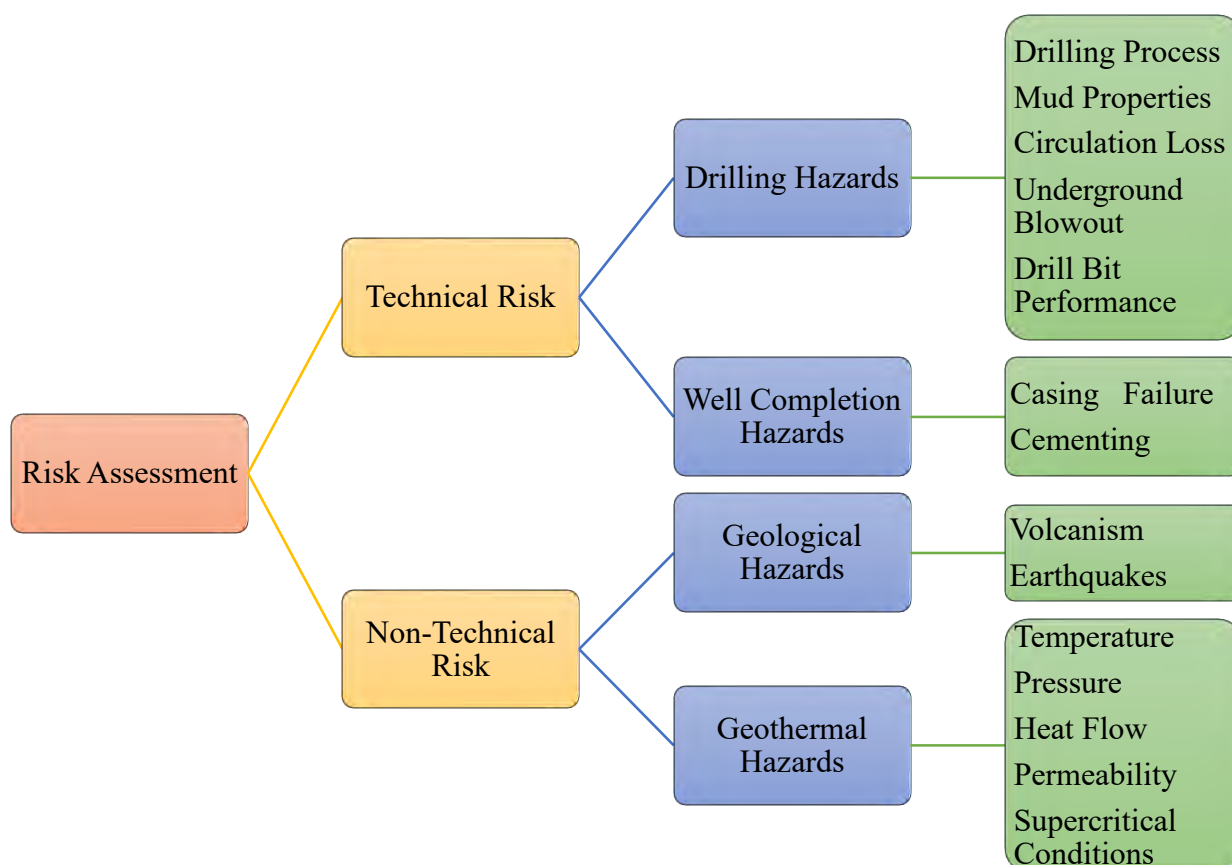


Figure 23: Hierarchical categorization of the risk assessment. The major risk types are related to several hazards

3. Results

3.1. Torque and Drag Calculation

The software summarizes the simulation of the individual operation modes in a spreadsheet, displaying the fail or pass for the tension, torque and stress categories (Fig. 24). A failure or warning for one of these aspects will be discussed in the following. The torque and drag calculations are performed under normal and abnormal conditions for the rotary drilling operation mode (Fig. 14).

Tension	Torque	Stress
Buckling	Yield	Axial
Rig Pull	Rig Max	Bending
Pipe Yield	Cxn MUT	Torsional
Cxn Yield		Hoop
		Radial
		Triaxial

Figure 24: Summary of torque and drag calculations, showing a detailed listing of different aspects of tension, torque and stress during drilling.

21" Hole – Intermediate Casing Section (110-450 m)

P_f @ 450 m = ≤ 2 bar; T @ 450 m ~ 225 °C

The tension, torque and stress limits were not reached under normal drilling conditions, indicating that the different operation modes have passed the simulation. However, the buckling hook load have exceeded the limit of the assembly (Fig. 25). This warning is a non-critical situation, but of potential concern. The true tension versus depth graph shows that the drill pipe is gradually subjected to compressional loads with increasing depth (Fig. 25). Lowering the weight on bit increases the hook load and will minimize the potential of helical buckling. The stress versus depth curve shows some 650 bar of von Mises at the surfaces, however, the yield strength of the pipe is almost ten times higher (Fig. 25). Drilling with water-based mud result to an insignificant increase of the hook load, surface torque and stress compared to the use of oil-based mud.

The simulation under abnormal conditions have shown the failure of connections because the calculated surface torque exceeds the recommended make-up torque.

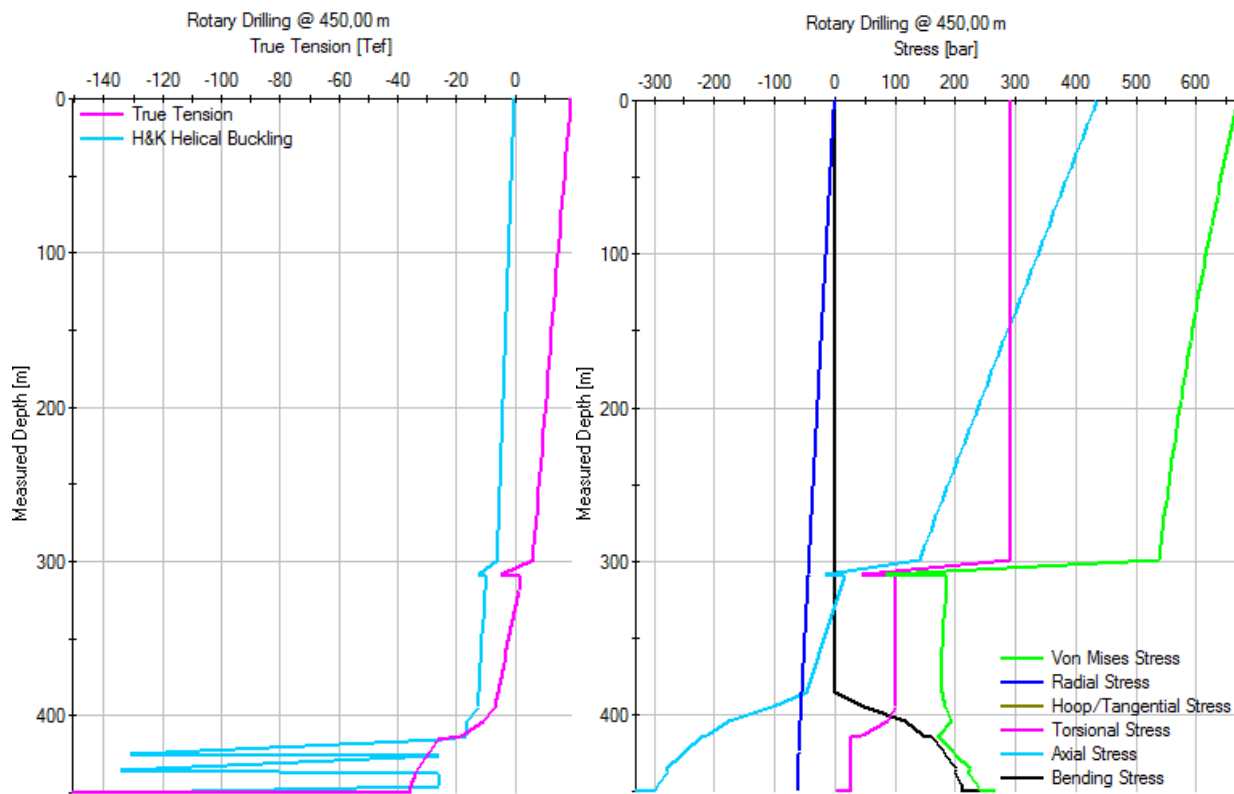


Figure 25: Graphs showing the true tension (left) and surface stresses (right) as a function of depth under normal conditions and based on the stiff string model.

17 ½" Hole – Anchor Casing Section (450-1,200 m)

P_f @ 1,200 m = 62 bar; T @ 1,200 m ~ 289 °C

The hook load, surface stress and torque have increased and show a similar behavior with depth as for the previously load case. The potential of buckling is a concern for the lower part of the drill pipe as the neutral point was determined a few decimeters above bottom. This corresponds with the location of the heavyweight drill pipes. The circulation of fluids yields to a higher hook load and a doubling of the von Mises stresses. The values are the highest when using a water-based drilling fluid (Table 12). Under abnormal conditions, the connections may fail due to high resultant bit torque at the bottom.

Table 12: Comparison of the hydraulic effect of two different fluids on the hook load, surface torque and the von Mises stress.

	Hook load (tons)	Surface torque (N·m)	Von Mises stress (bar)
Water-based mud	148	7,561	3,954
Oil-based mud	136	7,512	3,224

12 ¼" Hole – Production Casing Section (1,200-3,000 m)

P_f @ 3,000 m = 186 bar; T @ 3,000 m ~ 363 °C

The risk of buckling still exists during rotary drilling and can only be avoided by reducing the weight on bit. The surface torque has increased to 8,000 N·m, but decreases by circulating the fluids with a flow rate of 3,600 l·min⁻¹. On the other hand, an inclusion of hydraulics yielded to drill pipe failures due to excessive hoop and triaxial stresses. The hoop stress tries to split the pipe along its length. Fig. 26 shows the higher hoop and triaxial stresses compared to the yield stress of the drill assembly. The axial stress value approaches the yield stress maximum by applying a higher flow rate and may cause a collapse under even higher flow rates. The use of the oil-based mud mitigates the stress by about 1,000 bar compared to the water-based mud. Only a slow-down of the flow rate to 3,000 l·min⁻¹ or less yields to a significant reduction of the acting stresses.

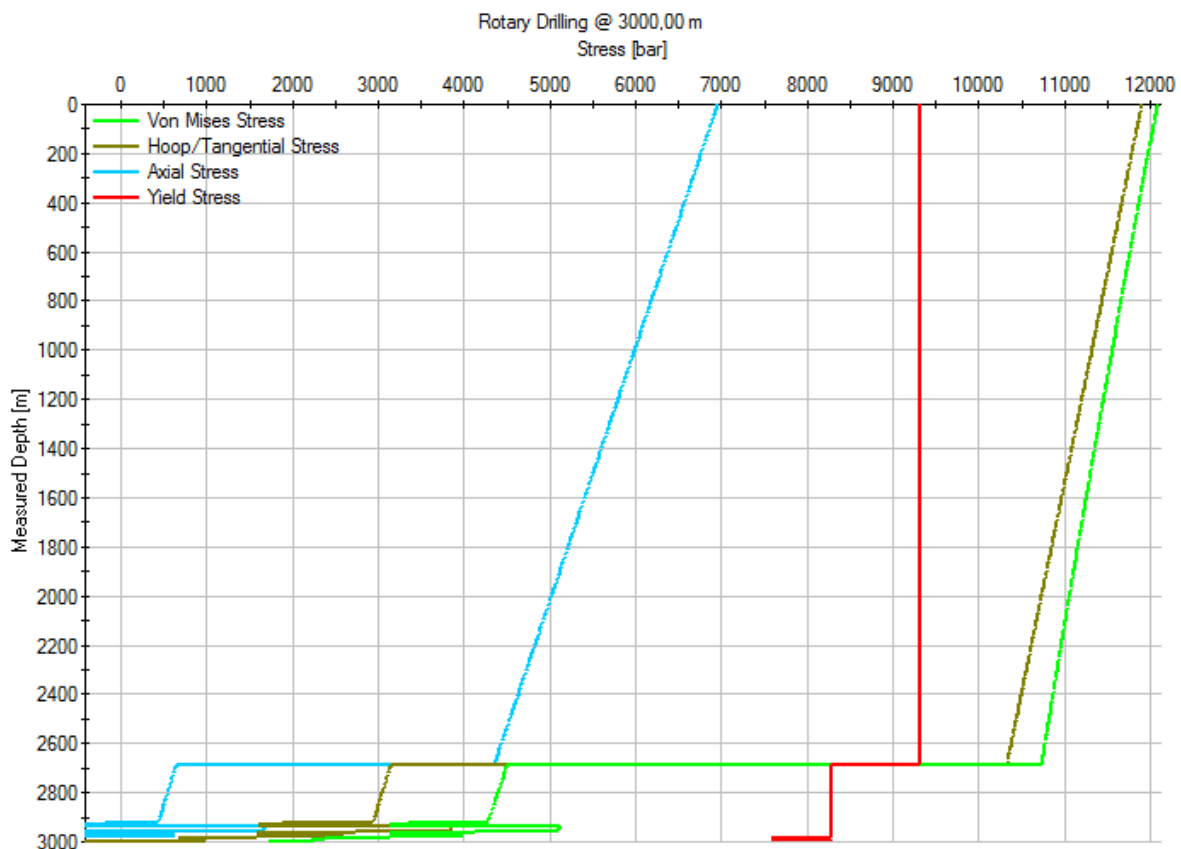


Figure 26: Graph showing the surface stress conditions for drilling the production casing section and circulation of drilling fluids at a flow rate of 3,600 l·min⁻¹.

The same applies to the other operation modes if exposed to hydraulics and high flow rates. The calculation of abnormal drilling conditions and no hydraulics have led to the warning that the surface torque exceeds the make-up torque. An inclusion of hydraulics would additionally indicate that the yield stress has been exceeded as described earlier.

8 ½" Hole – Production Liner Section (3,000-5,000 m)

P_r @ 5,000 m ~ 288 bar; **T** @ 5,000 m ~ 402 °C

The simulation indicates a potential concern of helical buckling. Table 13 shows a lower von Mises stress at 5,000 m depth than drilling to 3,000 m.

Table 13: Calculation results of the 17 ½" and 8 ½" hole sections under normal conditions.

Normal conditions @ 3,600 l·min ⁻¹ & OBM	Hook load (tons)	Surface Torque (N·m)	Von Mises Stress (bar)
@ 3,000 m	276	7,553	6,473
@ 5,000 m	189	7,572	4,095

The circulation of either oil-based or water-based mud at a flow rate of 3,600 l·min⁻¹ did not result to a stress failure mode as described for the 17 ½" hole calculation (Fig. 27).

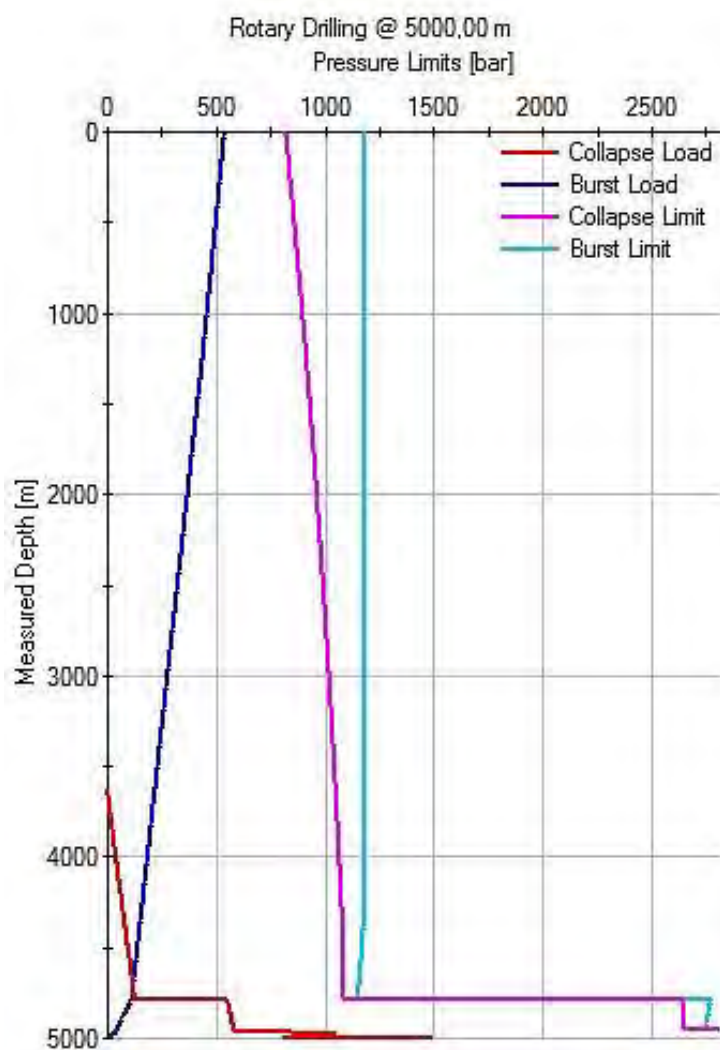


Figure 27: Collapse and burst pressure profile of drilling the production liner section to 5,000 m depth.

The simulation of abnormal conditions led to a torque warning which refers to the make-up torque of the connection. A slight increase of the von Mises stress could be observed, but it is of no concern for any stress failure. The use of water-based mud as the circulating fluid increases the surface stress by about 200 bar.

3.2. Hydraulics Calculation

Initially, the hydraulics calculations were run by circulating the water-based mud at a static flow rate of $3,600 \text{ l}\cdot\text{min}^{-1}$. The fluid was circulated in consideration of temperature effects according to the geothermal gradient and the specific heat coefficients and thermal conductivities (Chapter 2.10). Temperature modelling was conducted with a static mud inlet and air temperature of 15°C . The hydraulics calculation for each section basically follows the example input dialog in Fig. 15. The above mentioned flow rate and circulating time were changed in order to investigate the effects on the annulus and string temperature profile.

21" Hole – Intermediate Casing Section (110-450 m)

The hydraulics calculation was performed according the input dialog shown in Fig. 15 of Chapter 2.10. The total bit flow area of 3.10 cm^2 was calculate by assuming five nozzles. This value plus the flow rate are the basic input data to perform the pump pressure calculation option in order to determine the required pump pressure to circulate. The calculation has yielded to a maximum pump pressure of 323 bar, which is close to the maximum operating pressure of the T-1,600 triplex pump with a liner diameter of 6". Despite the high values a failure of the pump is not expected. The equivalent circulating density of the $1,400 \text{ kg}\cdot\text{m}^{-3}$ drilling mud exceeds the fracture gradient along the whole section (Fig. 28). The pressure profile while shows an identical gradient to the equivalent circulating density while running the assembly into the hole. A swab operation or pulling out of the hole shows the lowest equivalent mud weight (Fig. 28).

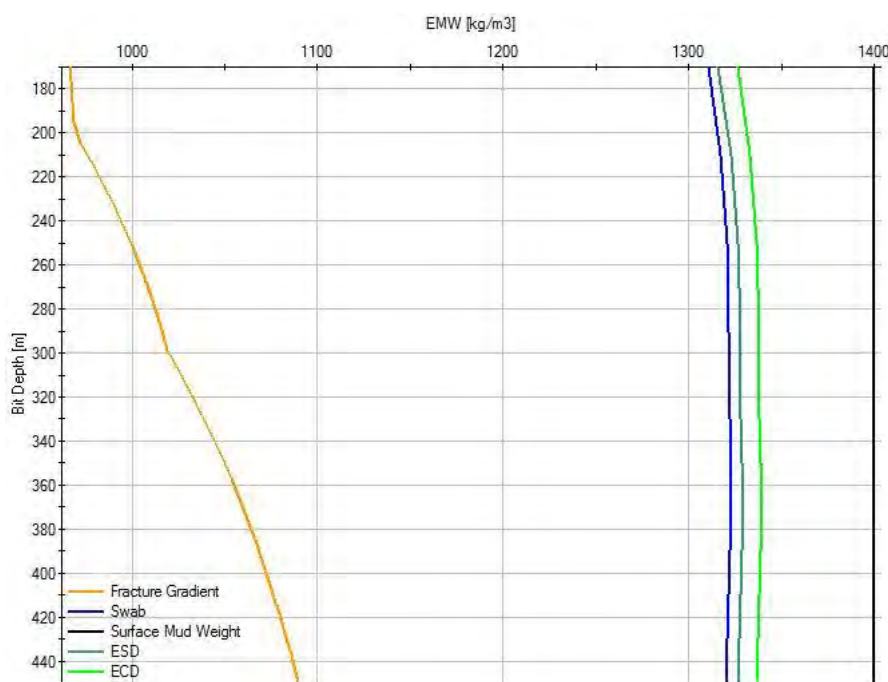


Figure 28: Graph showing the equivalent mud weight during drilling succeeds. The equivalent static and circulating densities exceed the fracture gradient along the intermediate casing section.

The equivalent mud weight versus bit depth profiles indicate that the hydraulics calculation have failed for the circulation of the defined drilling mud.

A circulation of fluids at a flow rate of $3,600 \text{ l}\cdot\text{min}^{-1}$ and for one hour has a major effect on the temperature distribution inside the pipe and annulus (Fig. 29). It can be seen that the string and annular temperature profiles are almost straight and identical at about $130 \text{ }^\circ\text{C}$. The circulating temperatures are greater than the constant density temperatures indicating that the fluid is less dense than the surface mud weight.

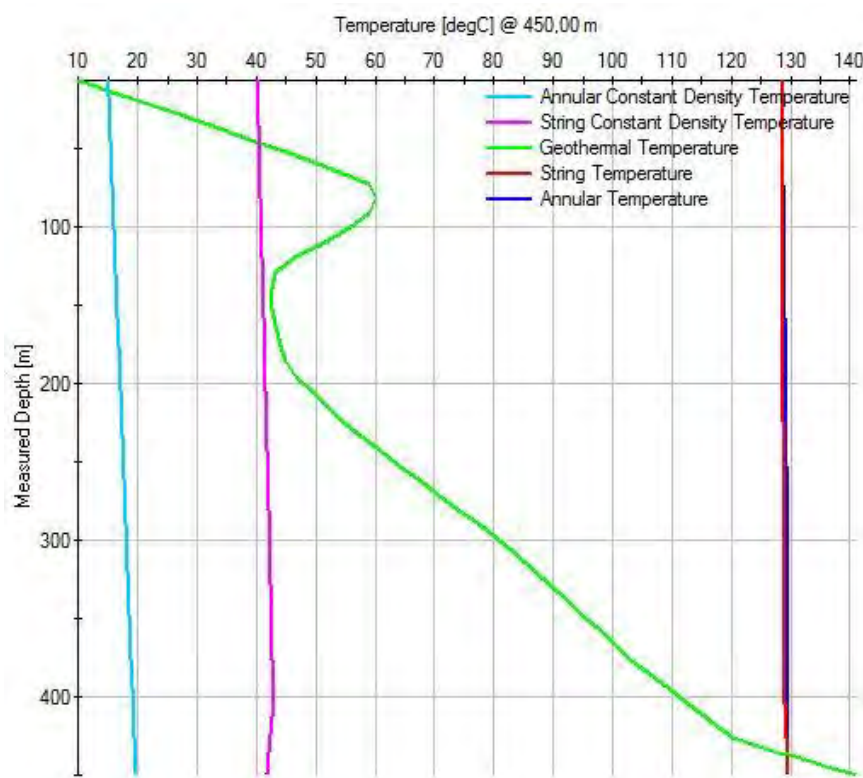


Figure 29: Temperature profiles showing the string and annular temperature after circulating for one hour. The constant density temperature profiles represent the temperature at which the thermal expansion effect is equal to the compressibility effect.

Simulation of hole cleaning has led to a successful and sufficient cuttings transport ratio and cuttings concentration within the annulus. The change of the flow rate has a significant effect on the equivalent mud weight, string pressure and the temperature in the pipe and annulus. A flow rate of $1,800 \text{ l}\cdot\text{min}^{-1}$, half of the initially defined rate, shows a reduced string pressure at the bottom by a factor of three. On the other hand, the equivalent mud weights increase and approach to the initial surface mud weight. The string and annular temperature decreased by approximately $50 \text{ }^\circ\text{C}$. A longer circulating time shifts the profiles again towards higher temperature, however, the effect is low with little temperature increase when extending the circulating time to 20 hours or more. The use of an oil-based mud did not show significant changes in the pressure, equivalent mud weight or temperature profile. Generally, the pressure and temperature has increased a little, but negligible.

17 ½" Hole – Anchor Casing Section (450-1,200 m)

The simulation has indicated any failure mode to occur during fluid circulation at a rate of $3,600 \text{ l}\cdot\text{min}^{-1}$. Fig. 30 shows that the equivalent circulation density decreased to $1,071 \text{ kg}\cdot\text{m}^{-3}$ at the bottom and is therefore below the fracture gradient. A lower flow rate of $1,800 \text{ l}\cdot\text{min}^{-1}$ would lead to fracturing due to exceeding equivalent mud weights above 600 m depth. Thus, the surge and swab operations also resulted in a failure mode.

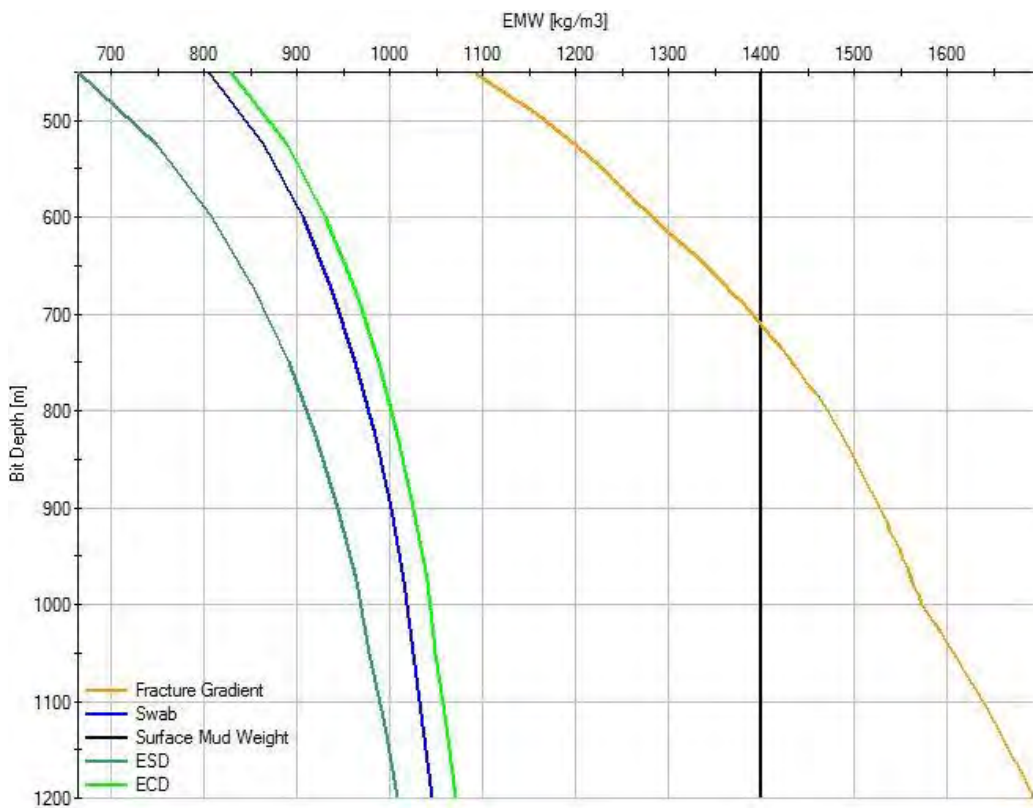


Figure 30: Equivalent mud weight versus bit depth during drilling of the anchor casing. The gradient of the equivalent circulating density increases less than the fracture gradient.

In order to keep the flow rate constant at $3,600 \text{ l}\cdot\text{min}^{-1}$, a pump pressure in the range of 800-1,040 bar is required for this section. The pressure exerted to the string peaks at 1,110 bar which is a factor of more than five higher beyond the fracture pressure at the bottom. Similar to the previous calculation, the reduced flow rate yields to only one third of the string pressure.

The temperature modelling under a high flow rate of $3,600 \text{ l}\cdot\text{min}^{-1}$ and no considered circulation time delivers a moderate temperature profile inside the anchor casing (Fig. 31). Both temperature profiles increase slightly and reach a maximum temperature of $70 \text{ }^\circ\text{C}$ at the bottom of the section. As said earlier, this would result to a failure mode and potential fracturing of the intermediate casing shoe.

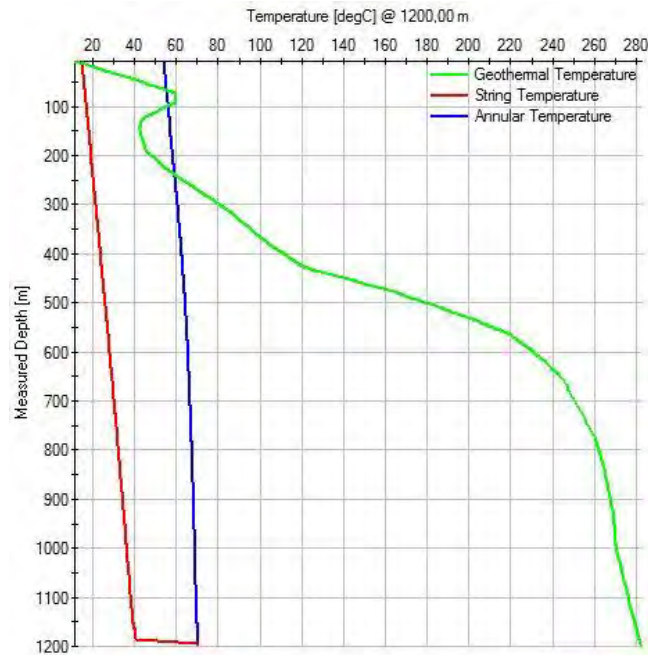


Figure 31: Temperature profile for the string and annulus at a flow rate of 3,600 l·min⁻¹.

12 ¼" Hole – Production Casing Section (1,200-3,000 m)

The fracture gradient along this section lies above 1,700 kg·m⁻³ and is therefore high enough to withstand the mud weight. On the other hand, the string is exposed to an increased pressure of 1,620 bar from the inside. This string pressure is highly influenced by the total flow area of the drill bit. An increase of the flow area from 1.66 to 4 cm² reduces the maximum string pressure to 930 bar (Fig. 32). The pressure, exerted by the equivalent circulating density lies within the margin of the pore and fracture pressure.

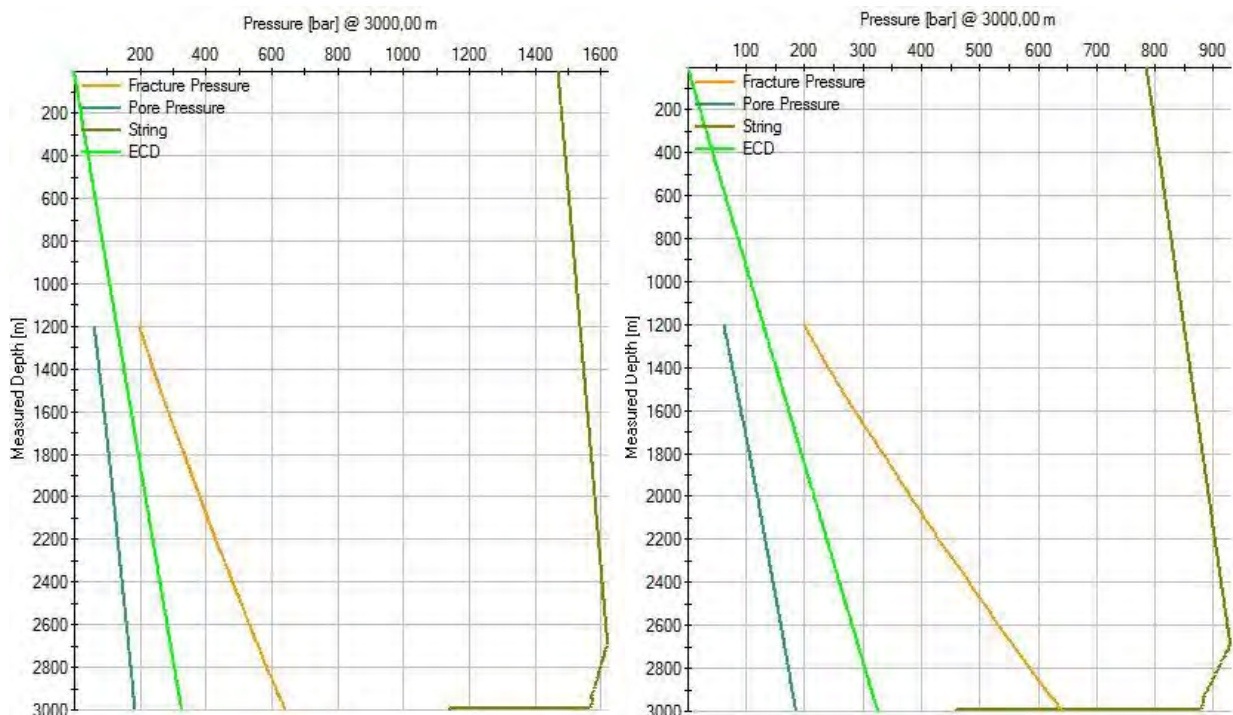


Figure 32: Pressure profiles for a total bit flow area of 1.66 cm² (left) and 4 cm² (right).

The thermal effect of circulating the fluid at a constant flow rate of $1,800 \text{ l}\cdot\text{min}^{-1}$ is shown in Fig. 33. As can be seen, the temperature at the bottom of the section rises up to $150 \text{ }^\circ\text{C}$.

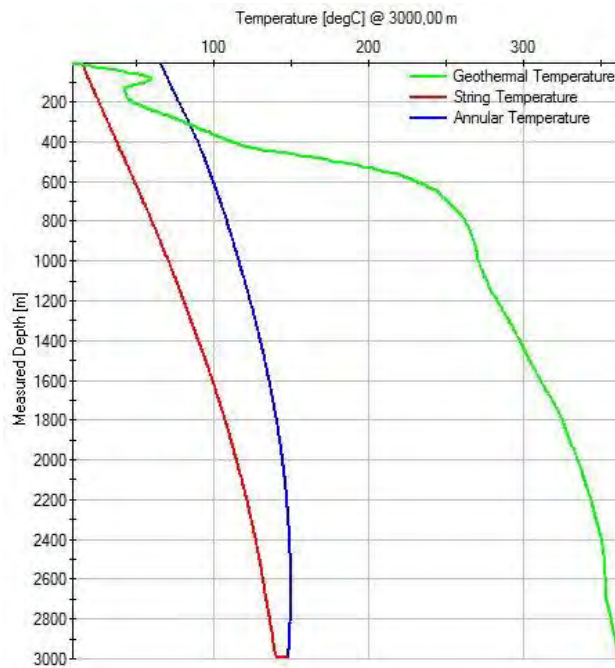


Figure 33: Graph showing the temperature profiles for the string and annulus if circulating at a moderate flow rate of $1,800 \text{ l}\cdot\text{min}^{-1}$

The circulation of fluids, either water- or oil-based fluids, result to any failure mode neither under a high flow rate nor after a long exposure of fluid circulation. A special concern is given to the extremely high temperatures of the mud when circulating with high flow rates.

8 1/2" Hole – Production Liner Section (3,000-5,000 m)

The following Fig. 34 summarizes the initial input parameters for calculating the hydraulics of the production liner which will be exposed to the expected reservoir at 5,000 m depth of IDDP-2. The below check box express that the simulation was successful and no limit was exceeded. The simulation of the thermal effect on the geothermal gradient shows that the string and annulus is exposed to high temperatures from bottom to top.

Wellbore		Wellpath		5020.00 m Assembly		8 1/2" Hole Perforated Liner Section		Rig		InnovaRig GFZ					
Inputs Circulating Fluid															
Calculate	Pump Pressure	Range Calc		<input checked="" type="checkbox"/>		Riser Booster		<input type="checkbox"/>							
Pump Pressure		kPa		Flow Rate				l/min							
Flow Rate	3600,00	l/min	Start Depth	3000,00	m	<input checked="" type="checkbox"/>		Annulus Loaded							
Bit TFA	8,00	cm ²	End Depth	5000,00	m	Rock Density	2500,00	kg/m ³	Cuttings Diam.	12,000	mm	Penetration Rate	2,50	m/hr	
Bit Pressure Loss		%	Depth Interval	200,00	m	<input type="checkbox"/>		Swab/Surge							
Pump	T-1600		Rows	10		RIH		m/min	POOH		m/min	<input type="checkbox"/> Closed Pipe <input type="checkbox"/> Open Pipe			
Liner	152,400	mm	Annular Pressure		kPa	<input checked="" type="checkbox"/>		Temperature Effects				Mud Temp. In	15,00	degC	
				Circulating Time		0h-0m						Riser Inlet Temp.		degC	
				Pit Volume		30000,00		l				Air Temp.	15,00	degC	
Pressure		Pump Pressure		<input checked="" type="checkbox"/>		Hole Cleaning		Cuttings Transport Ratio		<input checked="" type="checkbox"/>		Cuttings Transport Ratio (Riser)		<input checked="" type="checkbox"/>	
Density		ESD		<input checked="" type="checkbox"/>		Trip		Swab		<input checked="" type="checkbox"/>		Cuttings Concentration		<input checked="" type="checkbox"/>	
		ECD		<input checked="" type="checkbox"/>				Surge		<input checked="" type="checkbox"/>		Cuttings Concentration (Riser)		<input checked="" type="checkbox"/>	

Figure 34: Up: Database and additionally checked options for the simulation. Down: Summary of the simulation results.

The below comparison of temperature profiles show the effect after a high flow rate of 3,600 $\text{l}\cdot\text{min}^{-1}$ and a moderate rate of 1,800 $\text{l}\cdot\text{min}^{-1}$ (Fig. 35). The higher the flow rate the less exposed the drilling assembly towards high temperatures.

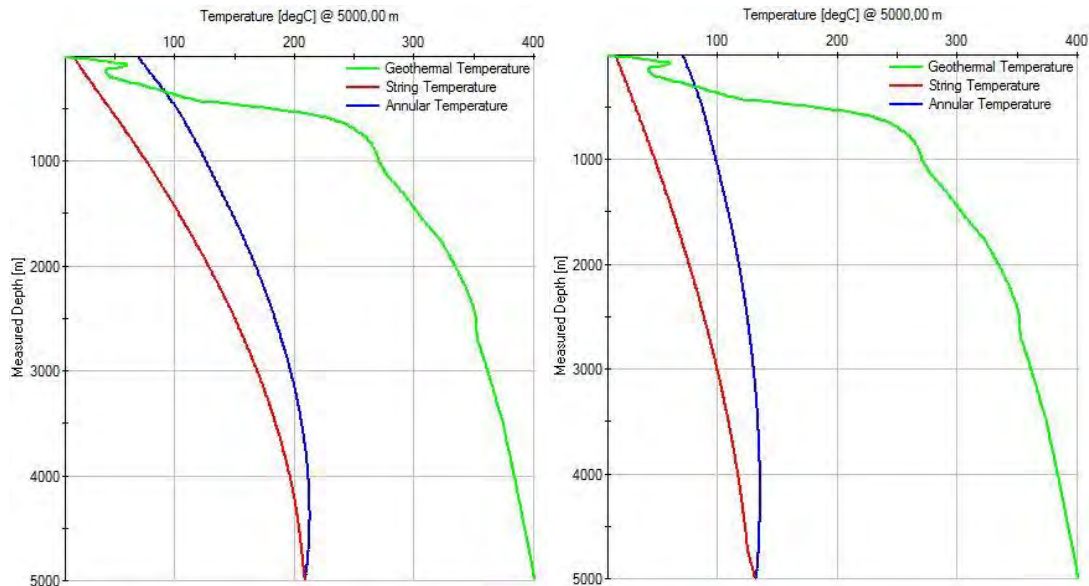


Figure 35: Graphs showing the effect of different flow rate to the temperature distribution along the hole section. A flow rate of 1,800 $\text{l}\cdot\text{min}^{-1}$ (left) gives a higher temperature than circulating the fluids at a static rate of 3,600 $\text{l}\cdot\text{min}^{-1}$ (right).

Another effect is expressed in the required pump pressure in order to keep the static flow rate. At the final depth of the well, a pump pressure of 455 bar is necessary to pump the fluids, whereas only one third is required if circulating with a reduced flow rate. Same as other calculations, the string pressure exceeds the fracture pressure at any depth. A greater nozzle size increases the total flow area of the bit and consequently reduces the string pressure. Fig. 36 demonstrates the approach to increase the total flow area to such values that the pressure inside the string becomes less than the fracture pressure. A minimum of 8 cm^2 is necessary when circulating under the high flow rate. At a low flow rate, an area of 1.8 cm^2 seems to be adequate.

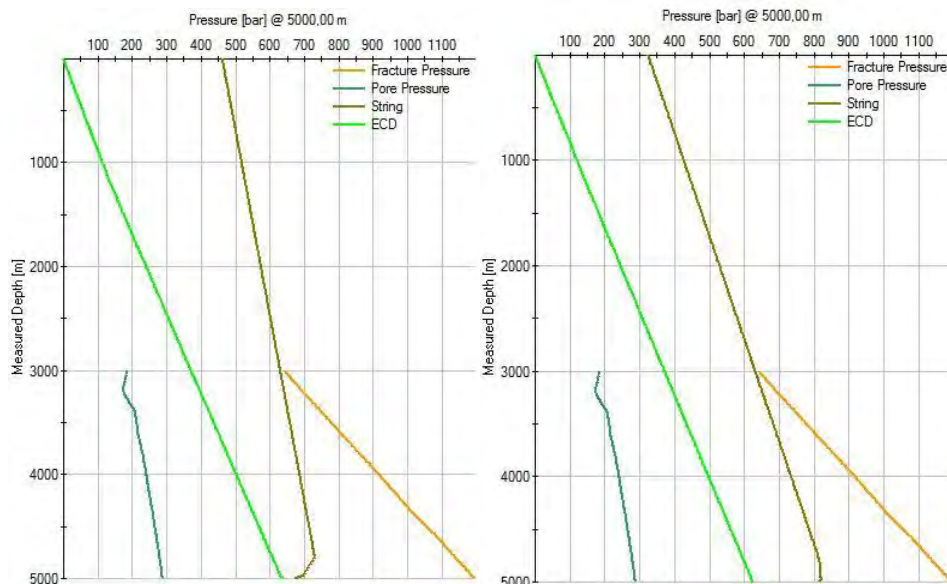


Figure 36: Graphs showing the string pressures at a high (left) and low (right) flow rate. A minimum of 8 cm^2 is required to keep the string pressure below the fracture pressure at a high flow rate. At a low flow rate, a total flow area of 1.8 cm^2 is adequate.

3.3. Casing Analysis

Each of the following casing section analyses will cover a selection of the defined load cases. If not stated otherwise, the results refer to the initially set calculation options, fluid densities and load case conditions (Chapter 2.11.).

18 5/8" – Intermediate Casing Section (110-450 m)

The intermediate casing section has passed the simulation and withstands the different load cases. A summary of the load case results points out, that collapse is the most possible failure mode to occur along the section. The minimum safety factor of 1.28 refers to a fully evacuated casing string which could fail due to collapse at a depth of 110 m (Table 14). The burst/ tension load case shows that a collapse failure is also likely to occur around the casing shoe.

Table 14: Load case summary for the intermediate casing section. The values and words highlighted in red signal considerable risks of failure.

Load Case	Min SF/DF Failure Mode	Min SF/DF @ Depth (m)	Safety Factor	Design Factor	Min SF/DF Component
Burst/ Tension	Collapse	450	1.31	1.25	Coupling
Collapse – Fully Evacuated	Collapse	110	1.28	1.25	Coupling
Collapse – Circulation loss	Collapse	110	2.17	1.00	Coupling
Tension/ Running	Collapse	450	8.16	1.25	Coupling
Worst Case	Collapse	110	1.28	1.25	Coupling

Fig. 37 shows that a possible collapse failure is most likely to occur where the design factor rated collapse load is closest to the pipe yield. The potential failure mode refers to the K-55 coupling with a collapse resistance or coupling yield of 24 bar.

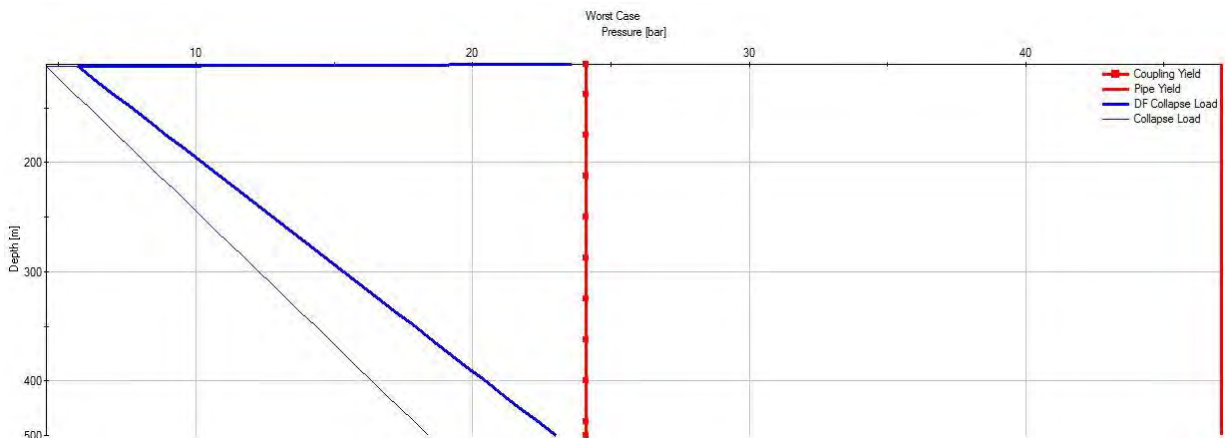


Figure 37: Worst case summary of all simulated collapse load curves. The coupling yield refers to the collapse resistance.

A drilling mud density lower than $1,400 \text{ kg}\cdot\text{m}^{-3}$ will not be able to withstand the external pressure and will inevitably lead to a collapse failure. The other failure modes, like axial, burst or triaxial are of no potential concern, since the margin between the safety and design factor is greater than for collapse.

13 $\frac{5}{8}$ " – Anchor Casing Section (450-1,200 m)

The summary plot of design versus safety factor of the worst case shows that all load cases meet the design criteria for burst, collapse and triaxial (Fig. 38). The axial mode is not displayed, as the margin is too large and therefore of no concern for this section.

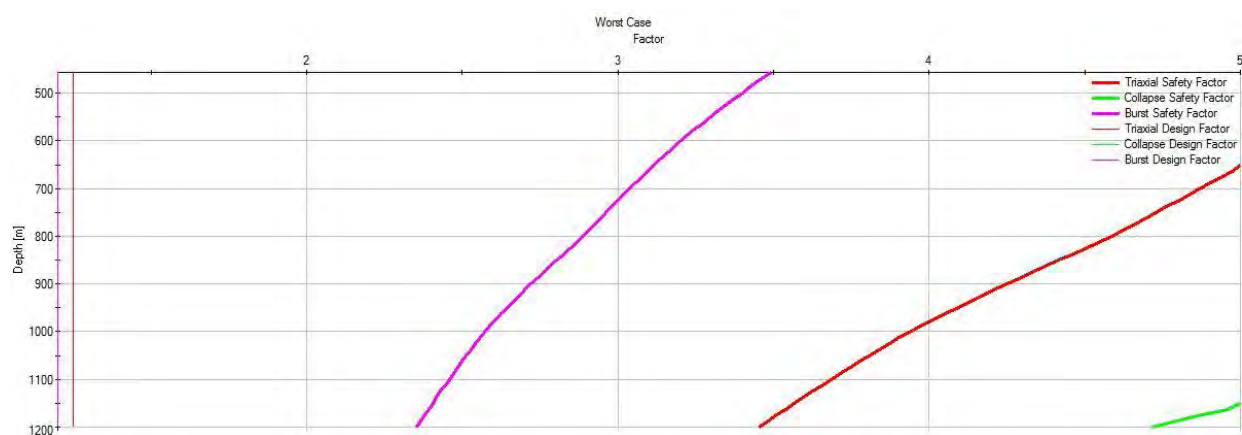


Figure 38: Curves summarizing the simulated safety factor for all possible failure modes, except for axial compression or tension.

The higher safety factors of the triaxial and burst failure modes are related to the kick load case. The internal pressure profile shows that an influx of 5 m^3 of geofluids would diminish on its way up the pipe. A higher volume of 50 m^3 yields to a reversed internal pressure profile and an increased pressure at the intermediate casing shoe (Fig. 39).

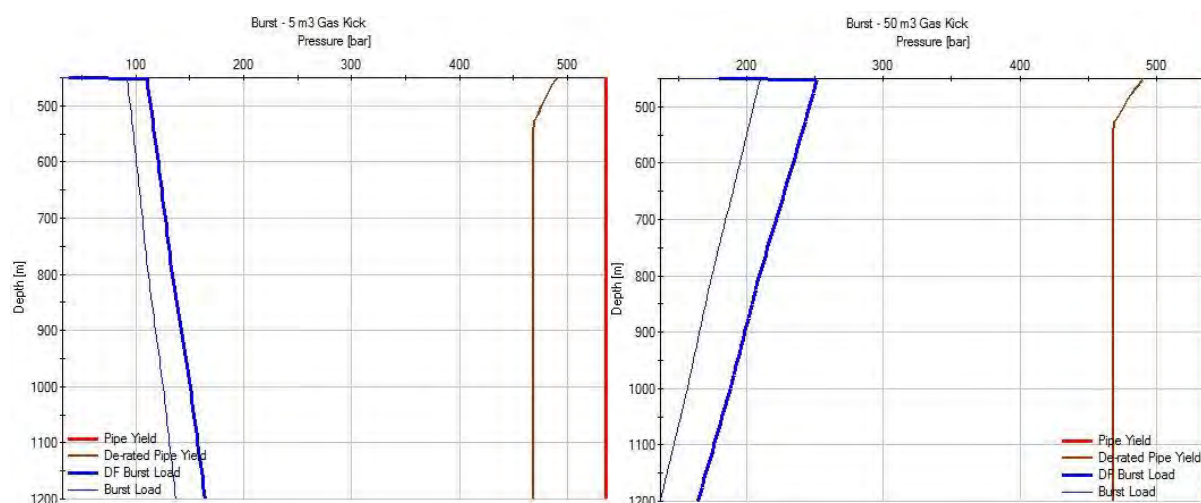


Figure 39: Internal pressure profiles of the burst – 5 m^3 kick load case (left) and the simulation of a kick with a volume of 50 m^3 (right).

A potential triaxial failure mode exists for the $86 \text{ lb} \cdot \text{ft}^{-1}$ casing joint in particular. The ellipse of plasticity visualizes that the burst and tension loading occurs in combination when a gas volume has entered the pipe (Fig. 40). A higher volumetric influx of gas would increase the internal pressure or burst load at constant tension load and consequently shifts the load curve closer to the connection limit. A loss of circulation in combination with a mud drop could result to a triaxial failure mode as well.

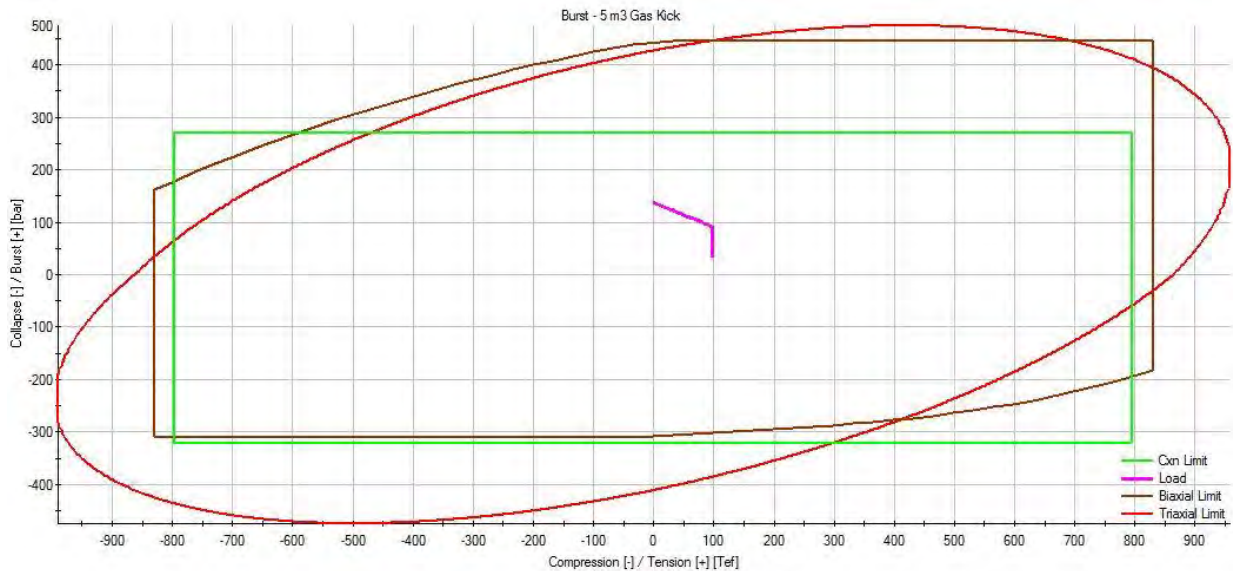


Figure 40: Ellipse of plasticity showing the combined load and the failure mode limits of the 5 m^3 kick load case.

In addition to the potential of triaxial failure, exists a possible casing collapse due to a fully evacuated string or during the pipe installation. The minimum safety factor for the collapse failure mode is with 4.72 still not close to the design factor of 1.25, however, a small additional external pressure load rapidly increases the potential of failure.

9 5/8" – Production Casing Section (1,200-3,000 m)

The simulation has revealed several failure modes, especially due to an influx of geofluids and circulation loss (Fig. 41). Both load cases have result to a burst and triaxial failure mode. The axial and collapse design criteria were meet by all load cases but show a potential to exceed the load limit in case of additional unexpected external or internal pressure (Fig. 42). A gas influx of 5 m^3 would result to a high internal pressure of 450 bar at the casing shoe which causes a burst load that exceeds the de-rated yield strength of the K-55 casing joint by 123 bar.

Load Case	Axial	Burst	Collapse	Triaxial
Burst - 5m ³ Gas Kick	✓	✗	✓	✗
Burst/Tension	✓	✓	✓	✓
Collapse - Fully Evacuated	✓	✓	✓	✓
Collapse - Lost returns with mu	✓	✗	✓	✗
Tension -Running	✓	✓	✓	✓

Figure 41: Pass and fail summary of load case calculations.

The high temperature reduced the burst resistance from 375 to 328 bar and makes the casing prone to burst in case of a mud drop in the annulus and a subsequent drop of the external pressure. The pipe yield under normal conditions would be sufficient to withstand a burst.

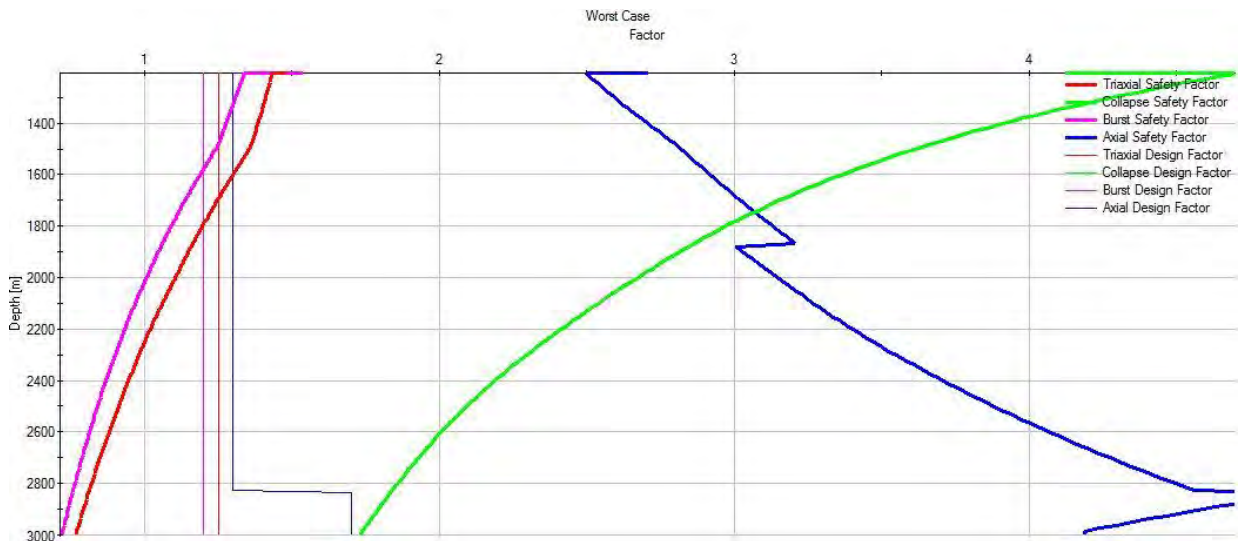


Figure 42: Relationship between the design factors and the calculated safety factors for axial, burst, collapse and triaxial analysis categories. The factors include the simulation results of all load cases. The collapse design factor curve is overlapped by the triaxial design factor

The triaxial failure is linked to the combined burst load and occurs in case of an influx of geofluids or due to a loss of circulation. A failure mode of concern is a collapse due to a full evacuation of the pipe (Fig. 43). The simulation has shown that the casing would collapse under an additional external pressure of around 70 bar. The collapse and burst resistance of the casing joints dictates the failure modes along the production casing interval.

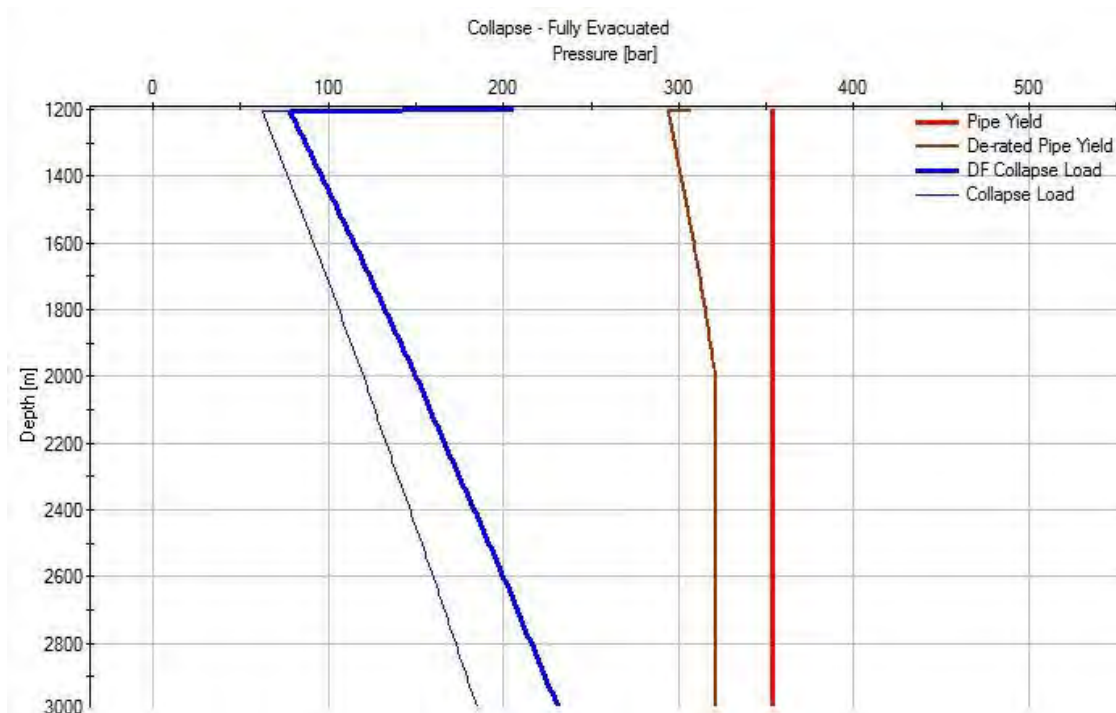


Figure 43: Graph showing the external pressure profile in case of a fully evacuated casing string. An additional 70 bar of external pressure would exceed the de-rated pipe yield limit.

7" – Production Liner Section (3,000-5,000 m)

The previously described collapse potential for a fully evacuated casing string is an actual failure mode for the production liner section (Fig. 44). The external pressure exceeded the de-rated pipe yield at a depth of around 4,000 m and increased to 288 bar at the casing shoe. The ellipse of plasticity in Fig. 44 shows that the combined tensional and external stresses affect both string elements, the casing joints and the couplings, and provokes a triaxial failure mode. The use of L-80 API grade for the couplings and joints would meet the design criteria for the burst and triaxial failure modes.

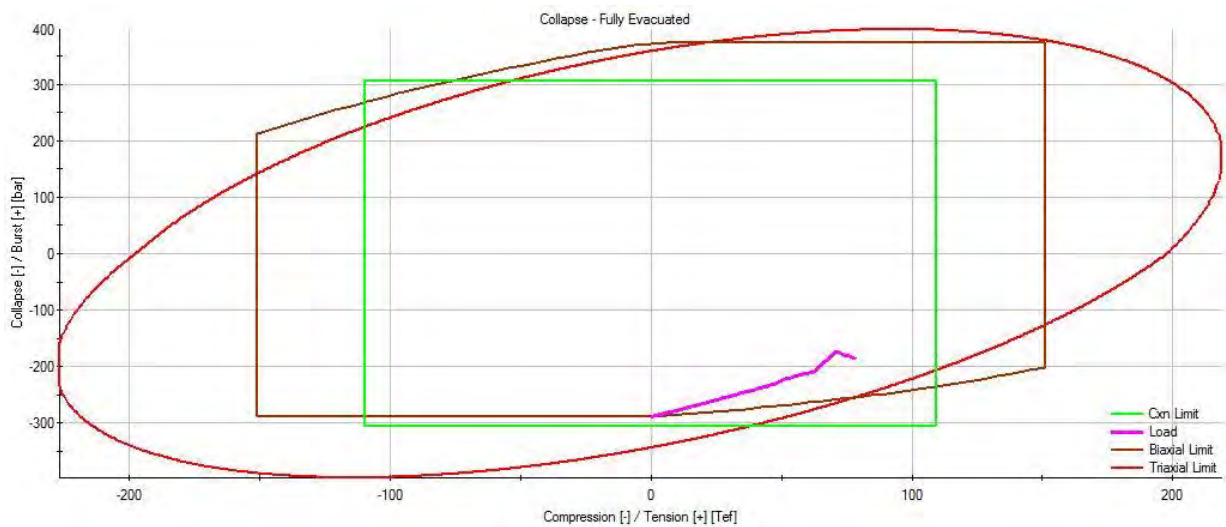


Figure 44: Ellipse of plasticity shows the collapse and triaxial failure modes for a fully evacuated production liner.

Another triaxial failure mode has been detected for the case of circulation loss and a subsequent mud drop. The excessive internal pressure exerted by the drilling mud inside the casing string has led to a burst of the casing joints and couplings along the entire liner section (Fig. 45). The extreme downhole conditions have a high effect on the pipe and coupling yield as the de-rated limits show.

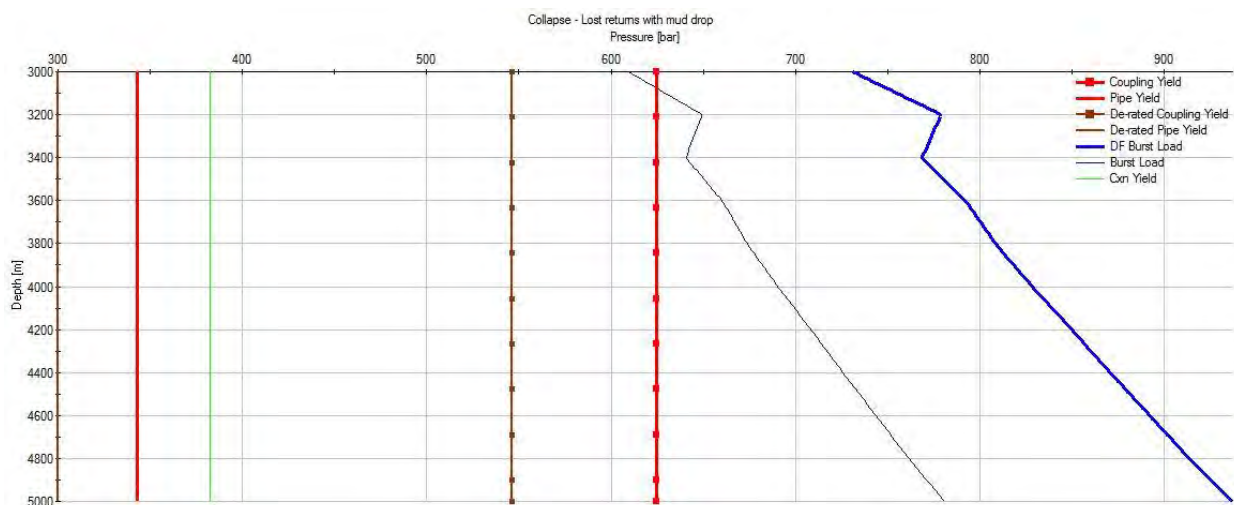


Figure 45: Internal pressure profile illustrating the burst failure mode after a circulation loss and drop of the mud level in the annulus.

3.4. Cementing Analysis

In the following, the cementing job results of the intermediate, anchor and production casing sections are shown. Initially, the calculation was run with both drilling fluids and a fixed flow rate of $500 \text{ l}\cdot\text{min}^{-1}$ for the cement slurry and $3,600 \text{ l}\cdot\text{min}^{-1}$ for the drilling fluids. These flow rates were changed to investigate the effect on surface and downhole parameters.

18 5/8" – Intermediate Casing Section (110-450 m)

Initially, the free fall calculation was run to pump a volume of 21.50 m^3 of cement slurry to fully fill the annulus from casing shoe to surface. Fig. 46 shows the pumped volume, flow rate and pump time as defined in the fluid and pump schedule.

5020.00 m Assembly 18 5/8" - Intermediate Casing Rig InnovaRig GFZ													
Inputs		Fluids		Pump Schedule		Friction Factors & Tortuosity		Hole Volume		Pipe Capacity		Annular Volume	
								93002.0 l		71718.6 l		21283.4 l	
Operation	Fluid	Volume Pumped [m ³]	Flow Rate [l/min]	hh:mm	Pump	Liner	Total Vol Pumped [m ³]	Total Time [hr]	Efficiency [%]				
1 Pump fluid	Lead Cement - API Class G	21.50	500.00	0h-43m	T-1600	152.400	21.50	0.72	97				
2 Pump fluid	HPHT - WBM	71.72	3600.00	0h-19m	T-1600	152.400	93.22	1.05	97				

Colour	Name	Volume [l]	Volume in Hole [l]	Fluid Density [kg/m ³]	Fluid Model	PV [mPa.s]	YP [Pa]
1	Displaced Fluid	260994.69		1400.00	Bingham Plastic	32.00	5.27
2	Lead Cement - API Class G	21283.41	21283.41	1750.00	Bingham Plastic	29.00	23.00
3	HPHT - WBM	71718.67	71718.67	1400.00	Bingham Plastic	32.00	5.27

Figure 46: Up: Pump schedule for cementing the intermediate casing section from casing shoe to surface. Down: Fluid schedule including the displaced fluid, cement slurry and the drilling fluid to be pumped at least.

The cement job was successful after one hour and has pumped a total volume of 93.22 m^3 . The use of above defined densities for the fluid and cement yields to a maximum equivalent circulation density of $2,023 \text{ kg}\cdot\text{m}^{-3}$, which exceeds the fracture gradient along and at the bottom of the hole. The pumping of cement slurry into the hole tends to a higher flow rate than planned and peaks at $2,250 \text{ l}\cdot\text{min}^{-1}$ when the total volume of the slurry has entered the borehole. The subsequent pumping of drilling fluid requires a lower flow rate than planned (Fig. 47). The entry of the cement slurry into the annulus comes along with an abrupt increase of the surface pressure and a reduced string hydrostatic pressure.

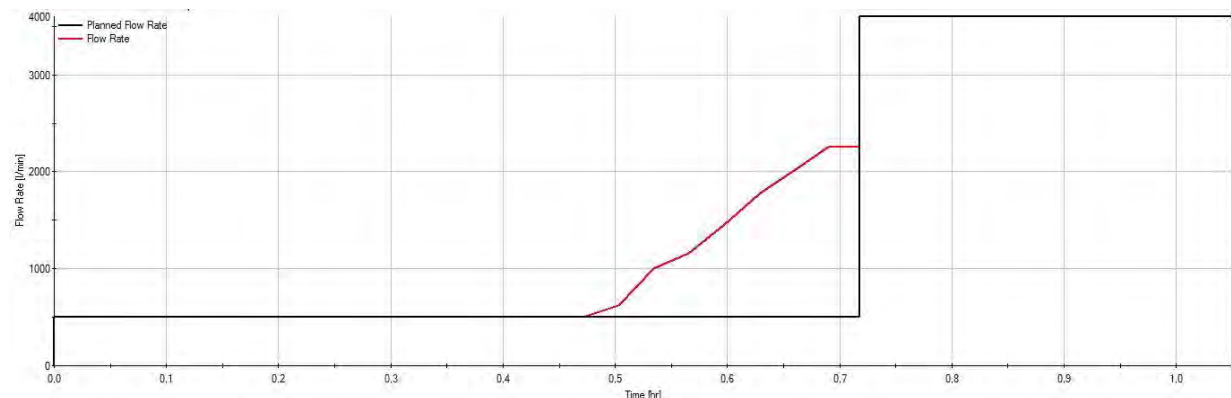


Figure 47: Chart displaying the planned and actual flow rate of the free fall calculation.

At the same time, the annular pressure loss steadily increases from 3 to about 12 bar during pumping of the cement slurry (Fig. 48). By pumping the cement slurry out of the hole and into the annulus decreases the hook load from approximately 92 to 88 tons at the end of the cementing job. In order to simulate the effect of the flow rate on the calculation results, the cement slurry was pumped at the same rate as the drilling fluid. The comparison has shown that the effect on the results is marginal and is mainly obvious in a smoothed dynamic profile of the surface pressure, ECD gradient and hook load. This effect is in the same way valid for the following cementing calculations.

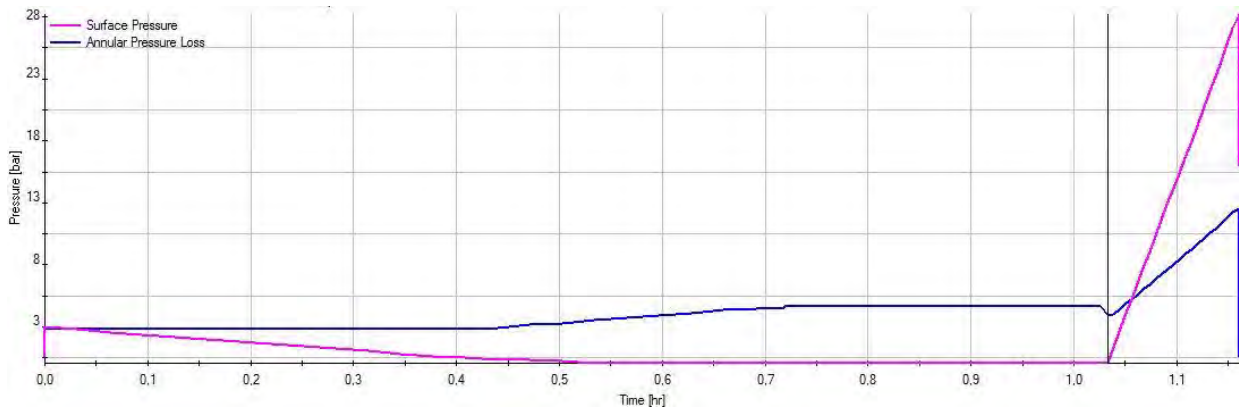


Figure 48: Chart showing the surface pressure and annular pressure loss during cementing of the intermediate casing and by the use of the free fall calculation. The black vertical line indicates the entry of cement into the annulus.

The use of the oil-based drilling mud instead of the water-based fluid leads to a different development of the surface and bottomhole pressures during pumping. The below Fig. 49 shows the surface pressure curve by pumping the oil-based mud into the intermediate casing and indicates an elevated pressure profile compared to the results when using the water-based fluid (Fig. 48). On the other hand, both calculations result to almost similar peak pressures at the end. The same behavior is valid for the bottomhole pressure profile. The pumping of oil-based mud throughout the calculation has led to a lower flow rate than planned. Other parameters, such as hook load or ECD, did not result to significant changes. These observations have also been found in the following calculation of the anchor and production casing sections.

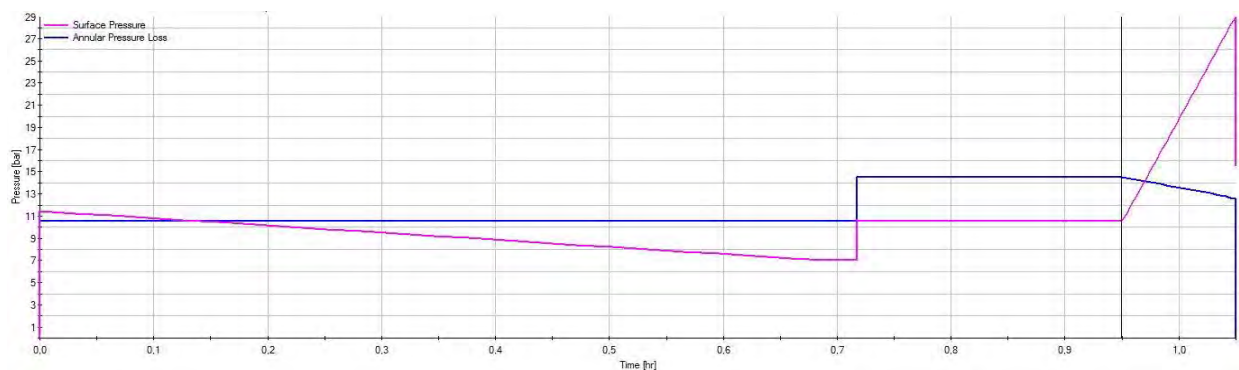


Figure 49: Chart showing the surface pressure and the annular pressure loss during cementing of the intermediate casing and by the use of the free fall calculation. The black vertical line indicates the entry of cement into the annulus.

13 5/8" – Anchor Casing Section (450-1,200 m)

The final design of the cementing job, as shown on the right hand side, does not express the actual situation at that stage. Previously, the intermediate casing section was cemented from its casing shoe at 450 m depth up to the surface (Fig. 50). This situation is not displayed in this schematic as the space between the intermediate and surface casing is filled with the displaced fluid. The software does not transfer the setting of the previously cemented casing section, but simplifies the calculation by assuming that the entire volume between the next and previous casing is fully filled with the displacement fluid. In reality, cement would have been placed between the intermediate and surface casing section. Thus, the volume of the displaced fluid and, consequently, the total volume is lower than calculated.

The anchor casing section was cemented just below the previous intermediate casing shoe as proposed by INAGSON et al. (2015). The simulation shows that the gradient of the equivalent circulating density exceeds the fracture gradient along the section. The fracture gradient increases more rapidly with depth and both gradient curves approach towards the bottom of the section (Fig. 42).

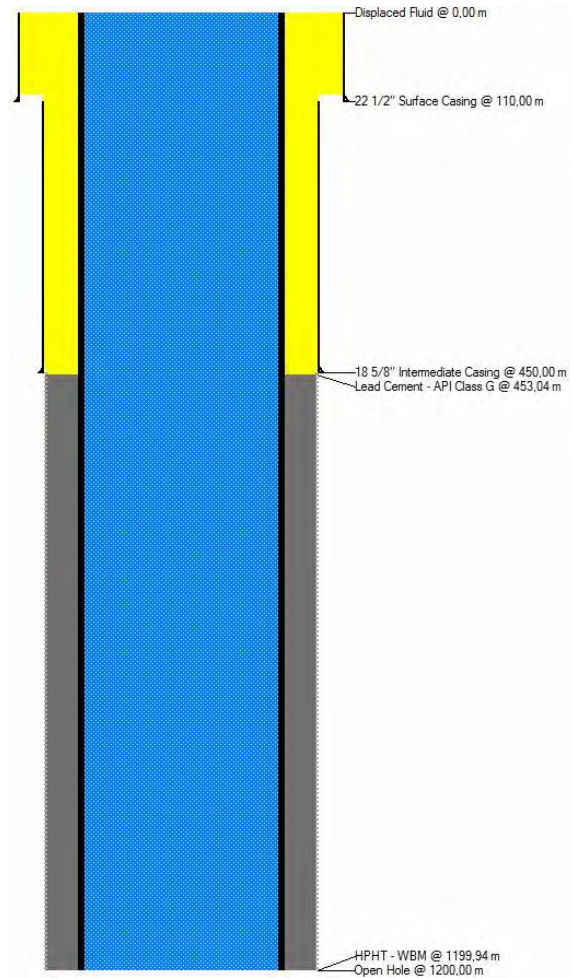


Figure 50: Fluid schematic of the borehole and top of the cement slurry in the annulus.

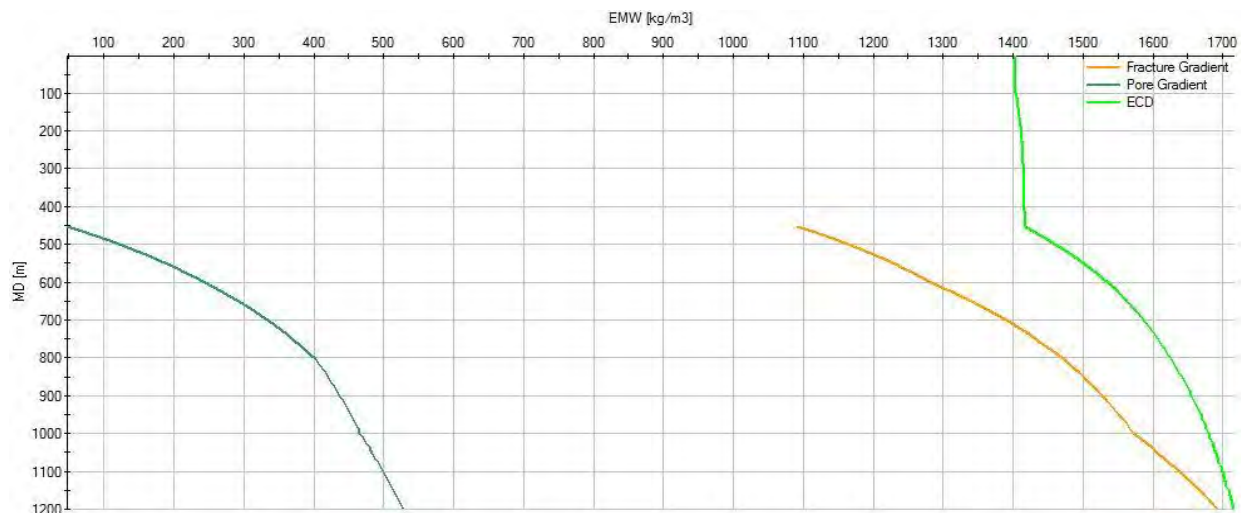


Figure 51: Gradient curves of the pore pressure, fracture pressure and the pressure exerted by the equivalent circulating density. The graph shows the simulated development of the equivalent mud weight along the entire borehole.

A look to the profile of the ECD gradient shows that the fracture pressure at the bottom of the casing section was exceeded just shortly before end of the cement job (Fig. 52). Similar to the previous calculation behaves the flow rate and pressure readings at the surface and bottomhole (Fig. 48 & 49). The hook load constantly decreases until the cement slurry has entered the annulus which causes a short bouncing up before it plunges to 133 tons.

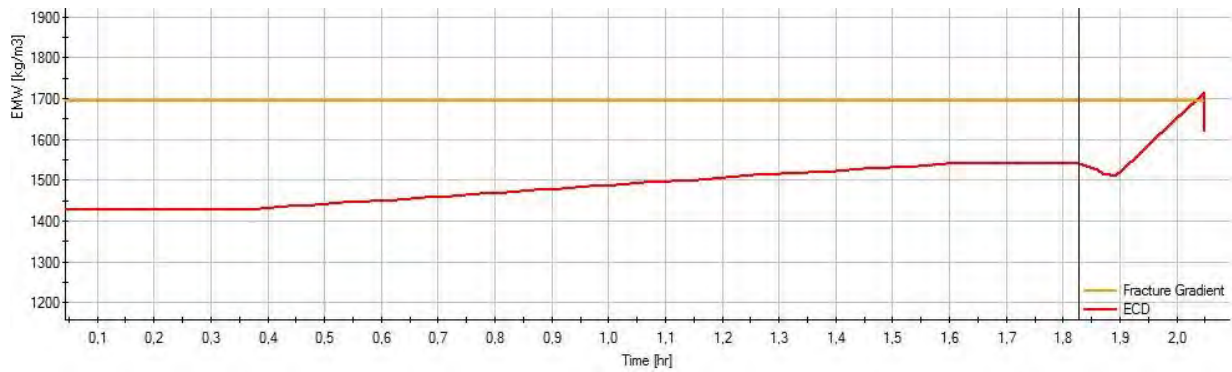


Figure 52: Graph showing the development of the ECD gradient at the bottom of the anchor casing section. The black vertical line indicates the beginning of fluid displacement in the annulus by the cement slurry.

9 5/8" – Production Casing Section (1,200-3,000 m)

The cementing calculation was successful with regard to the hole conditions during pumping of the fluids. Fig. 53 shows the depth profile for the pore gradient, fracture gradient and the equivalent circulating density. It can be seen that, other than the previous calculations, the fracture gradient was not exceeded at any depth. The equivalent circulating density increases less with depth resulting in a larger margin to the fracture gradient. The maximum bottomhole pressure, exerted by the equivalent circulating density, is around 525 bar and occurs when the cement passes into the annulus. Once the cement enters the annulus, a sharp increase of the surface stress was observed and peaked at 117 bar at the end of pumping.

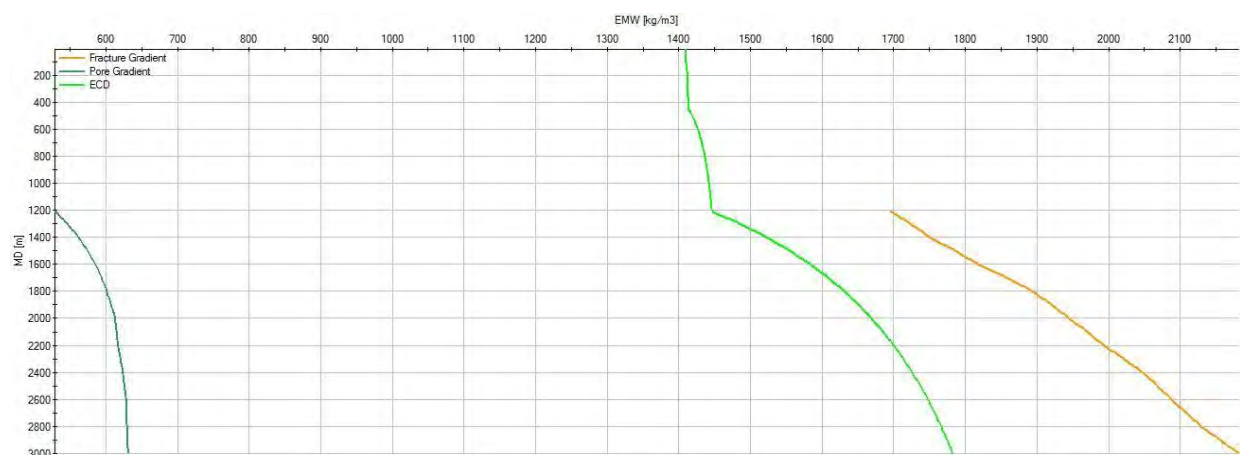


Figure 53: Graph displaying the gradient profiles for the pore pressure, fracture pressure and the equivalent circulating density pressure.

3.5. Risk Analysis

This subchapter examines the major risks arising from hazards of environmental, technical, constructional or operational nature. The risk assessment is then summarized in a sheet at the end of Chapter 4.3.

Geological Risks

The geological setting of the Reykjanes Peninsula originates from volcanic, tectonic and climatic events which took place in geological time scales. Still, the Peninsula experiences active volcanism and rifting along the spreading ridge (Fig. 2). Active tectonic movement of the two diverging plates induces earthquakes to form swarms of fissures and fractures, along which magma can migrate. The 3-D modeling of the Reykjanes system has revealed a sheeted-dyke complex with numerous intrusions of magma bodies, almost extending from great depth of 5,000 m or more (SCHERFF, 2016). The last effusive volcanic eruption took place around 800 years ago (FRÍÐLEIFSSON et al., 2003). The Reykjanes geothermal area is just beneath the zone of high seismicity at which most of the earthquakes occur at a depth of 1,000-5,000 m. A seismogenic zone, capable of generating earthquakes, is known to exist between 5,000 and 6,000 m depth (FRÍÐRIKSSON et al., 2015). Several thousands of earthquakes have been recorded during the summer of 1972 with the largest, accounting for 4.4 on the Richter magnitude scale (KLEIN et al., 1977). A higher number of micro-earthquakes have been recorded since the Reykjanes power plant have started its operation in 2006. The extraction of large quantities of fluids from the reservoir has caused a subsidence of around 100 mm during the first two years of production and a total of 320 mm from 1992 to 2014 (AXELSSON et al., 2015). It is assumed that, fluid extraction changes the stress field and triggers the generation of earthquakes and seismic fault movement (KEIDING et al., 2010). The geological and tectonic setting reveals several natural hazards which cannot be predicted accurately. Earthquakes and volcanic eruptions do not strictly follow a cycle and can happen any time.

Geothermal Risks

The geothermal risks emerge from the uncertainties of conditions below 2,700 m and especially at the bottom of IDDP-2. INGASON et al. (2015) approached an estimation of the pressure and temperature conditions below 3,000 m on the basis of the boiling point with depth curve and an extrapolation of logged values. This prediction assumes that the fluids in the Reykjanes geothermal system have 3.5 % of sodium chloride in solution and therefore more than the average amount in seawater. Nowadays, the deepest production well in the Reykjanes field is just over 3,000 m depth and most of the wells range between 2,000-2,500 m depth (FRÍÐLEIFSSON et al., 2011). Fluid extraction of greater depth could not be obtained, thus the salinity is not well

known and only assumed. The 3-D model in SCHERFF (2016) expresses that the temperature of the Reykjanes system does not follow a single geothermal gradient, but consists of a convective and conductive gradient. The temperature prediction according the boiling point with depth curve follows the convective trend. However, some of the wells in the Reykjanes field show a response back to a conductive gradient from around 2,500 m depth onwards (FRIDRIKSSON et al., 2015; FRIDLEIFSSON et al., 2014a). The expectation to find supercritical fluids or superheated steam is based on the interpretation of resistivity surveys which show a thermal plume or heat source at 10 km depth, just below the site of IDDP-2 (FRIDLEIFSSON et al., 2011). The interpretation of resistivity profiles led to a low resistivity column in the center of the Reykjanes system. This column was defined as the up-flow zone within the fractured system, promising higher permeability and temperature in order to approach supercritical conditions (FRIDLEIFSSON et al., 2014a).

Technical Risks

The process of drilling a 5,000 m deep well in a volcanic zone in Iceland also means to manage high pressure, high temperature, aggressive fluids and gases, stiff rocks and a fractured subsurface. The heterogeneous geology and the alternating facies makes it difficult to plan and control the drilling process. The stiffness of the basalt governs the running speed and finally the drilling program schedule of the project. Additionally, the drilling into basalt or hard formations in general wears down the drill bit and causes multiple tripping operations to change the bit. A sudden change of the bedrock changes the weight on bit and torque to such an amount that the drilling assembly is damaged or perhaps broken. The simulated high torque and increased rotational speeds have shown the high failure potential of the drilling assembly connections. The probability of helical or sinusoidal buckling is a problem at any time. An unexpected problem can also arise from drilling into locally molten basalt or fresh magmatic intrusions after a seismic event. This incident can cause pipe sticking or a total loss of the bottomhole assembly. As a result, fishing, milling and sidetracking are considerable operations, which are time-consuming and expensive. The highly fractured subsurface increases the possibility to encounter permeable zone, which can cause severe circulation loss. A loss of circulation results in hole cleaning and bit cooling problems. This case is a critical condition for the drilling assembly which can break or get stuck. The location of aquifers is quite well known for the upper 2,000 m of the field, but mainly undefined for greater depth. A loss of circulation during running the casing into the hole have been simulated with a mud drop in the annulus and the total evacuation of the casing string. The simulations have shown that all casing sections are prone to collapse or burst (Chapter 3). As simulations have shown, a high temperature environment reduces the pipe resistance to external or internal loads, making this more problematic in the case of a circulation loss.

4. Interpretation

This chapter aims, firstly, to evaluate the results of the simulation and, secondly, to assess the risks to occur when drilling into a highly fractured volcanic system under high pressure and temperature conditions.

4.1. Drilling Simulation

One of the major challenges of a geothermal project is the selection and formulation of an efficient drilling fluid to overcome the inherent conditions of HT wells, such as IDDP-2. The abundance of dense and stiff magmatic formations in the Reykjanes system induces a low penetration rate, higher bit wear and extended drilling time. As the geothermal field hosts a fissure swarm in shallow regions and a sheeted-dyke complex with increasing depth, the drilling fluid formulation must contain loss of circulation materials, such as high viscosity polymer pills. The pumping of polymer pills and cementing off the permeable zones have been an efficient tool when drilling the first IDDP well in Northern Iceland (PALSSON et al., 2014). This approach is in the same way advisable since several inflow zones are expected at 90 m depth, but more frequently when drilling into the current productive zone between 2,000 and 3,000 m. On the other hand, polymers have temperature limitations and thermal degradation of polymers begin above a temperature of about 150 °C. Such a temperature are going to be approached during fluid circulation in deeper parts of the production casing section (Fig 33). Torque and drag calculations have shown that drilling the upper 1,200 m, respectively the intermediate and anchor casing sections, is of low risk with a non-critical potential of buckling. It can be said that the sinusoidal or helical limit of a non-drillpipe component was exceeded. The circulation of fluids under the same high flow rate of 3,600 l·min⁻¹ would result to a burst failure of the assembly when drilling the subsequent production casing section. A non-critical operation can be achieved by simply keeping the flow rate below 2,500 l·min⁻¹ or less. The same measure has to be applied when rotating off bottom, tripping into or out of the hole. A failure potential by drilling the production liner section to 5,000 m was not observed. The burst failure of the production casing is not an issue of the drilling fluid properties, but the drilling assembly, particularly, the drill pipe. The 5" drill pipe gives a too low burst resistance and should be updated to an outer diameter of 6". The higher hook load for the production casing section originates from the installation of heavy drill collars and additional heavy weight drill pipes (Table 6). However, the use of the same assembly design for drilling the final section would not overcome the maximum hook load of the drilling rig. A managed hook load mitigates the potential of helical or sinusoidal buckling. To conclude,

drilling under normal conditions and circulating fluids did not show any failure mode of high concern. The use of water-based drilling mud slightly increases the drilling parameters, namely hook load, surface torque and stress. A stuck pipe and the operation to rotate with higher torque could lead to abnormal conditions under which the connections may fail by exceeding the make-up torque. Such kind of incident can happen when drilling into magma bodies, as such a problem has occurred during drilling of the IDDP-1 well. This incident has led to abandonment of the well (PALSSON et al. 2015). The loss of circulation could result to a similar pipe sticking incident due to poor cuttings removal at the bottom of the section. An immediate sealing of permeable zones is crucial to avoid pipe sticking and moreover to mitigate failure modes of cemented casing strings above the open hole section. Such a post cemented load case was simulated and will be described in the following.

The cementing calculations have revealed the possibility of fracturing during pumping. The equivalent circulating density, which increases with increasing depth, overcomes the fracture gradient above 1,200 m. On the basis of this, a reduced mud and slurry density is recommended to avoid the possibility of fracturing and additional loss of circulation. The high equivalent circulating density of up to $1,800 \text{ kg}\cdot\text{m}^{-3}$ at the bottom of the production casing does not exceed the fracture gradient. The installation of stage cementing windows at the top of the anchor and production casings is an efficient tool to reduce the high surface pressure when pumping the slurry into the annulus. Two stage cementing is also helpful to cement the 1,800 m long anchor casing interval sufficiently from above. Furthermore, it could also be of use if sealing of permeable zones during drilling was insufficient and the cement slurry is incapable of flowing up the annulus from below. Occasional circulation losses have not only economic consequences, but serious technical and operational casualties. The use of API class G cement for such a high temperature environment can lead to problems. A temperature limitation exists for the cement slurry in almost the same range as mentioned for the polymer additives. When exposed to temperature above $150 \text{ }^\circ\text{C}$, the thickening time is reduced and the rheological properties will gradually decrease with increasing temperature. The temperature resistance of the slurry can be increased with an addition of a significant amount of silica flour.

Assuming the intermediate casing string is set and cemented, a fluid loss while drilling the next open hole section results in a drop of the drilling mud level inside the casing string or a total evacuation in the worst case. As this incident may be casually the case in a fractured system, the string components experience a critical external load. As this load case represents a post cemented situation, the external pressure is governed by the cement column and pore pressure gradient profile from the previous casing shoe (Fig. 18). The annulus of the intermediate and anchor casings is fully cemented compared to the production casing section, which is partly cemented

and the displaced fluid additionally controls the external pressure profile. The external load increases with increasing depth and could reach up to 186 bar at the production casing shoe. The API K-55 is suitable to withstand the external load, same as for the anchor casing. In contrast to that is the same material grade prone to collapse at the couplings of the intermediate casing section. The likelihood of a collapse is the highest for every load case and most critical during a fully evacuated string, loss of circulation and installation. In order to avoid a failure mode, the high risk can only be mitigated by the selection of a higher nominal weight for the couplings. A 20" coupling of $109.35 \text{ lb}\cdot\text{ft}^{-1}$ provides a more secure resistance under defined design criteria and is also capable to withstand an additional external load of 15 bar at the most. A fully evacuated production casing string have the potential to collapse, which can be confined with the API L-80 grade for the joints. The same grade is able to avoid the simulated collapse mode for the production liner. However, the little margin between the safety and design factor means that the higher grade of T-95 is of better recommendation. The L-80 grade is appropriate to reduce the risk of the anchor casing to burst during an unexpected influx of geofluids with a volume of 5 m^3 . The load profile in Fig. 38 has shown that the lower joints are exposed to higher pressures than the upper part. According to this, the installation of T-95 joints in the upper 300 m, as the well design proposal indicates, is not necessary, but vice versa and with a lower API grade (INAGSON et al., 2015; Fig. 6). The burst and triaxial failure due to an underground blowout at the production casing level requires to change the material grade to T-95 for both, the couplings and joints. Naturally, a mud drop in the annulus, caused by a loss of circulation, decreases the hydrostatic pressure at the bottom, but also the counter pressure to the pressure inside the string. The simulation has shown, that a burst and triaxial failure is inevitably at the bottom of the production casing. The installation of L-80 would meet both design criteria. A T-95 grade would almost double the burst resistance, increases the safety margin to 100 bar and recommended to also meet the limits of the previous kick load case. The mud drop along the production liner section is fatal and difficult to manage. The high temperature conditions of $400 \text{ }^\circ\text{C}$ at the bottom have a vast impact on the resistance of the equipment and can reduce the yield by more than 100 bar. A burst and triaxial failure cannot simply avoided by a higher material grade of single elements, but requires a new assembly. The grade for the couplings must be at least L-80 to resist the acting internal pressure. In order to keep a uniform material grade for this section, the $26 \text{ lb}\cdot\text{ft}^{-1}$ joints must be replaced by the $46.4 \text{ lb}\cdot\text{ft}^{-1}$. These suggestions only apply for the actually occurring burst and triaxial loads, but do not meet the defined design criteria.

Table 15: Summary of the simulated failure modes for different load cases and casing levels. The weak points indicate the area of improvements with regard to the proposed well design in INAGSON et al. (2015). The suggestion of improvements are given as minimum upgrade measures

Section	Failure mode	Weak point	Minimum upgrade measure
Intermediate	Collapse*	Coupling	Nominal Weight of 109.35 lb·ft ⁻¹
Anchor	Burst*	Joint	L-80
Production	Collapse*	Joint	L-80
	Burst	Joint	L-80
	Triaxial	Joint	T-95
Liner	Collapse	Joint	L-80, T-95 recommended
	Burst	Joint	Nominal Weight of 46.4 lb·ft ⁻¹ and T-95
		Coupling	L-80
	Triaxial	Coupling	T-95

* Potential failure mode

An upgrade to T-95 for both elements is technical feasible and recommended, but still critical with regard to the couplings. The T-95 would shift the burst and triaxial design limits below the coupling and pipe yield limits. The alternative of 46.4 lb·ft⁻¹ joints reveals an axial failure mode for the load case of a fully evacuated liner. The axial load is the highest at the top of the liner, thus opposite to the burst and triaxial load profiles. This observation leads to a preferred installation of the heavier pipes with a grade of T-95 at the bottom of the liner. The remaining liner section can then be equipped with 38 lb·ft⁻¹ joints, but with T-95 at least. A mud drop due to circulation loss is a problematic incident throughout the entire wellbore and leads to fatal failure modes. The sealing of permeable zones and thus the mitigation of circulation loss is of high priority during drilling of the individual sections. Table 15 summarizes the possible and actual failure modes as simulated for different load cases and outlines the weak points of the assembly. An alternative selection of the equipment is stated as minimum upgrade measures.

As mentioned above, the burst and collapse resistance of the downhole equipment decreases with increasing temperature. A higher temperature reduces the yield of the equipment and consequently shrinks the margin between the design criteria limit and the thermally de-rated load resistance. The couplings are more prone to thermal degradation and can lose up to 80 bar or more of its yield. When drilling a section, the used drilling fluids are in the same way affected by high temperatures as well as the pressure environment. The equivalent circulating density is an important parameter to understand the changes in rheology and density due to pressure and temperature. A reliable prediction of this parameter requires the input of laboratory measurements at similar conditions as expected during drilling of the specific well (ROMMETVEIT & BJÖRKEVOLL, 1997). The temperature and pressure dependency was imported for the oil-based mud, but not for the water-based mud. Despite this fact, the hydraulic calculations have shown

that the equivalent circulating density is slightly lower for the oil-based than for the water-based mud at any depth. The density at the bottom of the production casing is around 20 % less than at the surface. This observation is different to what has been discovered from comprehensive experiments. According to McMORDIE JR. et al. (1982) is the density of an oil-based drilling fluid greater than that of a water-based mud at high temperatures and pressures. The discrepancy is possibly due to a different formulation of the fluids. Experiments have shown that the pressure dependency is much higher for oil-based muds, whereas a higher temperature effect was observed for water-based muds (ROMMETVEIT & BJÖRKEVOLL, 1997). It was calculated that the density of water-based mud decreases faster from top to bottom of the production casing section than it is the case for oil-based mud. Circulating at different flow rates affects the equivalent circulating density in such a way that the density versus depth trend is opposite. A flow rate of $1,800 \text{ l}\cdot\text{min}^{-1}$ decreases the density with depth, whereas twice the flow rate shows the highest circulation density at the bottom of the hole. Additionally, a higher flow rate is responsible for higher mud temperatures and lower mud densities. This phenomena relates to the well-known effect of fluid expansion due to geothermal heating and is higher for oil-based than for water-based muds with regard to the thermal expansion coefficient (Table 9). The compression due to the high pressure acts contrary to the expansion. The time dependency is less distinct and pronounced in a little drop of the density when circulating for 12 hours instead of 1 hour. A high temperature affected drop of the initial mud density could promote the possibility of an unexpected influx of geofluids and, therefore, a kick. Thus, cooling of the return mud with a cooling tower at the surface is an effective and essential process to keep the mud from becoming too hot. A higher mud inlet temperature increases the equivalent circulating density and can exceed the initial mud density. The reinjection of too hot return mud is of special concern in order to prevent high internal pressure and possible failure modes.

4.2. Thermal Modelling

The thermal effect on circulating fluids is a curious issue with regard to the rheological mud properties, well bore stability and downhole equipment. Thermal modelling of each selected hole section has shown that the flow rate, circulating time and mud type are those parameters most affecting the bottomhole fluid temperatures during circulation (RAYMOND, 1969). The circulating rate has a major impact on the temperature profile (Fig. 35). The lower the flow rate the less exposed is the well bore and casing strings to high temperatures, assuming a low mud inlet temperature. RAYMOND (1969) has experimentally determined that a geothermal gradient below $4 \text{ }^{\circ}\text{C}\cdot 100 \text{ m}^{-1}$ has little effect on the temperature difference between the fluid at the bottom of the hole and the outlet fluid. Due to the fact of a very high geothermal gradient up to $120 \text{ }^{\circ}\text{C}\cdot 100 \text{ m}^{-1}$ in the Reykjanes system, the outlet mud temperature is almost equal to the bottomhole

fluid (Table 17; Fig. 31). It can also be seen from Fig. 35 that, the bottomhole fluid temperature is significantly lower than the geothermal rock temperature when circulating at a high flow rate. It is important to keep the flow rate moderate in order to avoid too high temperature in the borehole, but also to avoid a burst failure mode due to high internal pressure. The high temperatures during circulation act as a thermal stress on the pipe and reduces its yield strength. The simulations have verified that the mud type rarely affects the temperature conditions during circulation. A higher temperature for the string and the annulus was found when circulating with an oil-based drilling fluid.

4.3. Risk Assessment

The site selection of IDDP-2 at the Reykjanes Peninsula involves a harsh environment in a volcanic and tectonic active area. Every seismic event can generate new fractures and fissures which may change the stress field, can cause well integrity problems or damages on the surface equipment, such as engines, pumps or the drilling rig. Furthermore, the fissures provide the pathways for hot magma to migrate. Earthquakes can re-open old fracture systems and enable hot fluids or magma to flow upwards into the Reykjanes system. Young intrusions of magma can change the temperature conditions around the well or even destroy the downhole equipment. In addition to that, the sheeted-dyke complex in greater depth holds the possibility of very hot basalt and perhaps molten magma. The localization of small molten magma bodies becomes more restricted with increasing depth as the resolution of resistivity surveys decreases. The first attempt in northern Iceland has shown that an interpretation of resistivity measurements with a low resolution can lead to a well abandonment due to penetration into a molten intrusion (PALSSON et al., 2014). A volcanic eruption through the fissure system or from a volcano, both proximal and distal, implies a potential hazard due to ash-fall or lave flow. The installation of a monitoring system can be helpful to detect arrhythmic patterns, indicating a potential danger, and to alert the crew of an expected earthquake. The occurrence of earthquakes is more likely to occur than a volcanic event in the near future and during the operational lifetime of the project. But a volcanic eruption in combination with a major earthquake can fatally damage the facilities or result in a reduction of the system's capability. The worst case scenario could have a moderate to high impact on functionality of operations. These scenarios endanger the safety of geothermal drilling and production throughout the lifetime of any well in the Reykjanes field.

The success of the Iceland Deep Drilling Project depends on findings of supercritical fluids or superheated steam in order to considerably increase the efficiency and energy outcome of geothermal wells. The prediction of downhole conditions, on the basis of assumptions about the

fluid composition and the extrapolation of logged gradients, implies obvious uncertainties. A higher salt concentration in the reservoir fluid shifts the critical point to greater values, consequently demands drilling deeper than 5,000 m. This scenario will affect the drilling, well completion and cementing design, because it becomes more prone to failures. A similar scenario can arise from a higher geothermal gradient than expected. According to this, the temperature can increase to higher values in shallower depth. The pressure conditions may then too low to develop a supercritical state of the fluids. A higher temperature changes the rheological properties of the drilling mud and cement slurry, which can then result in a bad cementing job and drilling difficulties. The above mentioned sheeted-dyke complex could cause very high circulation losses unless these problematic zones are not filled with cement or loss circulation materials. The knowledge of permeable zones is very important to avoid a problematic influx of gas or steam into the wellbore. The simulations have shown that even the influx of a small amount of gas volume could lead to a burst failure.

The restricted database, lack of information and different possible scenarios define several hazards to occur and a considerable geothermal risk for this project. The probability to fail by drilling into a supercritical reservoir is moderate to high and can have a marginal or even critical severity. The success of this project gives the direction of geothermal production in future. Nevertheless, the high temperature and high pressure conditions at great depth and still existent uncertainties can have a moderate to high impact on the drilling process.

The technical risks are directly related to above mentioned geological and geothermal hazards. The casing string analysis outlines that the grades of the connections and joints must be reviewed to avoid a failure in any simulated load case. Especially, the API K-55 was not suitable to withstand the internal pressure in case of an unexpected influx of geofluids or circulation losses during installation of the production casing and liner. The couplings are in most of the cases resistant to downhole conditions but show the potential to fail in the intermediate casing section and cause a collapse in the worst case. The probability of material failure increases with increasing downhole temperature and pressures. Secondly, the alternating lithologies can lead to abrupt changes in drilling parameters, such as torque and rotational speed, which then causes the damages on the equipment. Table 16 simply visualizes the probability, severity and impact of above described hazards and gives a summary of associated consequences. A discrete assignment to a specific hazard was in some cases not applicable and solved by defining a range for the possibility, severity or the impact factor.

Table 16: Risk assessment sheet for the IDDP-2 well at Reykjanes, Southern Iceland

<i>Risk assessment sheet for the IDDP-2 well at Reykjanes, Southern Iceland</i>						
<i>Hazards</i>	<i>Description</i>	<i>Consequences</i>	<i>Probability</i>	<i>Severity</i>		<i>Impact</i>
<i>Geological Risks</i>						
<i>Volcanism</i>	Lava flow, Ash deposits, magmatic intrusion	Fire, casing collapse, wellbore failure or loss, stop of project or production	C	2	1	II I
<i>Earthquakes</i>	Fractures, reopening of old structures, stress field change	Damage on surface facilities and downhole equipment, wellbore casualties, electricity and water supply failure	B	3	2	III II
<i>Geothermal Risks</i>						
<i>Supercritical Conditions</i>	No supercritical conditions or at greater depth	No production of supercritical fluids, no energy boost, failure of project's goal	B	2		II I
<i>Temperature and pressure</i>	Higher or lower gradients than predicted	Higher exposure to extreme conditions, material failure, limitations of drilling rig, mud properties, hydraulics	B	2		II I
<i>Technical Risks</i>						
<i>Material Failure (@ HT)</i>	Fatigue, wear, high torque, changing bedrock properties	Damage to drill bit and casing string, fishing of stuck pipe or total loss of pipe, delay in drilling process, costs	B	3	2	II
<i>Circulation Loss</i>	Permeable zones, aquifers, loss of circulation, drop of mud level	Collapse or burst of casing string, kick, hole cleaning and cooling difficulties	B A	2	1	I
<i>Cementing</i>	Insufficient cement job, problems in cementing	Well integrity problems, delay of drilling process, costs	C	3		III
<i>Underground blowout</i>	Unexpected influx of high amount of geofluids	Burst of casing string or connections, well integrity problems, delay in drilling process	C	3	2	III II

5. Conclusion and Outlook

Almost two decades ago was the kick-off for an approach that has the potential to be applicable nearly everywhere in the world. Now, almost two decades later, the approach is still at the beginning. Iceland is a leading country in research and project development of supercritical reservoirs. The execution of the pioneering IDDP project requires a detailed assessment of environmental, technological, operational, geological and geothermal risks. These risks evolve from a list of challenges the Iceland Deep Drilling Project has to cope with:

- * High pressure and high temperature conditions
- * Volcanism, earthquakes and tectonic movements
- * Highly fractured underground with complex geology
- * Aggressive gases and fluid compositions
- * Technological limitations... etc.

The risk assessment of the IDDP-2 well at Reykjanes identified several hazards to be linked to above points, such as, loss of circulation, molten magma bodies, re-opening of fractures, rock hardness, fatigue and equipment failures. A high risk is related to the weakness of the downhole equipment available for drilling at extreme conditions. The high temperature reduces the pipe and connection yields, making them more prone to technical failure. The simulation has outlined collapse and burst failures in case of circulation loss, drop of the mud level in the annulus and a full evacuation of the string. The modelling of temperature effects has shown a significant impact of the flow rate and circulating time on the downhole temperature distribution. A managed flow rate and the installation of a mud cooling tower keep the casing resistance high. The high thermal load reduces the yield of the pipe and connections and requires the selection of heat resistant materials. The identification of weak points at the bottomhole assembly and the determination of critical drilling conditions is of high importance. The improvement of this simulation depends on the access of logging data with regard to temperature, pressure, porosity, permeability, density and lithology. The modelling of downhole temperatures due to fluid circulation demands the knowledge of field specific thermal conductivity and heat capacity, and the behavior of the drilling fluids under downhole conditions. The simulation of thermal stresses, wear, circulation loss, an influx of geofluids helps to predict possible wellbore instability and equipment failures.

The bright future of supercritical fluid extraction will finally begin as soon as the technical obstacles of drilling, production and fluid handling, and the transportation of heat or electricity over long distances have been surmounted. When the day has come, Iceland is then, among others in the world, a major producer and supplier of “Green Power”.

6. References

- AXELSSON, G., ARNALDSSON, A., BERTHET, J.-C. C, BROMLEY, C.J., GUDNASON, E.A., HREINSDOTTIR, S., KARLSDOTTIR, R., MAGNUSOON, I.Th., MICHALCZEWSKA, K.L., SIGMUNDSSON, F., SIGURDSSON, O.** (2015): Renewability Assessment of the Reykjanes Geothermal System, SW-Iceland, In: Proceedings World Geothermal Congress 2015, Melbourne, Australia, 19-25 April, pp. 10.
- BISCHOF, J.F.** (2000): In: Ice Drift, Ocean Circulation, and Climate Change, Springer, pp. 215.
- BOURGOYNE JR., A.T., MILHEIM, K.K., CHENEVERT, M.E., YOUNG JR., F.S.** (1986): Applied Drilling Engineering, SPE Textbook Series, Vol. 2, Society of Petroleum Engineers pp. 502.
- CHEMWOTEI, S.C.** (2011): Geothermal Drilling Fluids, In: Geothermal training in Iceland 2011, Report 10, UNU-GTP, Iceland, 149-177.
- EIRIKSSON, J., LARSEN, G., BJÖRNSSON, H., SIMONARSON, L.A., HALLSDOTTIR, M.** (1994): Roadlog, In: Nordic Geological Excursion in Iceland, Quaternary Geology and Glaciology, pp. 100.
- ELDERS, W.A., FRIDLEIFSSON, G.O.** (2015): Investigating a Mid-Ocean-Ridge Hydrothermal System on Land: the Iceland Deep Drilling Project on the Reykjanes Peninsula in SW Iceland, In: Proceeding World Geothermal Congress 2015, Melbourne, Australia, 19-25 April 2015, pp. 9.
- ELDERS, W.A., FRIDLEIFSSON, G.O., BIGNALL, G.** (2012): Report of an IDDP-1CDP Workshop to Plan a 5km deep borehole (IDDP-2) into the root zone of an Analog to a Black Smoker on Land at Reykjanes Iceland, SAGA report prepared for the IDDP-1CDP Workshop 2012, Eldborg-Svartsengi, Iceland, Report No. 9, pp. 33.
- FRIDLEIFSSON, G.O., ALBERTSSON, A., ELDERS, W.A., SIGURDSSON, O., KARLSDOTTIR, R., PALSSON, B.** (2011): The Iceland Deep Drilling Project (IDDP): Planning for the Second Deep Well at Reykjanes, Geothermal Resources Council Transactions, Vol. 35, 347-353.
- FRIDLEIFSSON, G.O., ARMANSSON, H., ARNASON, K., BJARNASON, I.P., GISALSON, G.** (2003): Part I: Geosciences and Site Selection, In: Iceland Deep Drilling Project, Feasibility Report, G.O.Friðleifsson (ed.), Orkustofnun, OS-2003-007, pp. 103.
- FRIDLEIFSSON, G.O., ELDERS, W.A., ALBERTSSON, A.** (2014b): The concept of the Iceland deep drilling project, Geothermics, 49, 2-8.
- FRIDLEIFSSON, G.O., SIGURDSSON, O., ÞORBJÖRNSSON, D., KARLSDOTTIR, R., GISLASON, Þ., ALBERTSSON, A., ELDERS, W.A.** (2014a): Preparation for drilling well IDDP-2 at Reykjanes, Geothermics, 49, 119-126.
- FRIDRIKSSON, T., STEFANSSON, A., OSKARSSON, F., EYJOLFSDOTTIR, E., SIGRUDSSON, O.** (2015): Fluid Chemistry Scenarios Anticipated for IDDP-2 to be Drilled in Reykjanes, Iceland, In: Proceedings World Geothermal Congress 2015, Melbourne, Australia, 19-25 April 2015, pp. 9.

- Hefu, H.** (2000): Study on Deep Geothermal Drilling Into A Supercritical Zone in Iceland, UNU Geotherm. Training Programme Report. 7, Nat. Energy Auth. Orkustofnun, Reykjavik, pp. 33.
- HOLMGEIRSSON, S., GUÐMUNDSSON, A., PALSSON, B., BOASSON, H.A., INAGSON, K., PORHALLSSON, S.** (2010): Drilling Operations of the First Iceland Deep Drilling Well (IDDP), In: Proceedings World Geothermal Congress 2010, Bali, Indonesia, 25-29 April 2010, pp. 10.
- IBEH, C., SCHUBERT, J., TEODORIU, C.** (2007): Investigation on the effect of ultra-high pressure and temperature on the rheological properties of oil-based drilling fluids, presented at 2008 AADE Conference and Exhibition, Texas.
- INAGSON, K., ARNASON, A.B., BOASSON, H.A., SVERRISSON, H., SIGURJONSSON, K.Ö., GISLASON, Þ.** (2015): IDDP-2, Well Design, In: Proceedings World Geothermal Congress 2015, Melbourne, Australia, 19-25 April 2015, pp.12.
- KÅRSTAD, E., AADNØY, B.S.** (1998): Density behavior of drilling fluids during high pressure high temperature drilling operations, SPE Paper 47806 presented at the 1998 IADC/SPE Asia Pacific Drilling Conference, Jakarta, Indonesia, September 7-9, 227-237.
- KEIDING, M., ARNADOTTIR, T., JONSSON, S., DECRIEM, J., HOOPER, A.** (2010): Plate boundary deformation and man-made subsidence around geothermal fields on the Reykjanes Peninsula, Iceland, *Journal of Volcanology and Geothermal Research*, **194**, 139-149.
- KELLINGRAY, D.S., GREAVES, C., DALLIMER, R.P.** (1991): High temperature and high pressure rheology of oilwell cement slurries, In: *Rheology of Fresh Cement and Concrete*, Banfil, P.F.G. (Ed.), Spon, 159-169.
- KLEIN, F.W., EINARSSON, P. WYSS, M.** (1977): The Reykjanes Peninsula, Iceland, Earthquake Swarm of September 1972 and Its Tectonic Significance, *Journal of Geophysical Research* **82**, **5**, 865-888.
- McMORDIE JR., W.C., BLAND, R.G., HAUSER, J.M.** (1982): Effect of Temperature and Pressure on the Density of Drilling Fluids, paper SPE 11114 presented at the 57th Annual Fall Technical Conference and Exhibition, 26-29 Sept., 1982, New Orleans, C.A., pp. 7.
- PALSSON, B., HOLMGEIRSSON, S., GUÐMUNDSSON, A., BOASSON, H.A., INAGSON, K., SVERRISSON, H., THORHALLSSON, S.** (2014): Drilling of the well IDDP-1, *Geothermics*, **49**, 23-40.
- PENNEBAKER, E.S.** (1968): An Engineering Interpretation of Seismic Data, paper SPE 2165 presented at the SPE 43rd Annual Fall Meeting, Houston, Sept. 29 – Oct. 2, 1968, pp. 12.
- RAVI, A.** (2011): Experimental assessment of water based drilling fluids in high pressure and high temperature conditions, published Master thesis at Texas A & M University, Texas, USA, pp. 113, [online]: <http://oaktrust.library.tamu.edu/handle/1969.1/ETD-TAMU-2011-08-9925> (05.01.2016)
- RAYMOND, L.R.** (1969): Temperature Distribution in a Circulating Drilling Fluid, *Journal of Petroleum Technology*, **21**, No. 3, 333-341.

ROMMETVEIT, R., BJÖRKEVOLL, K.S. (1997): Temperature and Pressure Effects on Drilling Fluid Rheology and ECD in Very Deep Wells, paper SPEI/IADC 39282 presented at SPE/IADC Middle East Drilling Technology Conference, 23-25 Nov., 1997, Bahrain, 297-305.

SCHERFF, A. (2016): 3-D Modelling of the IDDP-2 Geothermal Reservoir at Reykjanes, Southern Iceland, unpublished Master thesis at Clausthal University of Technology, pp. 50.

THORHALLSSON, S., MATTHIASSON, M., GISLASON, T., INAGSON, K., PALSSON, B., FRÍÐLEIFSSON, G.O. (2003): Part II Drilling Technology, In: Iceland Deep Drilling Project, Feasibility Report, G.O. Friðleifsson (Ed.), Orkustofnun, OS-2003-007, Reykjavik, pp. 76.

THORHALLSSON, S., PALSON, B., HOLMGEIRSSON, S., INAGSON, K., MATTHIASSON, M., BOASSON, H.A., SVERRISSON, H. (2014): Well design for the Iceland Deep Drilling Project (IDDP), *Geothermics*, **49**, 16-22.

WOHLGEMUTH, L., HARMS, U., BINDER, J. (2007): InnovaRig – The New Scientific Land Drilling Facility, *Scientific Drilling Journal*, **5**, 67-69.

YAN, C., DENG, J., YU, B., LI, W., CHEN, Z., HU, L., LI, Y. (2013): Borehole Stability in High-Temperature Formations, *International Journal of Rock Mechanics and Rock Engineering*, **47**, 2199-2209.

Online Sources

HOFER, T. (2015): Online Conversion Tool [online]: http://www.orkuveysja.is/veysja/orkuveysja_en.html (15.12.2015)

NEA-OS (2012): Iceland Energy Portal [online]: <http://www.deine-berge.de/Rechner/Koordinaten/Dezimal/51,10> (10.09.2015)

SAMORKA (2014): IDDP-Next Steps [online]: <http://sw.swapp.lausn.is/doc/2825> (06.01.2016)

7. Appendix

7.1. Appendix A: Temperature and Pressure Profiles

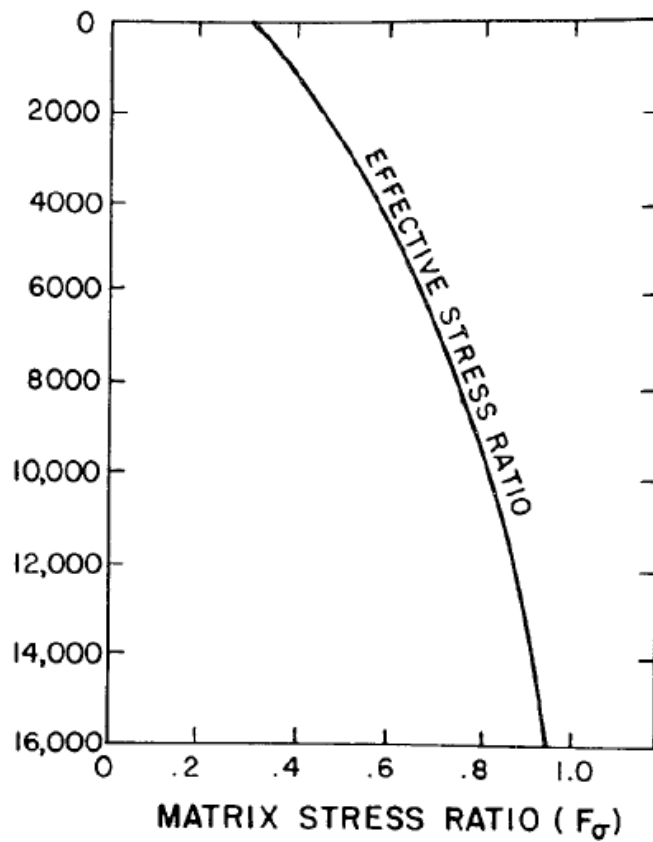


Figure 54: Pennebaker correlation curve for the effective stress ratio (BOURGOYNE et al., 1986).

Table 17: Temperature database according to data after SCHERFF (2016) and INAGSON et al. (2015). The geothermal gradients have been automatically calculated by the software Sysdrill.

Depth TVD (m)	Formation Temperature (°C)	Geothermal Gradient (°C·100 m ⁻¹)
0	10	
20	45	
40	69	120
60	79	50
80	88	45
100	94	30
120	104	50
140	113	45
160	122	45
180	134	45
200	145	60
250	174	55
300	197	58
350	207	46
400	217	20
450	225	20
500	234	16
550	245	18
600	253	22
650	260	16
700	267	14
750	273	12
800	275	4
850	278	6
900	281	6
950	284	6
1,000	287	6
1,100	288	1
1,200	289	1
1,300	290	1
1,400	298	8
1,500	302	4
2,000	329	5.40
2,500	346	3.4
3,000	363	3.4
3,500	375	2.4
4,000	383	1.6
4,500	392	1.8
5,000	402	2.0

Table 18: Pressure database for the IDDP-2 well. The pore pressures are according to data after INAGSON et al. (2015). The fracture pressure is based on the prediction method according to Pennebaker. The overburden pressure was calculated.

Depth TVD (m)	Pore Pressure (bar)	Pore Gradient (Specific Gravity)	Fracture Pressure (bar) (Pennebaker Correlation)	Overburden Pressure (bar)
100	1.3	0.13	9.4	25.5
200	1.4	0.07	19.0	50.9
300	1.5	0.05	30.0	76.4
450	2.0	0.05	48.1	114.6
600	14.3	0.24	75.4	152.8
800	31.5	0.40	115.4	203.7
1,000	45.7	0.47	154.2	254.7
1,200	62.1	0.53	199.2	305.6
1,400	77.1	0.56	240.2	356.6
1,600	91.9	0.59	285.2	407.5
1,800	106.2	0.60	334.3	458.4
2,000	120.3	0.61	381.4	509.4
2,200	133.2	0.62	430.0	560.3
2,400	146.9	0.62	481.8	611.2
2,600	160.3	0.63	532.3	662.2
2,800	173.0	0.63	584.6	713.1
3,000	185.8	0.63	641.8	764.0
3,200	197.3	0.55	693.8	815.0
3,400	209.1	0.63	750.9	865.9
3,600	219.9	0.61	804.5	916.9
3,800	230.9	0.62	860.6	967.8
4,000	241.7	0.62	916.8	1,018.7
4,200	251.1	0.61	969.4	1,069.7
4,400	261.4	0,61	1,023.6	1,120.6
4,600	270.9	0,60	1,085.4	1,171.5
4,800	280.4	0,60	1,138.8	1,222.5
5,000	288.4	0,59	1,194.5	1,273.4

7.2. Appendix B: InnovaRig

MAST		HOIST	
Height	51.8 m	Type	Hydraulic double-cylinder system
Hook load	3,500 kN (regular)	Stroke	22 m
		Power	2,000 kW
SUBSTRUCTURE		ROTARY TABLE	
Type	box-on-box	Bore	953 mm
Height	9 m rig floor (9 x 10m dimension)	Nominal load	4,450 kN
Casing load	3,500 kN	Dynamic load	3,500 kN
BOP trolleys	2 x 250 kN	Drive	hydraulic (max. 200 min ⁻¹ , 600 kW)
ROTARY TOP DRIVE		CORING TOP DRIVE	
Nominal load	4,450 kN	Nominal load	1,500 kN
Power	800 kW	Power	350 kW
Max. dyn. torque	48,000 Nm	Max. dyn. torque	12,000 kN
Max. RPM	220 min ⁻¹	Max. RPM	500 min ⁻¹
HYDRAULIC ROUGHNECK		MUD PUMPS	
Max. diameter	254 mm frame 1	Type	Electric (2 + 1 opt.)
Max. torque	508 mm frame 2	Power	1,300 kW
Max. load	4,540 kN	Max. pressure	350 bar
		Max. flowrate	2,200 L min ⁻¹
ELEVATORS		ROTARY TONGS	
Max. diameter	254 mm frame 1	Type	Hydraulic clamping
Max. diameter	508 mm frame 2	Diameter range	73 mm–508 mm
Max. load	4,540 kN		
PIPE HANDLER		MAGNETIC PIPE RACKING SYSTEM	
Drive	hydraulic	Type	Horizontal
Max. diameter	620 mm	Drive	Electric
Min. diameter	73 mm	Nominal load	45,000 N per magnet group
Lifting capacity	45,000 N		

Figure 55: Technical data sheet of the InnovaRig from the German Research Centre for Geosciences GFZ (WOHLGEMUTH et al., 2007).

7.3. Appendix C: Fann Dial Reading, Plastic Viscosity and Yield Point of OBM

Table 19: Listing of rheological properties of the oil-based drilling fluid after data from IBEH et al. (2008). The values refer to the test schedule under a constant pressure and variable temperatures.

P = constant at ~345 bar (~5,000 psi)				
Temperature (°C)	600 RPM (°)	300 RPM (°)	PV (mPa·s⁻¹)	YP (Pa)
~111 (~200 °F)	116	63	52	12
~167 (~300 °F)	74	40	33	8
~222 (~400 °F)	60	26	31	0
~278 (~500 °F)	65	35	32	5
~333 (~600 °F)	65	36	27	13

Table 20: Listing of the rheological properties of the oil-based fluid after data from IBEH et al. (2008). The values refer to the test schedule under a constant temperature and variable pressures.

T = constant at ~305 °C (~550 °F)				
Pressure (bar)	600 RPM (°)	300 RPM (°)	PV (mPa·s⁻¹)	YP (Pa) at ~278 °C (~500 °F)
~345 (~5,000 psig)	67	45	25	0
~689 (~10,000 psig)	95	64	30	5
~1034 (~15,000 psig)	122	81	41	12